Repeatable High-Yield Carbon Nanotube Growth by Moisture-Controlled Decoupled Chemical Vapor Deposition

by

Jinjing Li

A dissertation submitted in partial fulfillment
of the requirements for the degree of
Doctor of Philosophy
(Mechanical Engineering)
in The University of Michigan
2016

Doctoral Committee:

Associate Professor A. John Hart, Co-Chair, Massachusetts Institute of Technology
Professor Wei Lu, Co-Chair
Assistant Professor Neil P. Dasgupta
Professor Edward T. Zellers

DEDICATION

仰天大笑出门去
Laughing loud and stepping out

\- 李白 (唐)
\- Li Po (Tang)

也无风雨也无晴
Impervious to storm, yet impervious to shine

\- 苏轼 (宋)
\- Su Shi (Song)

ACKNOWLEDGEMENTS

My first taste of research started in the winter of 2008, when I was a junior student that was studying mechanical engineering. I can still remember some of the details during that interview, especially when my words became incoherent since I was so eager for that summer project for undergraduate student but I realized my background might not be really fitting nicely. At that time, the young, smart and energetic faculty sitting in front of me said, "Don't worry, I consider the passion to be more important at this point, rather than the experience in this field". Years later, I realized again and again how lucky I was to have the chance to work with Professor A. John Hart, and I would like to express my sincere respect and deepest gratitude to him for his clairvoyant guidance and solid support. During these years, as an admirable advisor, John always made time for his students despite his busy schedule. Without the support from him, I would never be able to achieve the doctoral degree.

I would like to thank my PhD committee members Professor Wei Lu, Professor Edward Zellers and Professor Neil Dasgupta for their time and efforts. They have offered invaluable advice throughout my research career and I really appreciate their support.

I would also like to acknowledge my excellent Mechanosynthesis lab mates. In no particular order, I would like to thank:

Dr. Sameh Tawfick, Dr. Eric Meshot, Dr. Mostafa Bedewy, Dr. Erik Polsen for exciting brainstorming and productive discussion; Dr. Alvin Orbaek White and Dr. Sebastian Pattinson for brilliant advice on the full picture of my dissertation; Dr. Davor Copic, Kendall Teichert, Megan Roberts, Dr. Jong G. Ok, Dr. Yongyi Zhang and Dr. Sei-Jin Park for training me on various software, equipment, and helping out with experiments. I would like to thank all my fellow Mechanosynthesizers. I really enjoyed the friendly, creative and constructive research environment which made my life of research full of joy and happiness.

I have spent a lot of time at fabrication and characterization facilities, and I would like to express my appreciation to Hongbin Zhao and Scott Hopkins from Pall Corporation, Dr. Kai Sun and Dr. Haiping Sun from the Michigan Electron Micro Analysis Lab (EMAL), Dr. Robert W. Hower and David Sebastian from Lurie Nanofabrication Facility (LNF), Dr. Arthur R. Woll from Cornell High Energy Synchrotron Source (CHESS), and Harald Eberhart from the University of Michigan Material Science and Engineering Department.

I would also like to thanks to the financial sponsors that have supported the research presented in this dissertation, Pall Corporation and the National Science Foundation. I would also like to express my appreciation to University of Michigan Department of Mechanical Engineering for a department fellowship.

Last but not least, I have a group of wonderful friends here in Ann Arbor, and my dear parents oversea in China. I cannot image how my life would have been without all of you and thank you for every moment we share in my life.

TABLE OF CONTENTS

LIST OF FIGURES

LIST OF TABLES

ABSTRACT

Aligned carbon nanotubes (CNTs) have become well known due to their outstanding properties. However, there remains a lack of understanding of the multivariate nature of CNT synthesis, and particularly how to achieve consistent production of aligned CNTs on industrially relevant substrates. This thesis presents a series of techniques for improved manufacturing of CNT forests, including achievement of higher density CNT forests and improved consistency of production.

First, decoupling of the catalyst annealing and CNT nucleation/growth steps is shown to attenuate moisture transients in the CVD system, and results in improvement in average CNT forest height by 21% and reduction of standard deviation by 76%.

Second, it is found that moisture improves the activation of catalyst particles at the beginning of CNT growth. But during later stage of CNT growth a 28% slower growth rate of forest height is led by a moisture level of 370ppm for 10 minute growth. Moreover, deposition of a small amount of carbon onto the reactor wall improves the CNT forest density by a factor of 2~4. X-ray photoelectron spectroscopy and transmission electron microscopy show that the carbon deposition causes the formation of a graphitic layer on catalyst particles, which helps activate particles to achieve higher density CNT forests.

Then, these findings are translated to perform CNT synthesis on metal alloys. CNT forests are synthesized on Haynes 556 alloy. It is shown that air oxidation at 825 ℃ and H_2/He reduction at 775 ℃ is required prior to hydrocarbon exposure in order to bring iron to surface as catalyst, and the presence of moisture during growth is required to achieve aligned forest. Finally, a hybrid filtration material is developed by synthesis of sparse tangled CNTs on sintered porous stainless steel filters. The CNT growth density on the porous substrate is tuned to give an increase in the particle capture efficiency of ~10^5 with a pressure drop of less than 15 psi. An analytical model is established to predict the relationship between pressure drop and flow rate, and rationalize the ideal CNT growth morphology on the filter.

CHAPTER 1
INTRODUCTION

1.1 Background and motivation

Carbon nanotubes (CNTs) were first identified in the scientific literature more than 25 years ago [1]; since then, CNTs have become one of the most important nanomaterials due to their excellent mechanical [2-6], thermal [7-10], chemical [11, 12] and electronic [13-18] properties.

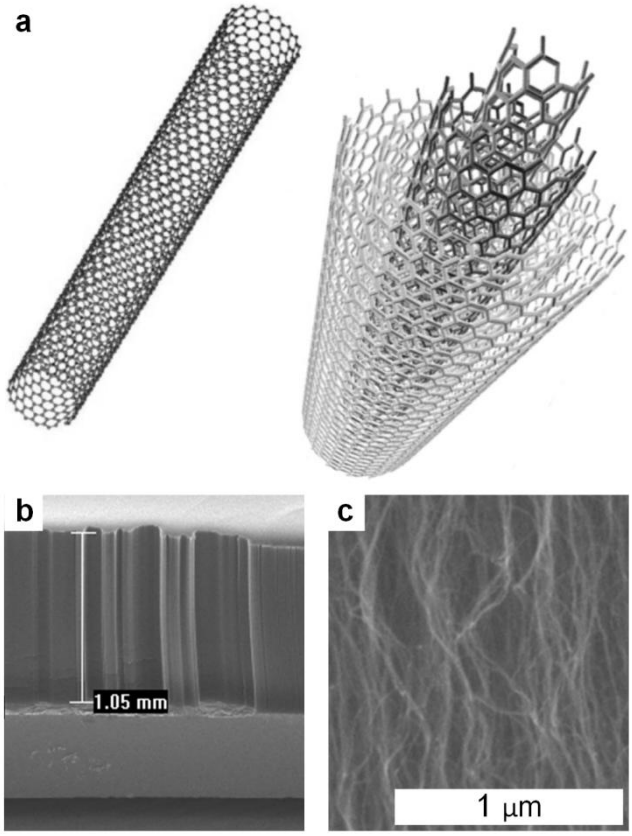

Figure 1.1 Carbon nanotube and CNT forest: (a), schematic of single-walled and multi-walled CNTs [19]. (b), SEM image of a CNT forest. (c), zoomed in SEM image showing individual aligned CNTs from CNT forest.

Individual CNTs are hollow tubes made of carbon atoms based on graphitic hexagonal carbon lattice [19]. As shown in Figure 1.1a, single-walled and multi-walled CNTs can be considered

as one or more layers of graphite that rolled up and formed a series of closed coaxial cylinders. The assembly of CNTs can be controlled to have different orders of alignment, such as random dispersion [20], horizontally aligned [21] or a collection of yarns [22]. In particular, this dissertation focuses on macrostructures that are composed of vertically aligned CNTs (CNT forests), shown in Figure 1.1b&c.

CNT forests attract researchers due to their instinct anisotropic structure – ordered 1-D alignment. Existing publications have already demonstrated applications requiring anisotropic properties, such as MEMS devices [23-25], unidirectional thermal conductor [26], supercapacitors [27] and semiconductor devices [28-30].

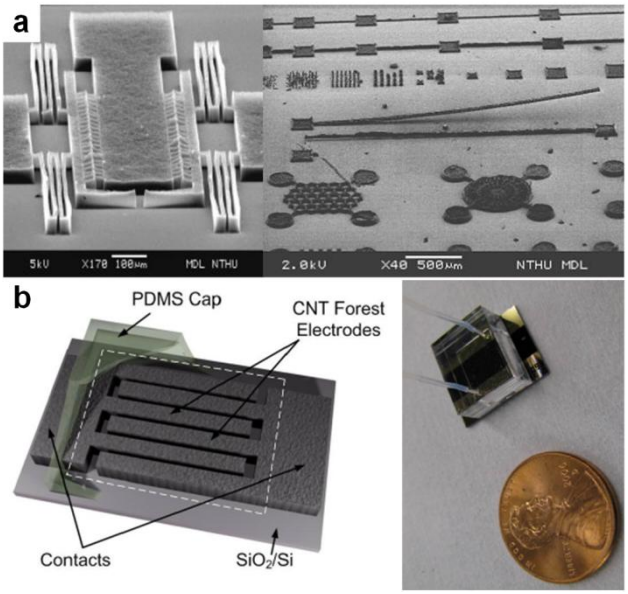

Figure 1.2 Applications that require consistent production of CNT forests. (a), micro-griper and cantilever that made of aligned forests [31]. (b), Supercapacitor that uses CNT forests as electrodes [32].

These applications require consistent production of CNT forests at controlled height and density. For example, the mechanical property of a micro cantilever device [31] composed by CNT forest (Figure 1.2a) can be significantly affected by the density of CNT forest. Fluctuation of forest density from batch to batch production will lead to inconsistent performance of the micro cantilever device. Similarly, when the CNT forests are used to build electrodes of a supercapacitor (Figure 1.2b) [32], the height of forests presents as one of the direct factors that will determine the capacitance of the supercapacitor.

The aligned CNT forests are typically produced by chemical vapor deposition (CVD) process,

due to its versatility for producing high quality CNTs. As shown in Figure 1.3a, there are three major stages in a typical CVD process. First the catalyst chip will be placed in a proper spot inside heating unit, and the substrate will be heated up to certain temperature which is suitable for catalyst annealing and CNT growth (usually about 700-850 ℃). Inert gases such as helium and argon can be used in this stage, and sometimes hydrogen is also included in this stage. Then it comes to the catalyst annealing stage, in which the substrate will be held at a constant temperature in reduced atmosphere, such as a mixture of helium and hydrogen. The catalyst film will break down and form nano-particles during the annealing stage. Finally, hydrocarbon gases such as ethylene or methane is introduced to the system. These hydrocarbon gases will decompose and form precursors, and react with catalyst particles to grown CNTs.

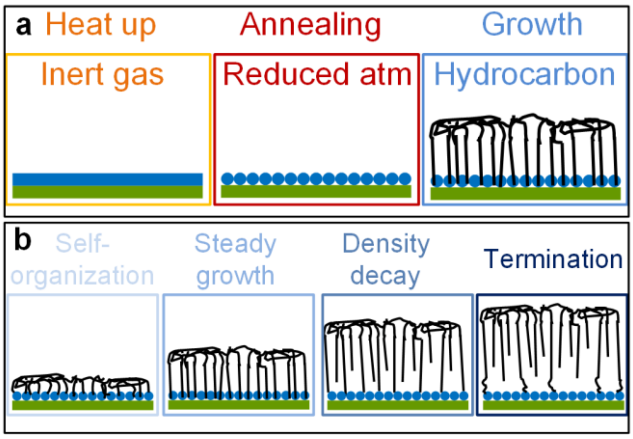

Figure 1.3 CNT forest produced by a typical CVD process: (a), three main stages that for forest production: substrate heat up, catalyst annealing and CNT growth. (b), four phases during the growth stage: CNT nucleation and forest self-organization, steady stage growth, density decay and termination of growth.

The CNT growth stage can be further divided into four phases. The collective mechanism of CNT forest growth revealed by Bedewy et al [33] has demonstrated the evolution of CNT alignment and density throughout the growth process, as shown in Figure 1.3b. CNT growth stage starts with activation of catalyst, nucleation of CNTs on catalyst particles and the self-organization of aligned forests. Then it comes to the steady growth phase, which the majority of activated catalyst particles are still producing CNTs. After that, some of the catalyst particles start to deactivate and stop from growing CNTs, which leads to a decay of forest density. Finally, the growth of CNT forest terminates after the density of remaining activated catalyst particles is not enough to support aligned forest growth.

As a result of modeling and theoretical calculation, it has been proposed that performance of carbon nanotube could be better than conventional materials. The Young's modulus of an individual CNT is expected to be in the terapascal (TPa) range [34], which is about one magnitude greater than that of steel. The electrical current density over individual CNT has been reported on the order of 10^7 A/cm^2 (2 magnitudes greater than typical materials), with ballistic transportation and does not dissipate heat [35].

Ideally, CNT forests can be fashioned with high density [36] and a high degree [37] of alignment. But in reality researchers have found the density of CNT forest obtained by CVD process to be less than 5% of the theoretical value, further to this it is common to find a significant degree of entanglement among the CNTs within the forest. The low density forests obtained from CVD process is due to the low activation rate of catalyst particles. Only a small portion of catalyst particles are activated during the CNT nucleation phase of the growth process. The lack of activation leads to empty space around each growing CNT, and further allows the CNTs to grow up with a high entanglement orientation. The causes of low activation rate of catalyst particles have not be fully understood yet, but previous research has shown one of the reasons could be deactivation caused by carbon coating [38].

Also, especially at the lab scale there are issues with batch-to-batch consistency [39]. Height and volumetric density of CNT forests produced in a long term study showed lack of consistency. Although a lot of details during the CNT forest synthesis are still not clearly understood yet, the collective mechanism of CNT forest growth [33] has indicated that properties of the catalyst, precursors, and substrates, and reaction conditions can greatly influence the product outcome [37, 38, 40-42].

Typical CVD process requires catalyst substrate remains in a fixed spot in the furnace throughout the heating, annealing and growth stages. With such a configuration, the inputs during different stages are coupled. Since it always takes time to reach steady state when adjusting inputs such as temperature, gas flow rate and moisture level, etc, researchers either have to stand with constant input throughout the entire CVD process, or to endure the transit caused by changing the input parameters. Such limitation of coupled effect brings difficulties to understand exact role of factors during different stages in CVD process. An alternative CVD process that can provide physical decoupling of each stage is required, in order to study the causes of inconsistency and low density in CNT forest production.

1.2 Scope and outline of this thesis

The goal of this dissertation is to understand the causes of variation in CNT forest growth, and discover techniques that can help improve consistency and density of CNT forest. Then, the applicability of CNT growth to industrially relevant substrates is studied, such as silicon wafer, high temperature alloy and stainless steel alloy.

Each of these topics, along with the results of CNT synthesis and property characterization, is presented in the following chapters:

Chapter 2 presents the design of a sample loading system that allows the physical decoupling of catalyst annealing and CNT growth steps. Then, the entire CVD system used for this dissertation, including moisture supply/record and vacuum control is described.

Chapter 3 presents a novel synthesis method that can improve the consistency of vertically aligned CNT forest growth by decoupling catalyst annealing and CNT nucleation/growth steps. A comparison to a reference CVD process where the sample sits in the furnace throughout the entire synthesis is performed, showing that decoupled process leads to taller CNT forests and reduces run-to-run variation. The approach in this chapter enables consistent lab-scale fabrication of CNTs for development of applications, and identifies key principles for translating batch-style CVD to continuous manufacturing.

Chapter 4 builds upon the decoupled synthesis process to determine how to increase the nucleation density of CNTs from the population of catalyst particles. Delivery of a small amount of carbon during catalyst annealing and supply of moisture during CNT growth is shown to enable this. With the help of the transfer arm assisted CVD system, detailed role of moisture at each phase during the CNT nucleation/growth process is elucidated. Furthermore, comprehensive characterization is carried out to study the impact of carbon preload during catalyst annealing. Fragments of single layer graphitic structure is observed on surface of catalyst particles after annealing with carbon supply, which indicates the carbon preload helps activate catalyst particles during annealing, and then lead to an initial greater nucleation/growth rate of CNTs at the starting phase of growth.

Chapter 5 demonstrates the direct growth of aligned CNT forests on the native surface of Haynes 556 super alloy, which is an industrial grade metal alloy. Heat treatments including oxidation in air and reduction in helium/hydrogen are applied on Haynes 556 alloy prior to hydrocarbon exposure, in order to bring catalytic and support elements such as iron and chrome to surface of sample for CNT growth. Supply of moisture during growth stage is also found to be an essential input to guarantee aligned CNT forest growth.

Chapter 6 presents the application of the growth techniques to the fabrication of CNT-enhanced porous stainless steel filters. An improvement of particle capture efficiency about 4-6 magnitudes after enhanced by CNTs is demonstrated. And an analytical model is established in order to elucidate the relationship between CNT packing ratio, pressure drop across enhanced device and particle capture efficiency.

Chapter 7 presents a summary of contribution of this thesis. Key questions with respect of consistent production of CNT forests are presented, along with proposed future directions that may be able to answer these questions.

CHAPTER 2
TUBE FURNACE SYSTEM FOR DECOUPLED, MOISTURE-CONTROLLED CHEMICAL VAPOR DEPOSITION

This chapter describes the CVD system that is designed and constructed for CNT growth in this thesis. First, the entire CVD system with associated modules is described. Then, each of the modules is introduced with further details and it is explained how this CVD system helps improve the control over catalyst annealing and CNT growth.

2.1 Background and motivation

During the past two decades of research on fabrication and application of vertically aligned CNT forests, many chemical and mechanical aspects of CNT nucleation and self-organization are revealed [33, 43-47]. As a result, many recipes have been developed for catalyst preparation and chemical vapor deposition to achieve control of the key attributes such as CNT diameter and areal density [48-51].

As introduced in Chapter 1, the entire synthesis process can be divided into several different stages, such as substrate heat up, catalyst film annealing, CNT nucleation and growth, etc. In nearly all published CVD processes for CNT growth, the catalyst substrate is loaded at a stationary point inside the furnace and remains there during the consecutive introductions of the annealing and growth gas mixtures. Limited by such sample loading mechanism, input factors during these different stages are "coupled" together: First, the input from an earlier stage will unavoidably be passed to and affect the following stage. Second, the change of one input will lead to the change of another input.

For example, if researchers would like to study the CNT growth at different temperatures, one of the two ways they could choose is to keep an identical temperature input throughout both annealing and growth stages. In such case the temperature for these two stages are coupled, and it becomes hard to distinguish if the difference in growth results is induced in

annealing, or growth, or both stages. Furthermore, the change of temperature during annealing will also change the decomposing temperature of hydrocarbon, which coupled three factors together: catalyst annealing temperature, hydrocarbon decompose temperature and CNT growth temperature.

The other choice is to hold temperature at one stage as a constant, while changing the input for the other stage. But since most of the CVD systems are heated by resistor coils, it is going to take time to switch from one temperature to another. Since the catalyst chip sits at a stationary spot during all these stages, this chip has to suffer the transit of temperature. The responding time of temperature transit will depend on the difference of temperature between two adjacent stages, which means the impact of temperature from the previous stage will be passed to the following stage and brings additional variables into the study.

The coupled effect can happen on factors like moisture concentration and gas composition. In a typical tube furnace CVD system, the flow rates of gases are controlled to furnace by digital mass flow controllers (MFC). Similarly, the control of moisture level is achieved by adjusting the ratio between moisture-rich gases and gases that have lower moisture levels. The different gases are delivered by stainless steel or PTFE tubing, and the reactor chamber is continuously purges with these gases. Since the total flow rate during CVD process is about 500-1000 sccm while the internal volume of gas delivery lines and reaction chamber in the CVD system is about 0.5 Liters, it takes time to reach steady state when switching from one composition to another. With traditional CVD system, it becomes almost impossible to achieve non-crosstalk study with different inputs from catalyst preparation and CNT growth, since the change of inputs as temperature, gas flow, moisture concentration and other factors need to take time to respond. Furthermore, with such a CVD system it is also not convenient to apply techniques like fast heating and fast cooling, which could be necessary in certain research purposes. For example, fast cooling allows to “frozen” catalyst chip right after the end of catalyst annealing and study the size and density distribution of catalyst particles right before CNT growth.

Other researchers have also noticed similar disadvantages of existing typical CVD systems. For example, Sakurai et al [40] has established a CVD system using an infrared lamp furnace in order to enable rapid heating and cooling. But with such design, the transition caused by the change of gas flow is still not avoided. On the other hand, Liu et al [52] transfers the

entire quartz tube during the CNT synthesis process, in order to selectively expose substrate to different gas mixtures Liu's work is able to avoid the transition caused by change of gas composition, but it will take much longer time to heat up the substrate before it reaches growth temperature.

There are also alternative designs of CVD reactor called "cold-wall" systems [42, 45, 53-55]. In such designs only the substrate will be heat up, while leaving the rest of the reactor (especially the reactor wall) remains in lower temperature. One of the advantages of the cold wall system is similar to the infrared lamp furnace: rapid heating and cooling for substrate. But since the substrate still stays in the reactor and contact with the gas atmosphere, the cold wall system still can not fully avoid the coupled effect.

In order to enable improved control over the catalyst annealing and CNT nucleation stages, it is necessary to decouple the exposure steps to the respective gas atmospheres. I then come up with the idea of constructing a substrate delivery system attached to the CVD system. Substrate samples are going to be loaded on a piece of quartz boat, and this quartz boat is further connected with a transfer arm. The transfer arm can be operated anytime during the CNT synthesis process, so the substrates can be transferred inside and outside of the furnace, at any spot that assigned due to research purposes.

2.2 Integrated CVD growth system

The entire CVD growth system is shown in Figure 2.1a. The whole system is composed of a few sub-modules such as CNT synthesis module, sample loading module, moisture control module and vacuum module. A detailed schematic of the entire CVD system labeled with gas flow directions is shown in Figure 2.1b.

The gases are supplied from compressed tanks, controlled by digital MFCs and delivered through 1/4" stainless steel tubing. One of the MFCs drives a branch of helium flow through the water bubbler at very low flow rate (less than 29 sccm) to bring moisturized helium gas to the system, and then joined the rest of the flow with a T-connector. The mixed flow of gases is then driven through a hygrometer in order to measure the moisture concentration of the stream before it enters the tube furnace.

The sample loading module is attached on the exhaustion end of the furnace, and allows catalyst chips to be transferred into the tube furnace by a quartz boat holder. There are two outlets from the sample loading module. Both of them are connected to the exhaust vent.

Between one of the outlets and the exhaust vent, there is the vacuum module, which allows the CVD system to be pumped down below 1 Torr. Further details of each module are going to be introduced in the following part of this chapter.

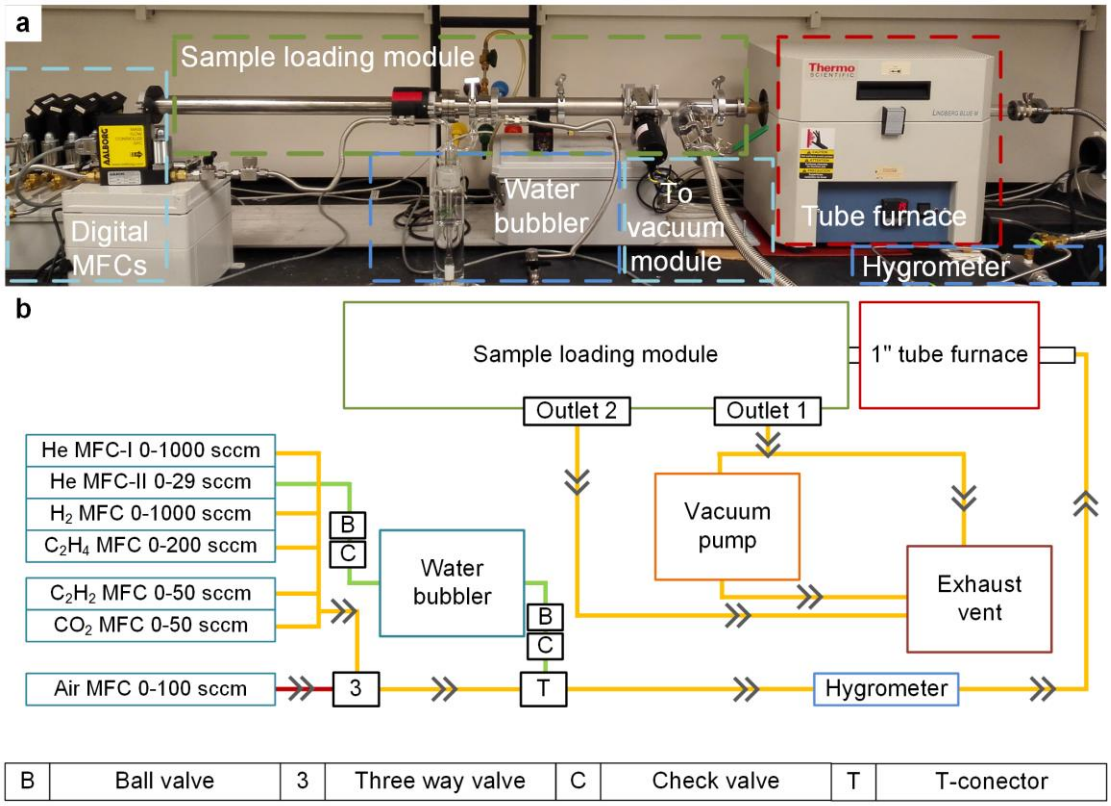

Figure 2.1 Tube furnace system for decoupled moisture-controlled chemical vapor deposition. (a), photo of the entire system labeled with sub-modules. (b), schematic of the system labeled with flow directions.

2.2.1 CNT synthesis module

The CNT synthesis module is composed by two major parts: digital MFC group and 1" tube furnace. Seven digital MFCs are used to provide quantitative control of the gases: helium (main stream, dry), helium (through water bubbler), hydrogen, ethylene, carbon dioxide, acetylene, and air. There is a three-way valve installed between the air MFC and other MFCs, so the oxidizer (air) will not be able to deliver together with flammable gases (H_2, C_2H_4 and CO_2) in order to prevent explosion caused by careless operation. The horizontal tube furnace (Thermo Scientific Lindberg/Blue M Mini-Mite, FT55035 COMA-1) is fitted with a quartz

tube (25 mm OD, 22 mm ID). The flows and temperature were controlled and recorded using a LabVIEW program.

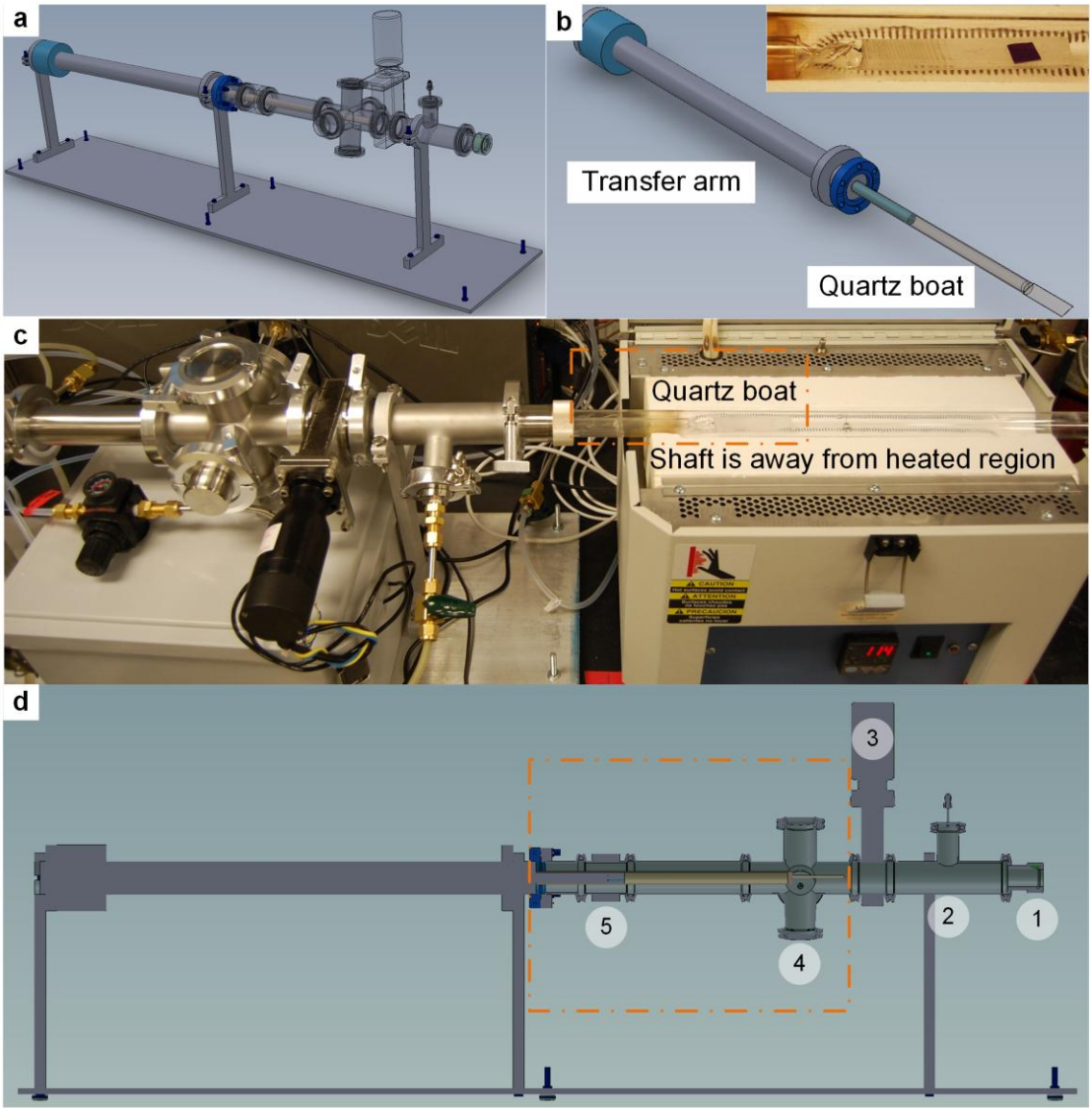

Figure 2.2 Schematic of sample loading module. (a), entire transfer arm sample loading system, supported by aluminum alloy stands. (b), quartz boat installed on the magnetic coupled transfer arm. The inset is a photo of catalyst chip held by quartz boat. (c), a photo showing sample loading module connected with tube furnace. (d), cross section view of the transfer arm system.

2.2.2 Sample loading module (transfer arm)

The schematic of the entire sample loading module is shown in Figure 2.2a. The key part of the module is a vacuum compatible transfer arm (VF-1695-18, Huntington Mechanical Laboratories), which has a stainless steel shaft that is magnetically coupled to a handheld movement ring located outside of the sealed chamber. This transfer arm needs to be operated at a temperature no greater than 200 ℃, in order to prevent demagnetization at high

temperature. The end of the transfer arm is fitted with a custom quartz boat (18 x 75 mm), which holds the catalyst-coated sample, as shown in Figure 2.1b. The inset of Figure 2.1b is a photo image showing a piece of catalyst chip sits inside the furnace which is held by the quartz boat. From the schematic it can be observed that the front of the quartz boat (brown color) is a few inches further away from the tip of the stainless steel shaft (green color). This design guarantees that when the quartz boat is sitting at the growth spot inside tube furnace, the stainless steel shaft can still stay outside the heat region and remain close to room temperature. A photo of the sample loading module connected with the 1" tube furnace is shown in Figure 2.3c. It shows that quartz boat is staying inside the furnace, while the stainless steel shaft is away from furnace and not shown up in this photo.

The cross section view of the transfer arm system is shown in Figure 2.2d. The whole system is placed at the downstream side of the tube furnace. From right to left, the numbers in white circles indicate the important parts in the transfer arm system: (1), 1" quick connector that connects with the exhaust end of the 1" quartz tube. (2), KF-40 t-connector, with a gas outlet. (3), pneumatic gate valve. (4), KF-40 6-way cross, which can be installed with gas analysis instruments, view port, thermal couple, vacuum pump and other devices according to requirements. (5), another gas outlet. Part (2) and (4) can be replaced by any other types of KF-40 connector with the same length, according to specific requirements of the researcher and tube furnace that is to be used. The region labeled with the orange dashed line is the load-lock chamber, and this load-lock chamber, gate valve (3) and KF-40 t-connector (2) are always staying at room temperature. On the other hand, the space inside the tube furnace is called the reactor chamber. The temperature of reactor chamber can vary from room temperature to 1000 ℃. The sample loading module can help improve the control over catalyst annealing and CNT growth stages in the following way:

Step 1, substrate is loaded on the quartz boat and positioned to any preferred spot in reaction chamber. The outlet (2) is closed and outlet (5) is open. Gas stream for annealing can purge through the reaction chamber and load-lock chamber and remain consistent in these two chambers.

Step 2, after catalyst annealing is finished, the substrate chip is carried back to the load-lock chamber by the transfer arm. Outlet (2) is open and gate valve (3) is closed. Now the substrate can cool down in the load-lock chamber with the same atmosphere as it was

annealed.

Step 3, now the gas composition, temperature and moisture concentration can be adjusted. Since gate valve (3) is closed and the load-lock chamber is at room temperature, the transit process happening in the reactor chamber is insulated from the substrate.

Step 4, open gate valve (3) and close outlet (2) after the input conditions in reactor chamber reaches the steady state, transfer substrate to the same spot (or a different spot) in the reactor chamber for CNT growth.

The sequence of operations listed above enables non-crosstalk control of inputs during catalyst annealing and CNT growth stages. Now, the exposure steps are decoupled to the respective gas atmospheres.

2.2.3 Moisture control module

Schematic of the moisture control module is illustrated in Figure 2.3a, and a photo of the water bubbler is shown in Figure 2.3b. To control the moisture level in the system, a small branch of Helium flow is delivered by a low flow rate (0-29 sccm) Helium MFC through a gas washing bottle (CG-1114-14, Chemglass). This split Helium flow is later joining the main stream moisturizes the gas mixture for CVD process. Deionized water is filled in the gas washing bottle as the source of water vapor supplied for growth. There is a pair of ball valve and check valve installed both before and after the water bubbler. The ball valves are used to shut off the bubbler and prevent the moisture diffuse from the bubbler to main flow of gas stream, when the dry condition (<10 ppm) is required. The check valves are installed to prevent potential back flow that may drive the water inside bubbler to the low flow rate He MFC. The mixture of gases passes through a hygrometer (Khan Cermet-II, Fluid Energy) before entering the tube furnace, so the moisture level of the gas stream can be monitored.

By keeping the total flow rate added from both Helium MFCs as constant, this moisture supply system can adjust the water vapor concentration in the growth system from 10 ppm to over 900 ppm without changing the composition of gas supply for CVD growth, as shown in Figure 2.3c. The flow rate labeled on the plot indicated the amount of Helium flowed through the water bubbler, and the total flow rate of the entire gas stream was always kept at 600 sccm, which is the standard flow rate during the CNT growth stage.

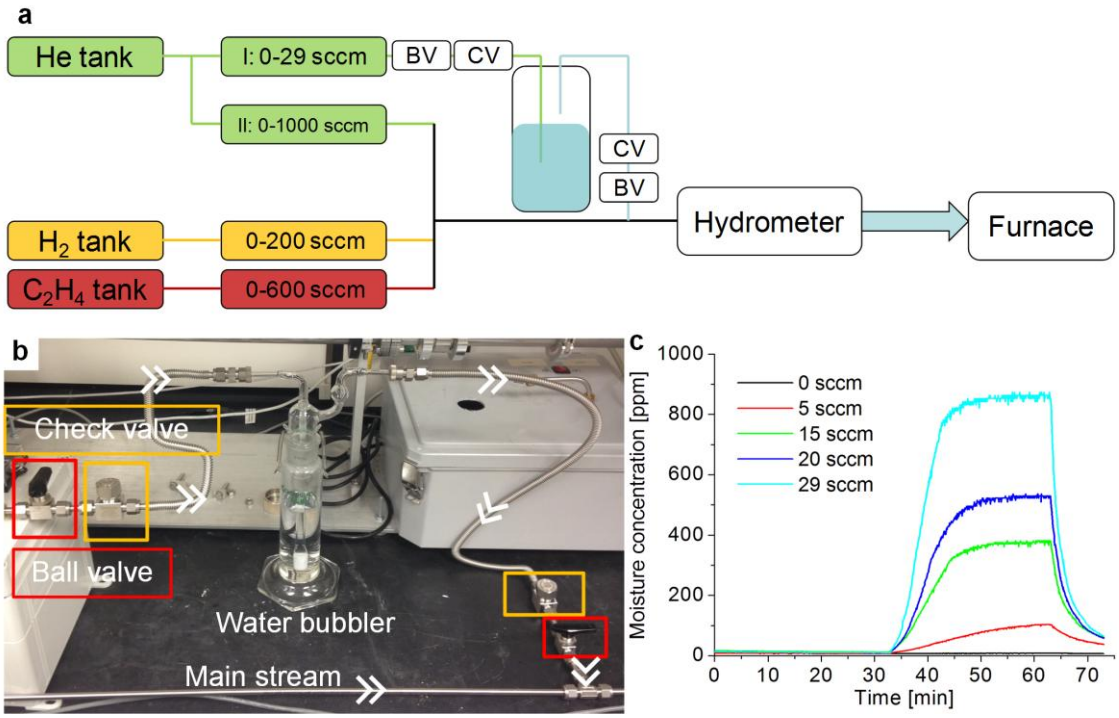

Figure 2.3 Moisture control module. (a), schematic of the moisture control module. BV stands for ball valve and CV stands for check valve. (b), photo of the water bubbler and flow stream through it. (c), concentration of moisture can be adjusted from 10 ppm to about 900 ppm by the moisture control module while keeping the total flow rate constant at 600 sccm.

The hygrometer has a ceramic moisture sensor with 80μ sintered metal guard, and the recommended flow rate is 1-5 L/min. The hydrometer can be operated with a pressure from vacuum to 5000 psig, and in the range of temperature from -40 ℃ to 60 ℃. The temperature in the lab and pressure in the growth system fit into the operating conditions of the hygrometer, but the typical flow rate applied in this research is about 0.5-0.6 L/min, which is about a half of the lower limit of the recommended flow rate. The low flow rate used in the research may lead to a lag of reading on the hygrometer. As a result, it takes time for the hygrometer to reach a steady state reading of the moisture concentration in the CVD system. The waiting time to reach a steady state reading will be longer if the difference between the initial moisture level and the steady state level is smaller.

2.2.4 Vacuum Module

A vacuum pump (DS 302, Varian) is connected to one of the outlet from the transfer arm system. A pressure transducer and reading unit (RVC 300, Pfeiffer) is attached with the pump to provide in-situ reading of pressure inside the growth system.

According to the specific goals of the studies described in the foregoing chapters, the various modules are used individually or in combination.

CHAPTER 3
HIGHLY CONSISTENT ATMOSPHERIC PRESSURE SYNTHESIS OF CARBON NANOTUBE FORESTS BY REDUCTION OF HYDROCARBON AND MOISTURE TRANSIENTS

This chapter is in large part reproduced from publication in preparation: Jinjing Li, Mostafa Bedewy, Alvin Orbaek White, Erik S. Polsen, Sameh Tawfick, and A. John Hart, Highly consistent atmospheric pressure synthesis of carbon nanotube forests by dynamic decoupling of catalyst annealing and hydrocarbon exposure.

This chapter describes a synthesis method that can improve the consistency of vertically aligned CNT forest growth by decoupling the catalyst annealing and carbon exposure steps. The decoupling is achieved using the sample loading module introduced in the previous chapter, which can move the substrate rapidly into and out of the CVD tube furnace. For the decoupled recipe, catalyst substrates are taken out of the furnace after annealing, while the atmosphere inside tube furnace is switched to CNT growth condition. The substrates are sent back to furnace a few minutes later after the gas composition inside the furnace reaches the steady state. Compared to a reference CVD process where the sample sits in the furnace throughout the process, the decoupled method improved the forest height by 21% and reduced the run-to-run variance of height by 76%. Furthermore, by studying the growth performance at controlled moisture levels (5-8 ppm and 15-30 ppm) using the decoupled process and the reference process, it is elucidated that the improvement in consistency is due to the stable moisture level during growth. As quantified by X-ray scattering, CNT forests grown by the decoupled method also have significantly greater alignment. The approach in this chapter enables consistent lab-scale fabrication of CNTs for development of applications, and identifies key principles for translating batch-style CVD to continuous manufacturing.

3.1 Background and introduction

Consistent synthesis and precise control of key properties such as height, density, diameter,

alignment of CNT forests are essential to their translation from lab-scale experimentation to are required when transferring laboratory scale technique to industrial applications such as thermal interfaces [56, 57], CNT forest embedded MEMS [31, 58], and high strength yarns and thin sheets [22, 59]. It is expected that high density CNT forests will have outstanding bulk properties compare to conventional materials. Unfortunately, researchers found that in reality, the density of CNT forests obtained by chemical vapor deposition (CVD) process is usually less than 5% of the ideal value, and this is limited by the nucleation density of the CNTs (i.e., the catalyst activity) as well as the density of catalyst particles on the substrate. Addition to the low density of CNT forest, a significant degree of entanglement among the CNTs within the forest is also observed.

Even with the disadvantages described above, CVD is the mainstream method of CNT forest synthesis, and atmospheric pressure synthesis is most attractive due to its simplicity and scalability. As introduced in Chapter 1, CNT forests produced by a typical CVD recipe will experience three main stages: substrate heat up, catalyst annealing and CNT growth. The gas atmosphere is going to be switched from one stage to the next. Due to the nature of the gas delivery system, it needs to take time to reach a new steady state when switching the gases, and such limitation makes the input factors coupled together during these stages (introduced in Chapter 2). Previous research has also shown huge variation of CNT forest growth can happen with this typical CVD process [39]. The sources that caused this variation has not been fully understood yet, but they could be moisture concentration in the growth system, residue carbon on reactor wall, impurities diffused into growth system from ambient, etc.

Moisture is known to influence CNT growth in the range thousands of ppm [60], hundreds of ppm [61], less than ppm levels [62], and even less than ppb levels [63]. For example, Noda et al [61] studied the impact of moisture on growth of SWNT forest in the range of a few tens to hundreds of ppm. They reported increased moisture content (from 0-300 ppm) would lead to a decrease of forest height when catalyst film is thin (<0.5 nm) but moisture is crucial to obtain millimeter-scale SWNT forest when supply of hydrocarbon was increased from 0.10 vol% to 0.6 vol%. They also found the termination of growth could be due to two mechanisms, catalyst deactivation and catalyst coarsening, and due to these two termination mechanisms millimeter scale forest could be achieved from either slow growth with low temperature and low hydrocarbon pressure or short growth with high temperature and high concentration of hydrocarbon [64]. As a conclusion, they suggested water prolongs catalyst

lifetime under excess C_2H_2 supply, but deactivates small catalyst particles and degrades the quality of CNTs.

On the other hand, Noy et al [62] focused on the impact of trace amount of oxygen containing species (ppm level, moisture and other impurities from supplied gases) can significantly modify kinetics of aligned CNT forest growth, and they suggest purification of reaction gas composition is essential to obtain reliable forest growth at atmospheric CVD conditions. Lulevich et al [63] also demonstrated that the absence of moisture (sub-ppb level) will cause catalyst layers to turn into micrometer scale particles that didn't lead to CNT forest growth.

Addition to moisture, the introduction of the hydrocarbon source can also affect forest production and consistency. In typical synthesis procedure, substrates are first annealed in a hydrogen-containing atmosphere then followed by addition of the carbon source. Due to the intrinsic response rate of the electronic mass flow controller (MFC), it takes several seconds to reach the set point when one or more of the partial flow rate is changed. And furthermore, the transient of chemical composition of the mixed gases from anneal condition to growth condition persists over several tens of seconds due to the flow rate (500-600 sccm) relative to the volume of quartz tube (about 200-300 cm^3 in furnace). This results in even longer transient in the chemistry of the atmosphere, and in particular the composition of thermally generated hydrocarbons that are known to influence CNT growth. Therefore, it can be imagined that the rate of change between exposure conditions for the annealing and growth steps would influence the outcome of the CVD process, such as by governing the rate at which CNTs consecutively nucleate from the catalyst particle population on the substrate. My hypothesis was that establishing a stable gas composition and moisture level inside the tube furnace prior to inserting the sample would lead to significantly improved consistency of CNT forest height and density via atmospheric pressure CVD.

This chapter studies the influence of the transient between the annealing and growth stages on the consistency of CNT forest synthesis by atmospheric pressure CVD, and on metrics of the synthesis process. In the following part of this chapter, it is demonstrated that decoupling the annealing and growth stages improved the mean height of forests by 21.0% and reduced run-to-run variation in height by 75.7%. The small angle x-ray scattering (SAXS) data also showed the alignment [33] of the CNT forest produced by decoupled recipe is improved (Herman's factor 0.62-0.68) compared to forests obtained from a reference typical CVD

process (0.44-0.50).

3.2 Methods and experiments

3.2.1 Substrate preparation

Supported catalyst thin films are deposited by sputtering (Lab18, Kurt Lesker) of Al_2O_3 (10 nm) followed by Fe (1 nm) on thermally oxidized (100) silicon wafers [47]. The silicon wafers coated with the catalyst are then cut into rectangular pieces (4x8 mm) using an automatic dicing saw (ADT-Dicing, Model 7100). The wafer pieces are sonicated in a beaker containing acetone, for 8 minutes (Crest Ultrasonics Model 1100D, power setting 6), after which the acetone is discarded and replaced with fresh acetone, and then sonication was repeated for 8 minutes at the same setting. The sonication procedure is repeated once again using methanol, and then 2-propanol, and then the substrate is removed using tweezers and dried in a gentle nitrogen stream.

3.2.2 CNT synthesis

CNT forests are produced using the tube furnace system with sample loading module (transfer arm) as introduced in Chapter 2. As shown in Figure 3.1a, the transfer arm is installed downstream to the tube furnace so the substrate chips are transferred into the furnace through the exhaust end of tube furnace. The temperature of the sample holder attached to the transfer arm is measured by affixing a thermocouple (Omega, XCIB-J-2-6-3) connected to a data acquisition card (National Instruments, USB-TC01).

CNT synthesis according to the 'decoupled recipe' is performed as follows (Figure 3.1b):

Step 1: The catalyst-coated substrate is placed onto the quartz boat attached to the transfer arm, the system is sealed, and the arm is used to place the leading edge of the sample at the desired location (unless otherwise noted, 7 cm downstream from the furnace control thermocouple).

Step 2: The system is purged with He (100 sccm, 99.999% Cryogenic Gases) and H_2 (400 sccm, 99.998%, Cryogenic Gases), and C_2H_4 (150 sccm, 99.5%, Cryogenic Gases) to remove any residual oxygen from the gas lines, for 5 minutes at room temperature. Next, the flow is switched solely to He (1000 sccm) for 5 minutes.

Step 3: Prior to heating of the furnace, the flow is switched to H_2 (400 sccm) and He (100 sccm) and held for 10 minutes at room temperature.

Step 4: The furnace is then heated to 775 ℃ over 10 minutes. Upon reaching the set point

temperature the flow is held for a further 10 min. During this stage, the catalyst film is chemically reduced and dewets into nanoparticles.

Step 5: The transfer arm is then used to move the sample from of the heated area of the furnace into the load lock area, at which point the gate valve is closed immediately; allowing the sample to cool in the same atmosphere in which it was annealed while flow is maintained in the furnace tube. As the study was carried out, we noticed that there is no significant difference on growth results no matter the gate valve is open or closed during this step. In order to reduce the complexity of the recipe and avoid potential mistakes from operation, the gate vale was then kept open during the entire CVD process. Some of the experiments awere carried out with the gate valve closed in this step, while the rest were carried out with the gate valve kept open. The operation of the gate valve for each group of experiments will be specified in the next section.

Step 6: Two minutes after the gate valve is closed, the flow into the furnace is changed to H_2 (100 sccm) and He (400 sccm). One minute after that, C_2H_4 (100 sccm) is added. This flow is maintained for a further 7 minutes before proceeding to the nest step.

Step 7: The gate valve is opened and the transfer arm is used to insert the sample (to 7 cm downstream from the control thermocouple). This configuration is maintained for the desired growth duration (from 10 seconds to 30 minutes).

Step 8: Upon completion of the growth duration, the furnace cover is lifted quickly, and the transfer arm is used to move the sample into the load lock position, outside the heated region of furnace. This ensures the sample cools rapidly, while the same gas flow is maintained for an additional 5 minutes.

Step 9: The flow is switched to He only (1000 sccm); the load-lock is opened and the sample is removed after it has cooled to below 100 ℃.

After repeated synthesis experiments a dark residue of carbonaceous material is found within the quartz tube. To prevent accumulated contamination this carbon material is removed between each experiment. This is carried out via oxidation at 875 ℃ for 30 minutes by flowing air through the tube (100 sccm, extra dry air, Cryogenic Gases).

Control experiments were also performed using a reference CVD method, wherein the samples are not removed from the hot zone of the furnace between anneal and growth stages. Specifically this procedure matches step 1-3 and the first 19 minutes of step 4 of the decoupled procedure. However for the last minute of step 4, gas flow is changed to He (400

sccm) and H_2 (100 sccm), then one minute later of C_2H_4 (100 sccm) is added to the stream for 10 minutes. Upon completion of CNT growth the furnace cover is quickly lifted while sample remains at the growth spot. The same gas flow is maintained for another 5 minutes and then changed to He (1000 sccm) for a further 5 minutes until such time that the sample is removed for analysis.

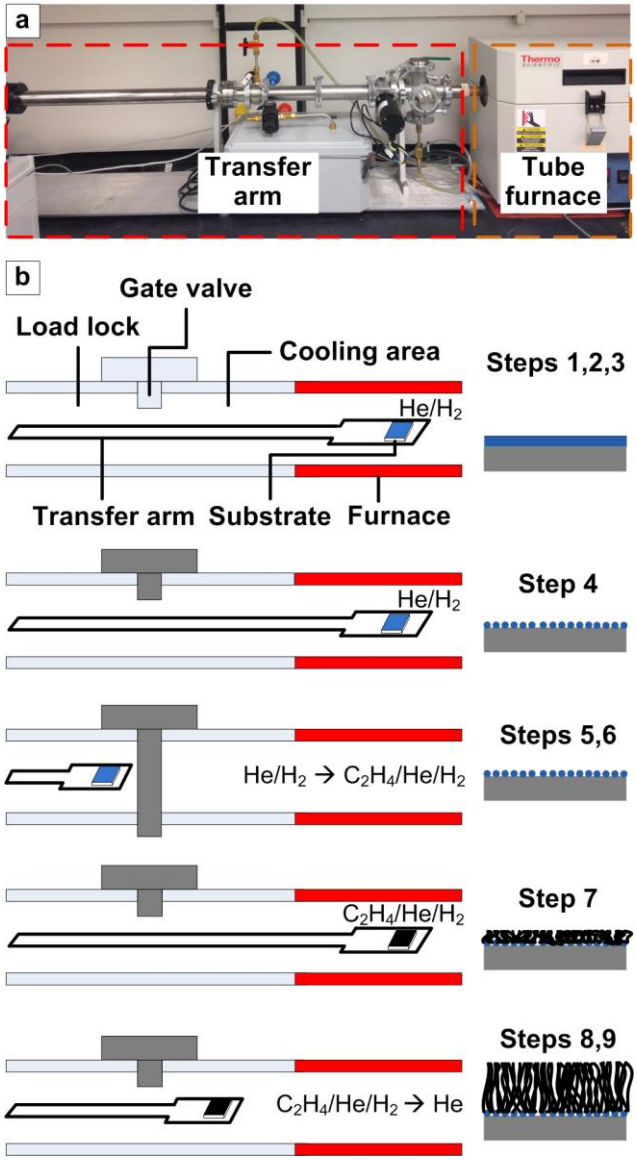

Figure 3.1 System and method for decoupled CNT synthesis: (a), system with magnetically coupled transfer arm downstream of the tube furnace. (b), schematic sequence of process steps. The transfer arm moves inward from left to right and is isolated from the furnace by a gate valve.

3.2.3. Control of transient moisture level

Experiments are also performed with varies of moisture levels in the CVD system. Four conditions are referred in this study: (I) humid condition, (II) dry condition, (III)

H_2O-assisted dry condition and (IV) bubbler controlled condition. The gate valve is closed during step 5 and then opened in step 7 for case I, while the gate valve is always kept open during the entire CVD process for case II, III and IV. Under the humid condition, the moisture level entering the CVD system was found to range from 50-250 ppm and was established following the routine outlined in Section 3.2.2, with a hydrogen tank that had an average moisture level about 300-400 ppm. The dry condition (5-8 ppm, variation throughout a typical experiment) is achieved by the additional step of an overnight purge of He (100 sccm) through the furnace system prior to carrying out the routine outlined in Section 3.2.2, and results from these reactions are denoted as groups C and D. The H_2O assisted dry condition was achieved by replacing the normal He gas tank by calibrated He/H_2O source (A31 100 ppm H_2O in Helium, certified mixture, Cryogenic Gases). Results from this set are denoted as groups E and F, which hold a moisture concentration of 15-30 ppm during growth stage (step 7. Section 3.2.2).

Because these experiments were carried out with 500-600 sccm total gas flow, compared to the 1000-5000 sccm operation condition for the hygrometer, the response of moisture reading may be slower than the actual evolution of moisture content in the reaction (As mentioned in Chapter 2). The moisture record during growth is 23-30 ppm, but I suggest the actual moisture concentration during growth could be greater. The steady state moisture concentration was settled to 60-70 ppm after 90 minutes of continuous purging at growth condition.

In order to provide better control of moisture concentration during the CVD process, a water bubbler assisted moisture control module is integrated to the CVD system at the end of this study (introduced in Chapter 2). With the help of the moisture control module, the concentration of moisture inside the CVD system can be adjusted from a few tens of ppm to about 900 ppm. Under the bubbler controlled condition, step 3 is take off from the decoupled recipe (Section 3.2.2), and moisture is added to the CVD system after the third minute of step 6 of the decoupled recipe. Instead of maintaining the flow for a further 7 minutes, the flow is maintained for a further 17 minutes.

3.2.4. Characterization

Mass of CNT forests are measured by a micro balance (Ohaus Discovery DV215CD). Substrate is measure before and after the CNT growth, and difference between these two

measurements is the mass of CNT forest. For each measurement the substrate is measured for three repeats, and the mass of the substrate is the average of the three repeats. There is usually only 0.01~0.02 μg difference among the three repeats. Scanning Electron Microscopy (SEM) images of the CNT forests are taken by using a Philips XL30 FEG SEM with a working distance of 10 mm and electron beam voltage of 10 kV. Transmission Electron Microscopy (TEM) images were taken using a JEOL 3011 at 300 kV and 113 mA. Atomic Force Microscopy (AFM) imaging is performed using a Bruker Dimension Icon in tapping mode. Small angle X-ray scattering is performed at the Cornell High Energy Synchrotron Source (CHESS, G1 line, wavelength 0.13nm) with a beam size of 100 μm in height to quantitatively map the alignment and diameter of CNTs with the CNT forests, as described in previous publications of our lab [55, 65-67].

3.3 Kinetics of decoupled CNT growth

The overarching goal of this study was to understand how the consistency of CNT forest growth was influenced by the stability of the moisture level in the CVD system, and to enable precise and repeatable control of the forest height using the rapid sample insertion. Using the transfer arm, the sample is manually inserted or withdrawn from the furnace within a duration of approximately 15-20 seconds.

In order to study the kinetics of CNT growth using the decoupled recipe, samples are produced using an identical annealing sequence (steps 1-6, Figure 3.1b), but with growth times ranging from 10 seconds up to 30 minutes. The starting time growth time (t = 0) is defined when the sample reaches the growth position and the motion of the transfer arm is stopped.

As shown in Figure 3.2, a CNT forest is first observed at 15 seconds (Figure 3.2a inset). The height of forest then increases nonlinearly with time during the first 60 seconds, and then the height kinetics become approximately linear until 20 minutes. Termination (i.e., cessation of height increase) occurs between 20 and 30 minutes, and the average forest height is 1.93 mm after 30 minutes growth.

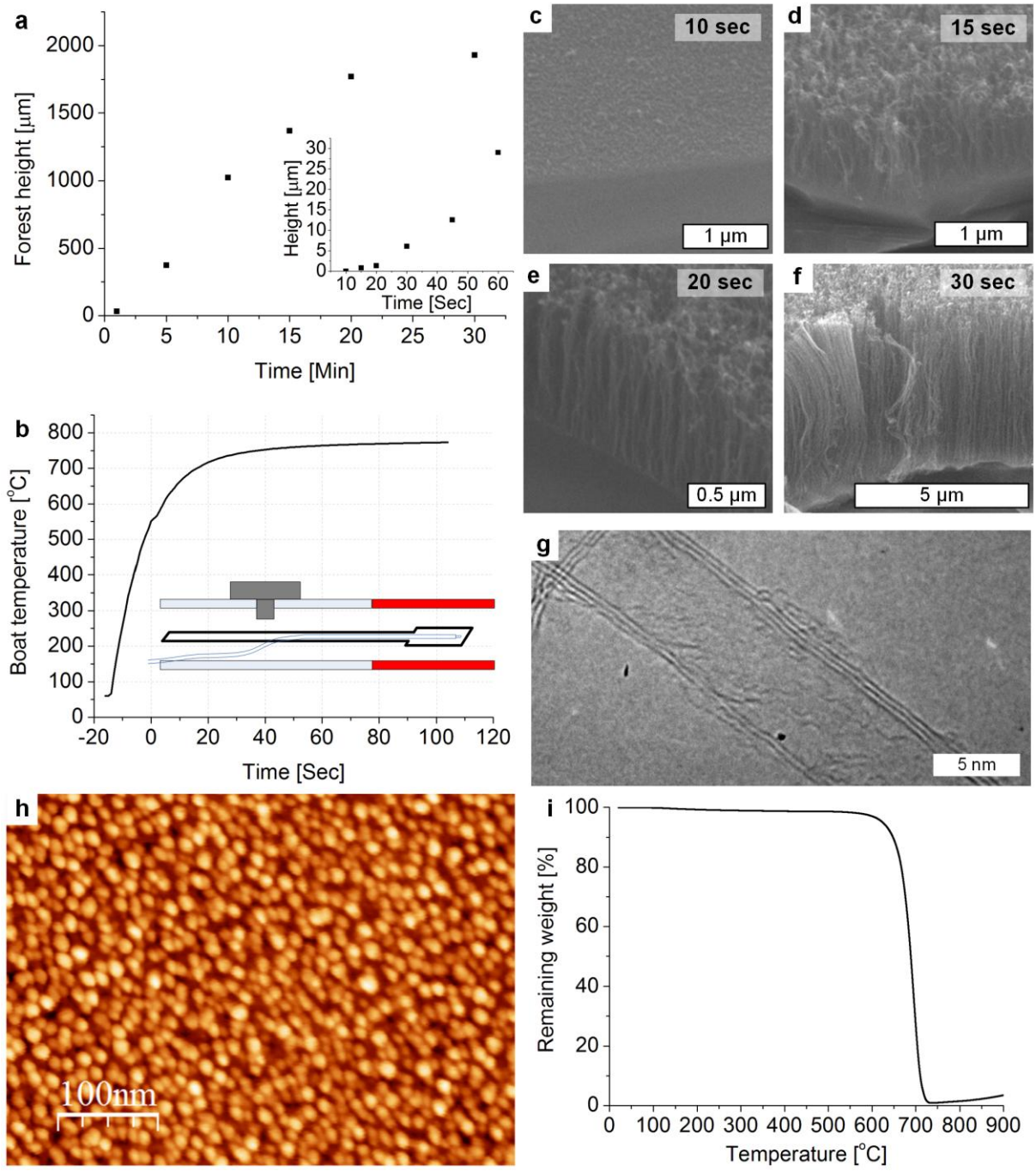

Figure 3.2 Height kinetics of CNT forest growth by rapid insertion to the stable hydrocarbon atmosphere after the decoupled catalyst annealing step. (a), Forest height versus time showing quasi-linear kinetics and abrupt termination at 20-30 minutes; inset showing nonlinear kinetics within the first minute of hydrocarbon exposure. (b), Temperature rises as the sample is inserted to the heated furnace, measured by attaching a thermocouple to the quartz boat. (c)-(f), SEM images of samples exposed to the hydrocarbon atmosphere for the durations noted. (g), TEM image of an individual CNT isolated from a CNT forest sample grown by decoupled recipe for 10 minutes. (h), AFM image obtained from surface of as annealed catalyst chip. (i), mass loss of a decouple recipe produced forest in air flow as temperature rises, generated by TGA.

I suggest the initial nonlinear CNT height kinetics is caused by the heating of the substrate during insertion to the furnace, as measured by a thermocouple attached to the quartz boat (Figure 3.2b). CNT growth begins while the substrate temperature is still increasing, yet after it has reached a minimum temperature for CNT nucleation. During the transfer (15-20 seconds), the sample temperature increases from 50 ℃ to 550 ℃. It takes a further 100 seconds for the boat temperature to reach 775 ℃ which is the set-point temperature of growth. Upon reaching threshold temperature (about 650~700 ℃) CNT nucleation occurs, at such time that a critical density of CNTs forms then a process of self organization of the CNTs ensues, thus leading to the onset of forest growth (Figure 3.2c&d). There is a gradual increase of alignment and density observed from Figure 3.2d to Figure 3.2e, which indicates the activation of catalyst particles may continue for a few seconds. The CNT forest starts to lift off as soon as the density of activated catalyst particles reaches the lower limit for aligned forest growth [33], and after this the density continues to increase thus causing further improved alignment.

TEM analysis of a typical decoupled sample gave an average CNT diameter of 8.1±0.5 nm (Figure 3.2g), which is comparable to the average height of catalyst particles determined by AFM (9.48±1.23 nm, Figure 3.2h). The AFM observation of well-formed catalyst particles after the annealing step also suggests that the annealing step, prior to withdrawal of the sample from the furnace (step 6 in Section 3.2.2), achieves complete reduction and de-wetting of the catalyst film. Thermo gravimetric analysis (TGA) of the samples produced by decoupled recipe suggests that 96% of the mass was lost between 600 ℃ and 735 ℃ (Figure 3.2i). Because an oxidation temperature greater than 500 ℃ is always associated with purer, less defective CNT samples [68, 69], the 96% of mass loss above 600 ℃ indicates that CNT forests obtained from decoupled recipe are high purity CNTs.

A detailed record of temperature evolution during the entire CVD process with decoupled recipe is shown on Figure 3.3. Figure 3.3a shows the temperature measured at the substrate and at the center of the furnace along with the setting temperature, and it is clear that the temperature on the substrate is cooled down while the center of the furnace still remains at 775 ℃. Figure 3.3b shows the temperature of the substrate right after the anneal stage. It takes about 4-5 minutes for the substrate to cool down to room temperature. Figure 3.3c shows the temperature of the substrate right after the end of the growth stage. It drops down below 400 ℃ in less than 15 seconds after taken out from the heated region, which implies

the reaction is quenched rapidly, and the growth of forest is quickly halted. The termination of the reaction can be precisely controlled by the sample loading module.

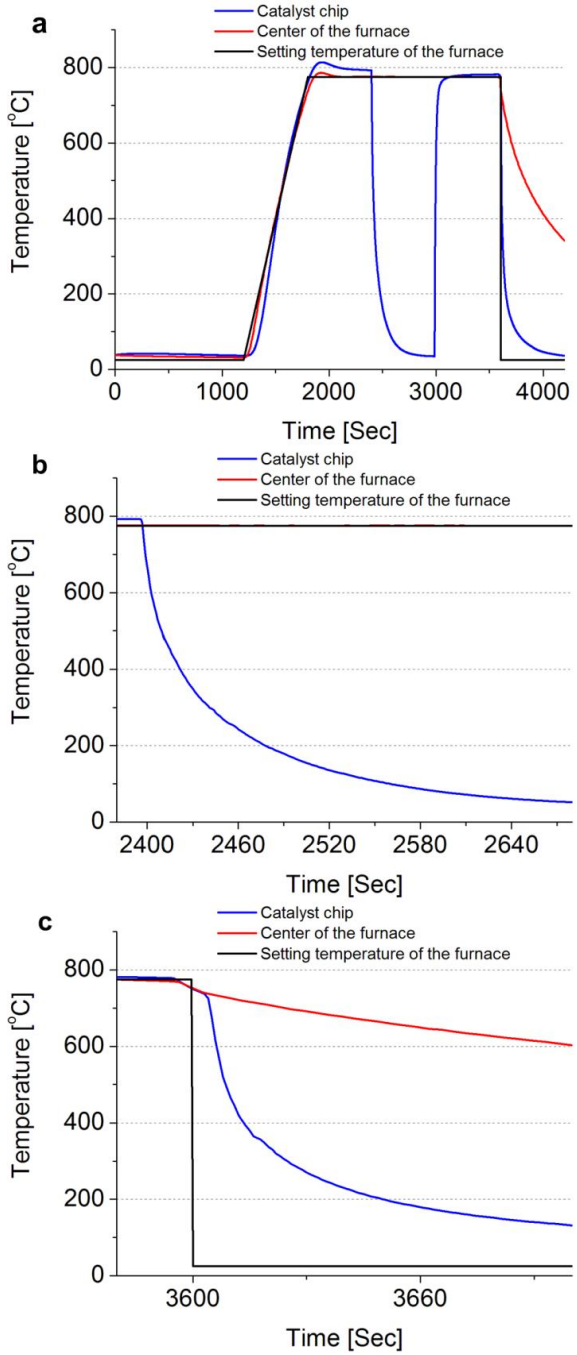

Figure 3.3 Evolution of temperature during the entire CVD process. Catalyst chip was placed at 7 cm downstream from the center of furnace during anneal and growth stages. (a), records of temperature evolution through the entire CVD process. (b), temperature of the substrate after annealing. (c), temperature of the substrate after growth.

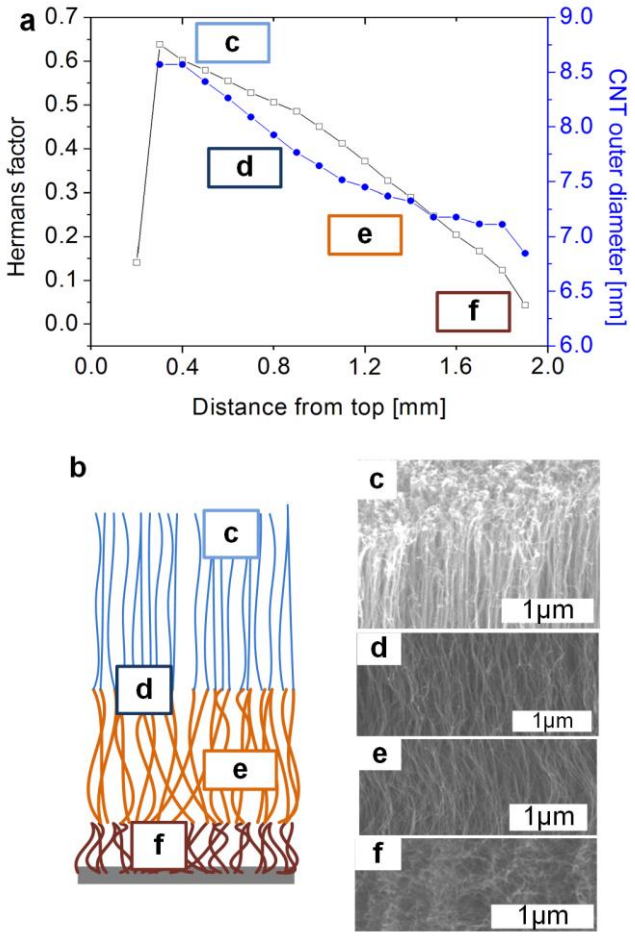

Figure 3.4 Alignment of CNT forest grown for 30 minutes by decouple recipe. (a), evolution of CNT diameter and forest alignment according to height. (b), schematic of forest alignment from top to bottom. (c)-(f), high resolution SEM images taken from the 30 minutes growth forest at different spots indicated in (b).

X-ray scattering is used to perform a quantitative analysis of the CNT alignment. The Hermans orientation parameter is calculated based on a mathematical model fitted to the scattering data from SAXS images taken at regular vertical positions from bottom to top of the forest [33, 65, 66, 70, 71]. This orientation factor (***f***) quantifies the average orientation of the ensemble of individual CNTs within the X-ray beam path, in relation to a reference direction [70]. So, f is a measure for the mean square cosine of the angle between the CNT direction and the reference direction (perpendicular to beam direction):

$$\boldsymbol{f} = \frac{1}{2}(3\langle\cos^2\phi\rangle - 1) \qquad \text{(Equation 3.1)}$$

And the mean square cosine of the angle can be calculated from the integration of the corresponding intensity distribution *I(ϕ)* of the X-ray scattering data about the beam's axis:

$$\langle\cos^2\phi\rangle = \frac{\int_0^{\frac{\pi}{2}}(I(\phi)\sin\phi\cos^2\phi)\mathrm{d}\phi}{\int_0^{\frac{\pi}{2}}(I(\phi)\sin\phi)\mathrm{d}\phi} \qquad \text{(Equation 3.2)}$$

Data is acquired at specific height intervals and the Herman factor plotted accordingly and shown in Figure 3.4a. The Herman factor can be seen to decrease steadily from top to bottom of the forest, suggesting CNTs are losing alignment as the growth going on. As a result, the part of the CNTs that formed at the end of the growth are less aligned, and more tangled, as compared to those that are formed during an earlier stage of growth. It is noticed that the crust has low Hermans factor (0.15), which agreed with the SEM image of tangled crust shown in Figure 3.4c. However, precise quantification of that is not possible because the top of the forest is not perfectly flat, and the crust is much thinner than the beam spot height. Figure 3.4b shows a schematic of the evolution of forest alignment across the full height of the 30 minute grown sample (not including the top crust), and the decline of CNT alignment with continued growth is also be proven by the SEM images in Figure 3.4c-f. Similar as described in the collective mechanism of CNT forest growth [33], I suggest the lost of alignment observed from forest produced by decoupled recipe can also be caused by deactivation of catalyst particles and density decrease as growth going on.

3.4 Run-to-run consistency and forest alignment improved by decouple recipe

To assess the consistency of repeated CNT growth experiments using the decoupled recipe, several samples are produced under identical conditions and compares to a control group obtained by a reference process (Section 3.2.2). 10 samples are produced using decoupled recipe and 6 samples are using reference process under identical conditions with 10 minutes of growth, and SEM is used to measure the height of forests. Results are shown as box plots in Figure 3.5a. Forest heights obtained from decoupled recipe reach an average of 1.02 mm which is 21% greater compared to forests obtained with reference process (0.85 mm) for the same growth time. The standard deviation of height for the decoupled recipe is 0.04 mm, which is 76% less than the standard deviation for reference process (0.17 mm). The coefficient of variance (standard deviation divided by average height) is only 4.0% with decoupled recipe, compared to 20% for reference forests.

X-ray scattering is also used to compare the CNT alignment between samples produced by the decoupled recipe and reference process. As shown in Figure 3.5b, all 8 samples are grown for 10 minutes and their alignment factor follow the same trend: the alignment first increased at the top of the forest, then decreased approaching the bottom. The maximum orientation factor is always greater for decoupled recipe samples, and the rate of decay is lower. At the bottom of reference forests, alignment factor of two out of the four samples decreased below

0.1, which indicates growth of forest had self-terminated [33]. On the other hand, Herman's factors for decoupled samples are still above 0.45, which indicated the growth from decoupled recipe had not self-terminated yet at the end of the 10 minutes. This agrees with the kinetics we show in Figure 3.2a.

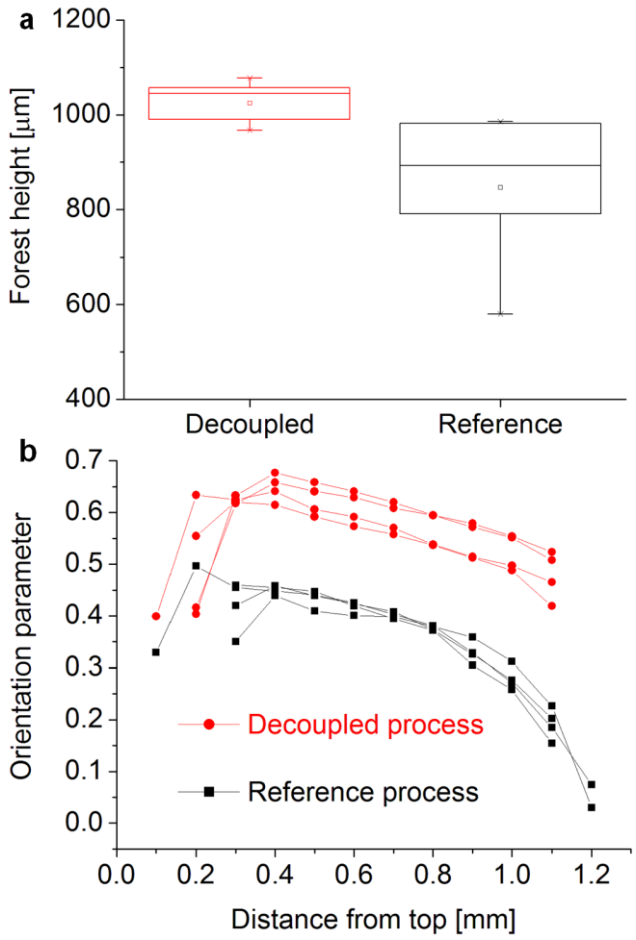

Figure 3.5 Comparison of height consistency and alignment variation between decoupled and reference recipe produced CNT forests. (a), Comparison of height variation two sample groups. All samples shown in this figure were exposed to the hydrocarbon atmosphere for 10 minutes. (b), spatial mapping of alignment (Hermans orientation factor) within CNT forests produced by decoupled process, compared to reference growth process.

Because the substrates from both decoupled recipe and reference recipe experienced the exact same anneal process, it is reasonable to consider the catalyst particle size and distribution are also the same. As a result, the status of substrate before hydrocarbon exposure is the same for both recipes. The lifetime of catalyst particles is improved from 10 minutes to about 20-30 minutes by only adding the decoupled step into the CVD process

3.5 Influence of moisture on growth consistency

To elucidate the reason for improved run-to-run consistency along with the greater alignment of CNTs using the decoupled recipe, the moisture content of the CVD system at each stage of the CVD process is measured and shown in Figure 3.6a (black curve). As introduced in Chapter 2, a hygrometer is installed in the CVD system and records the moisture concentration of gas stream before entering the tube furnace. A variation of moisture from 50 ppm to 250 ppm was observed during the entire synthesis process. This fluctuation was caused by a few reasons: first, moisture level from each gas tank (Helium, Hydrogen and Ethylene) could be different. It is used to happen in our lab that a Hydrogen tank that contained moisture level greater than 300ppm was used during this part of study; second, moisture residue in different gas delivery lines would also be different due to their own daily use rate. As a result from these two facts, it takes time to reach steady state when all gases are mixed. This record of moisture variation shows that the water vapor content during anneal stage (step 4) is very stable due to the 30 minute purge prior to the anneal (Figure 3.6b). But then when C_2H_4 is added to the reactor, there is a significant change of moisture content from about 220 ppm to 100 ppm during the decoupled step (step 5&6). By withdrawing the sample and allowing the moisture transient to settle, the moisture level is much more stable during CNT growth (80-95 ppm). Figure 3.6c also shows the much larger fluctuation of moisture during a particular growth stage for the reference process compared with decoupled recipe.

From the findings above, it can be concluded that decoupling the annealing and growth stages by removal of the substrate from the CVD chamber during atmospheric pressure synthesis introduces two important improvements to forest synthesis: (1), quick introduction of substrate to hydrocarbon rich and chemically stable atmosphere. (2), skipping of the transience caused by switching atmosphere from anneal to growth. From the previous study in Section 3.4, the influences from these two improvements are coupled. I next performed a comparison study to understand the effect from moisture content and the decoupled step separately. From previous work [39] of my colleges, continuous purging of system under a small flow of inert gas while at rest is suggested in order to reduce the variability in CNT growth. Furthermore, monitored and recorded by the hygrometer, gas streams come from He, H_2 and C_2H_4 tanks are confirmed to have baseline moisture concentrations all below 10 ppm. With 100 sccm of He continuously purging in the system, it's now able to maintain a moisture level within growth system to be always below 10 ppm during the entire synthesis process. From this baseline, with the help of a calibrated Helium tank that holds 100 ppm

moisture, a series of experiments is carried out which is listed as “Control of transient moisture level” in Section 3.2.3.

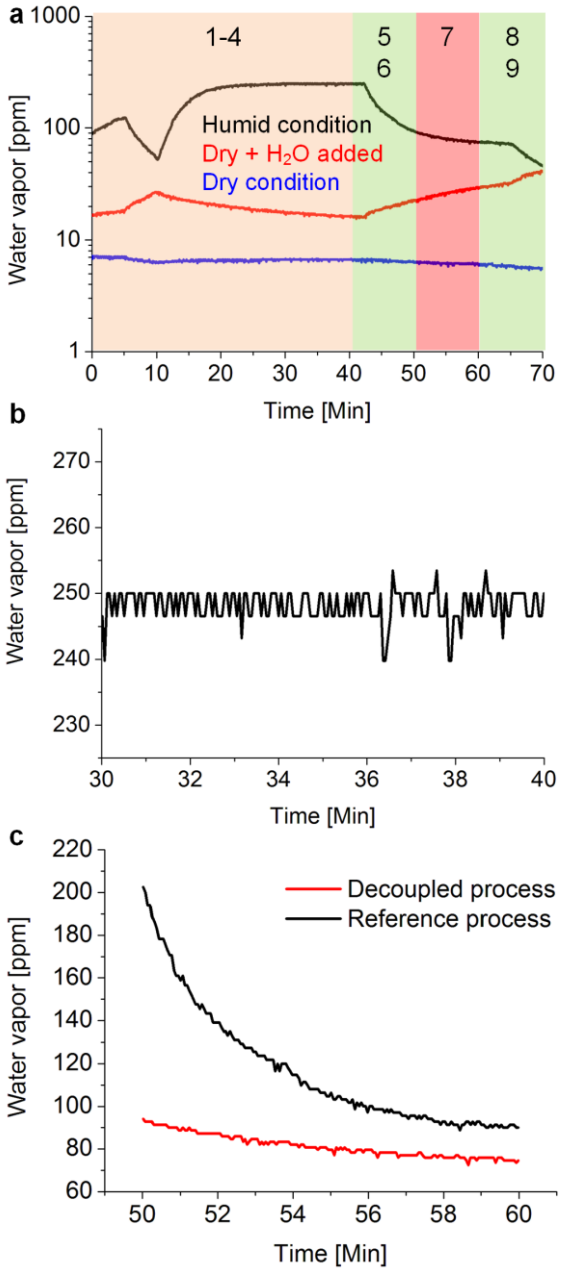

Figure 3.6 Moisture transients measured within the CVD system. (a), Moisture levels versus process time, measured at the inlet of the tube furnace, for the conditions noted and described in the text. The numbers correspond to the stages of the decoupled recipe, referring to the sample placement, as in Fig. 3.1. (b), Close view of the stable moisture level between 30-40 minutes, at which time the annealing step (step 4, Figure 3.1) is performed by the decoupled process. (c), Comparison of moisture transients during the CNT growth step (hydrocarbon exposure, step 7).

A detailed list of proposed experiments is shown on Table 3.1, along previous completed experiments discussed in Section 3.4. The moisture condition described in Section 3.4 is

denoted as the humid condition (Case I), and the groups of experiments obtained by the decoupled recipe and reference process to be group A and group B, respectively. Then experiments are proposed to be carried out in dry condition, which the fluctuation of moisture during a typical experiment is only from 5 to 8 ppm (Case II). In case II there is also a group for decoupled recipe (Group C) and a group for reference recipe (Group D). By comparing the CNT forest height and consistency between Case I and Case II, it should be able to distinguish the contribution from quick introduction of substrate and less fluctuation of moisture during growth stage.

In order to understand the importance of controlled amount of moisture during decoupled synthesis, Case III the H_2O assisted dry condition is also added to the study. In this study the regular Helium source (pre-purified Helium, less then10ppm H_2O) is replaced by a calibrated He-H_2O tank (100ppm H_2O). According to the recipe, the calibrated He-H_2O tank provides moisture reading of 23-30 ppm during growth stage for decoupled recipe (Group E) and 15-22 ppm for reference recipe (Group F). The results are listed in Table 3.2.

Table 3.1 Experiment design: study of CNT forest growth with decoupled recipe and reference recipe at different moisture levels

Case	Group	Recipe	Moisture (anneal/ growth) [ppm]	Purpose
I:	A	Decoupled	200-220 / 80-95	Initial results with huge fluctuation
Humid condition	B	Reference	200-220 / 100-220	of moisture during CVD process
II:	C	Decoupled	5-8 / 5-8	Study effect of the decoupled step
Dry condition	D	Reference	5-8 / 5-8	with low and consistent humidity
III: H_2O assisted	E	Decoupled	17-22 / 23-30	Study the effect of controlled
dry condition	F	Reference	17-22 / 15-22	moisture input on decoupled recipe

Table 3.2 Height, mass and volumetric density of forests produced by decoupled and reference process under different moisture conditions

Group	Moisture (ppm)	Recipe	Height(μm)	CV	Mass(μg)	CV	Density (μg/mm^3)	CV
A (I)	80-95	Decoupled	$1.02*10^3$	0.04	-	-	-	-
B (I)	100-220	Reference	$0.84*10^3$	0.20	-	-	-	-
C (II)	5-8	Decoupled	$7.9*10^2$	0.06	402	0.07	15.9	0.10
D (II)	5-8	Reference	$5.9*10^2$	0.05	243	0.07	12.9	0.09
E (III)	23-30	Decoupled	$1.04*10^3$	0.05	633	0.06	19.0	0.04

F (III)	15-22	Reference	$0.64*10^3$	0.11	345	0.15	16.9	0.11

Height, mass and density of the CNT forests obtained from decoupled recipe and reference process are presented in Figure 3.7, and from this figure the great advantage of decoupled recipe can be observed compares to reference process. In Figure 3.7a, the height of CNT forests from all the six groups are plotted. It's clear that for each pair of decoupled recipe and reference process under the same moisture level, the decoupled recipe would provide an overall taller CNT forest. A similar trend can also be found for mass and density of forests: samples obtained by decoupled recipe are always greater than reference recipe under the same humidity conditions.

For Case II, although the height, mass and density from decoupled recipe are all greater than reference recipe, the coefficient of variance stays the same for both Group C and Group D. This result suggests that once a consistent control of moisture at low level (<10 ppm) is guaranteed, the consistency between decoupled recipe and reference recipe are almost the same. Since there is still improvement of all these three properties by decoupled recipe, I conclude this improvement should be contributed by the rapid introduction of substrate to stable hydrocarbon atmosphere.

Furthermore, besides Case I, Case III also states the improvement of consistency is due to less fluctuation of moisture during the growth stage achieved by the decoupled step. Although the reading of hygrometer showed similar degree of moisture fluctuation of moisture during growth for decoupled recipe (23-30 ppm) and reference recipe (15-22 ppm), the actual fluctuation inside the furnace may not be the same. As mentioned in Section 3.2.3, due to the intrinsic property of Cermet-II hydrometer, the reading of moisture may respond slower than the actual trend of moisture evolution in furnace. And since the reference recipe missed the decoupled step, the substrates processed with decoupled recipe should experience less transit of moisture during growth stage, compared to reference recipe.

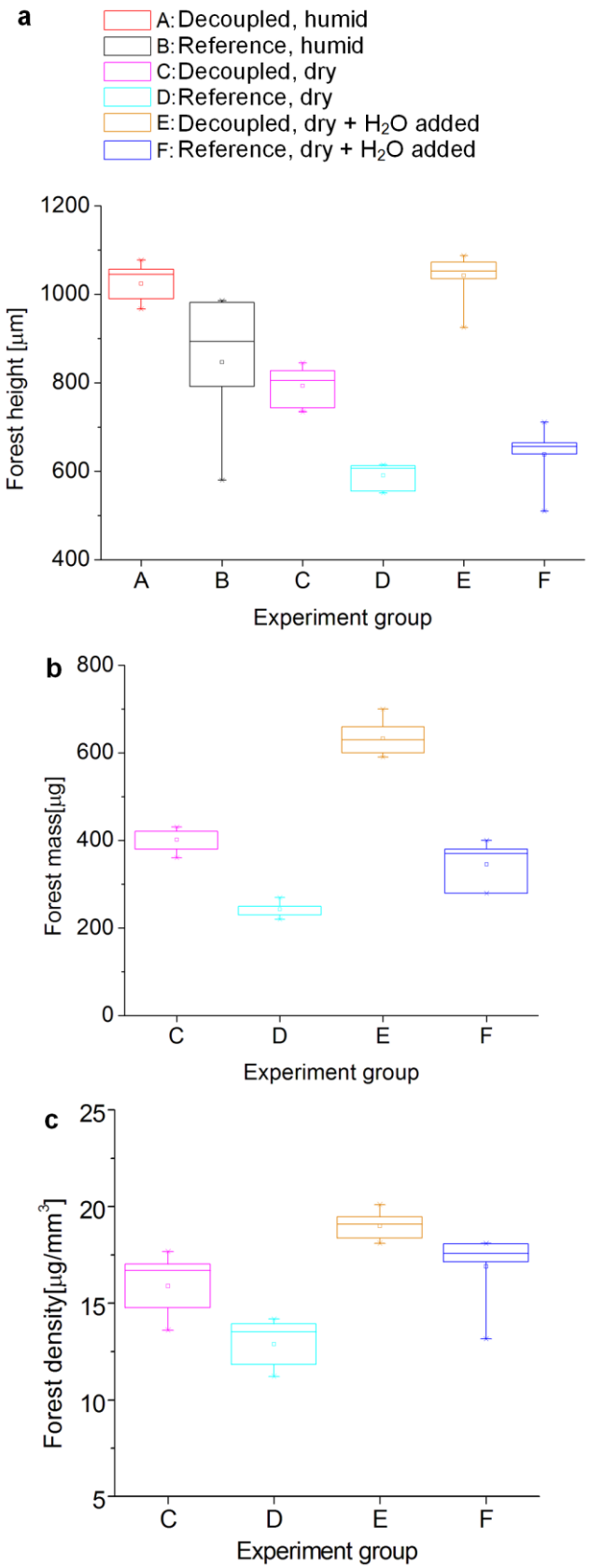

Figure 3.7 Statistical comparison of CNT forest under different moisture control conditions described in the text: (a) height, (b) mass and (c) density

3.6 Influence of moisture during growth stage

Study from previous sections has elucidated the influence of moisture on growth consistency and growth kinetics, but the method used to generate moisture concentrations was limited. It could only prepare moisture concentration at very few non-adjustable levels, but not were able to provide a quantitative control of moisture levels within a certain range. In order to give better control of moisture concentration during the CVD process, a water bubbler assisted moisture control module is established and integrated to the CVD system (section 2.2.3). A series of growth are carried out at different moisture levels, and the results are shown on Figure 3.8. Figure 3.8a shows evolution of moisture level during the entire CVD process. All samples carried out in this section are annealed for 10 minutes with a moisture concentration less than 15 ppm, while they are grown at four different moisture levels: less than 15 ppm, at 40 ppm, at 120 ppm and at 450 ppm (and the growth time varied from 3 minutes to 40 minutes as shown on Figure 3.8b). The group generated with moisture level less than 15 ppm is the same condition as the "baseline" (dry condition) described in section 3.2.3. Due to the batch to batch fluctuation of moisture concentration from the gas tanks, the baseline moisture level can vary from 5~15 ppm. The record of moisture demonstrates that quantitative and decoupled control of moisture concentration between annealing stage and growth stage can be achieved by the new CVD system we designed.

Since all samples are annealed at the exactly same condition, the difference on growth results can be all contributed to growth stage. The kinetics of forest height shown on Figure 3.8b states there are two distinguished groups of results: forests produced with dry condition (<15 ppm) and forest produced with moisture assisted condition (40, 120 and 450 ppm). Growths from both groups are terminated at about 20 minutes, but the growth rates of forest height are different. Linear regression of forest height from 3 minutes to 20 minutes shows the growth rate is 52.3 μm/min for dry condition, and it is 67.8 μm/min, 73.6 μm/min and 77.7 μm/min for 40, 120 and 450 ppm, respectively. A 29.6% improvement of growth rate is observed from baseline condition to 40 ppm, but the improvements from 40 to 120 ppm and 120 to 450 ppm are only 8.6% and 5.6%, respectively.

The results claims that the improvement of CNT production due to the presence of moisture during growth stage is much more significant when moisture concentration is increased from a few ppm to a few tens of ppm, rather than increasing the moisture level from a few tens of ppm to hundreds of ppm. This results is different from previous study reported by Futaba et

al [72], which provided the same moisture concentration during the entire CVD process. Futaba et al stated the forest production can be improved when increasing moisture level from 25 ppm to 150 ppm, while the growth of forests will be worse if the moisture level is further increased from 200 ppm to 300 ppm. Combined with study from Oliver et al [39] that reported a decrease of catalyst particle density caused by increased moisture concentration during anneal stage, I suggest the conflict between our result and Futaba's result is due to the different moisture input during anneal stage.

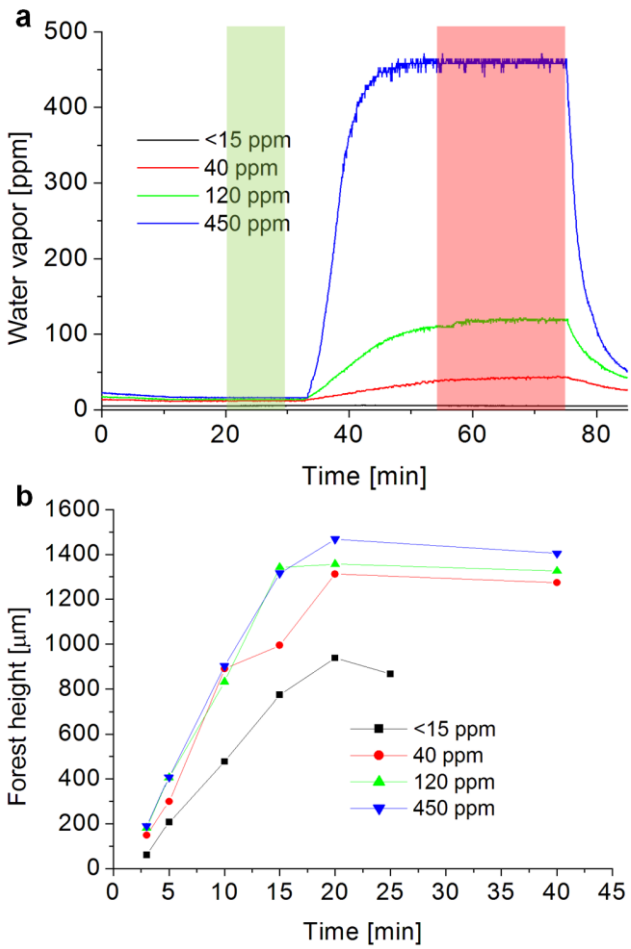

Figure 3.8 Forest obtained from decoupled recipe with different moisture input during growth stage. (a), Records of moisture concentration during the entire CVD process. The four trials demonstrated here were all produced with 20 minutes growth time. The regions coated with green and red colors indicate moisture levels during anneal and growth stages, respectively. (b), kinetics of height of CNT forests produced with moisture levels less than 15 ppm, at 40 ppm, at 120 ppm and at 450 ppm during growth stage.

3.7 Discussion

Operationally, when the sample is treated in a decoupled fashion, it is exposed to a more

stable atmosphere during the critical stage of CNT nucleation.

From Case I through Case III, decoupled recipe always shows greater height and mass compare to reference recipe in the same case regardless of moisture input in the system. The common feature among forests produced by decoupled recipe in all three cases is the sudden exposure of substrate hydrocarbon atmosphere. Substrate processed with reference recipe has to stay in furnace and experience the concentration of hydrocarbon and hydrocarbon precursor to rise up from zero to steady state concentration, while decoupled recipe suddenly introduces substrate to the rich and stable atmosphere of hydrocarbon precursor. As mentioned in Section 3.4, Herman's factor shows a better alignment is achieved by decoupled recipe at the beginning of growth compare to reference recipe in Case I. The better alignment at the beginning of growth suggests more CNTs are grown compared to reference recipe. And calculated from Case II&III, which height and mass are recorded for all samples, the density of the CNT forest produced by the decoupled recipe is always greater compare to reference recipe. Since the anneal process for decoupled recipe and reference recipe is identical, the greater number density of CNTs from decoupled recipe clarifies higher activation rate of catalyst particles. So I can conclude that the sudden exposure of substrate to hydrocarbon-rich atmosphere can lead to greater activation rate of catalyst particles which increases the alignment of the CNTs within the forest.

On the other hand, moisture is also critical for forest synthesis. Previous research from Stadermann et al [60] showed that water concentration greater than 2500 ppm leads to a decrease of CNT growth rate, and they suggest this decrease is due to the etching of graphitic carbon by water. Their optimal result was obtained at 1/330 for the water/ethylene ratio, and height of forest was about 300-400 μm after 10 minutes growth. Futaba et al [72] had also reported the influence of moisture concentration on forest height, but they suggest an optimal water/ethylene ratio of 1/1000 for their SWNT forests (800 μm for 10 minutes growth), while moisture input was constant during the whole CVD process. Wyss et al. [63] integrated gas purifiers to their growth system and eliminated impurities such as moisture, acetone and O_2. When removing moisture to the sub-ppb level, they showed that high mobility and coarsening of Fe catalyst particles caused no growth. In my study, the tallest and most consistent results were achieved by introduce a small amount of moisture compare to the dry baseline growth, representing a water/ethylene ratio less than 0.06/1000. With the present of He-H_2O tank, a water/ethylene ratio about 0.2/1000 was obtained according to the reading from hygrometer

during growth. Due to the slow response of hygrometer (mentioned in 3.2.3) I suggest the actual water/ethylene ratio during my best condition could be as high as 0.4/1000.

The consistency of forest production is also improved by decoupled recipe when there is fluctuation of moisture during growth stage. Looking at the forest height from all six groups, decoupled recipe always keeps the coefficient of variance of height around 0.05 (0.04, 0.06, and 0.05 for group A, C, and E), while corresponding data for group B,D,F are 0.20, 0.05 and 0.11. Decoupled recipe holds at the same level of variance regardless of moisture conditions, which suggests influence of inconsistency caused by fluctuation of moisture from anneal to growth is almost eliminated by decoupled recipe. The remaining 5% of variance in height from decoupled recipe could due to several reasons: the consistency of manual furnace operation of the transfer arm (i.e., sample placement, insertion rate), systematic error from the MFC, difference of catalyst thickness (which is about 5% from center to edge for typical 4" wafer used in this study), etc. I also noticed there is visible carbon black gradually deposited and cumulated on the inner wall of load lock chamber in the transfer arm system after several tens of experiments, and this effect could also be a potential source causes fluctuation in future growth.

Therefore, the decoupled recipe could be further improved with fully automatic operating process, as demonstrated by my college Ryan Oliver [73].One other source of the inconsistency could be the trace amount of oxygen-containing species introduced from the batches of gas tanks, surrounding atmosphere introduced by samples loading between experiments, remaining air captured in the load lock chamber and also hollow body of quartz arm (Chapter 2, Section 2.2).

3.8 Conclusion

In this chapter, it is first demonstrated that the CNT forests produced by decoupled recipe have better alignment (Herman's factor: 0.62-0.68) compares to forests produced by reference process (Herman factor 0.44-0.50) when grown using water vapor in the range 50-250 ppm throughout the whole synthesis process. Furthermore, by studying the growth performance at controlled moisture levels (5-8 ppm and 15-30 ppm) by decoupled recipe and reference recipe, the improvement in consistency is stated to be attributed to the stable moisture level during growth, whereas the improvement in CNT forest height is attributed to the presence of a richer and stable hydrocarbon precursor atmosphere upon the introduction of catalyst.

The decoupled recipe not only provides improved production of CNT forest, but also enables more freedom to study the growth mechanisms. Physical separation of anneal and growth stages would allow researcher to study impact of certain input on each stage individually without interaction with the other one. With the moisture control module integrated into the CVD system, we first studied the influence of moisture during growth stage excluding its influence from anneal stage, and showed the improvement of CNT production due moisture during growth stage is shown to be much more significant at a few tens of ppm, compares to hundreds of ppm.

CHAPTER 4
IMPROVEMENT OF CNT FOREST DENSITY BY CARBON-ASSISTED CNT NUCLEATION AND MOISTURE-CONTROLLED CNT GROWTH

This chapter describes a novel synthesis method for high density CNT forests by increased activation of catalyst particles. First, a study of the role of moisture during different phases of hydrocarbon exposure is presented, and the importance of moisture at the onset of hydrocarbon exposure is revealed. Then, it is shown that exposure of the catalyst to a small amount of carbon ('preloading') prior to introduction of the nominal hydrocarbon source for CNT growth significantly increases the nucleation density of CNTs from the catalyst population. In turn, this enables CNT forest synthesis with density up to 212 μg/mm^3. The density of CNT forest produced with preloading of carbon is always 3~4 times as much as that for the forests produced without preloading of carbon. Finally, a series of characterization is carried out to demonstrate the preloading of carbon formed a layer of graphitic structure on catalyst particles before growth started, which may help activate catalyst particles to achieve higher density CNT forests.

4.1 Impact of moisture during growth stage

4.1.1 Benchmark of previous work

Many studies have reported that synthesis of CNT forests is very sensitive to the presence of moisture during hydrocarbon exposure (i.e., the 'growth stage'). Hata et al [41] reported using H_2O as a weak oxidizer in order to selectively remove amorphous carbon without damaging the SWNTs at growth temperature, and as a result the water enhanced lifetime of the catalyst and made SWNTs grow easily from lithographically patterned catalyst islands. Later on, the same group (led by Futaba et al) [72] published how the kinetics of water assisted aligned forest growth at atmosphere pressure with moisture concentration of 50-290 ppm, and found the best performance was obtained at 140 ppm. They reported the maximum height of forest were obtained with a water/ethylene ratio around 1/1000. Then Yamada et al [38] characterized the chemistry on catalyst surface using elemental mapping and suggested

the presence of water helped remove carbon coating and revive catalyst activity.

Moreover, Stadermann et al [60] surveyed how CNT growth was influenced by water concentration up to 6000 ppm and reaction pressure from 100 to 1000 Torr. They stated the tallest CNT forest obtained within the stated range was observed at approximately 750 Torr. Whereas, growth rate decreases if water concentration exceeds 2500 ppm. Stadermann realized their optimal moisture concentration for forest height is about 1/330, which is about three times as high as reported by Futaba et al. Hasegawa et al [61, 64] also reported millimeter-tall CNT forests achieved with and without presence of water, and suggested that water prolonged the lifetime of the catalyst, but at the same time it also deactivated small catalyst particles and degraded the quality of SWNTs. Then Wyss et al [63] turned to seek the importance of moisture when the synthesis environment was desiccated down to ppb level of moisture/Oxygen. They stated the extinction of water in synthesis environment would leave the surface of catalyst particles in a metallic state (as opposed to as metal oxide), this increased the mobility of catalyst particles and caused coarsening during annealing at high temperature, and finally resulted in no CNT growth.

Previous studies had studied the impact of moisture on CNT growth from different aspects, but the reported results were different from researcher to researcher, some of the conclusions were even contradicting of each other. For example, the optimal moisture concentration for forest height was reported as 1/1000 by Futaba et al [72], while Stadermann et al [60] suggested it was 1/330. Optimal lifetime of catalyst was achieved with a moisture concentration of 140 ppm by Futaba [72], while In et al [62] reported a decay of catalyst lifetime for moisture concentration greater than 10 ppm. Most of the literatures listed above [38, 41, 60-62, 64, 72] didn't specify whether the impact of water was contributed from catalyst annealing stage or CNT growth stage. But Oliver et al [39] reported increased concentration of moisture from a few tens of ppm up to one thousand ppm would lead to a density decay of catalyst particles during anneal. The contradictions from all previous works indicated that the role of moisture during the entire CVD process could be very complicated, and the final impact of moisture may be an integration of individual effects from each stage. Furthermore, Bedewy et al [33] showed that CNT forest growth during hydrocarbon exposure can be divided into four phases: 1) nucleation and self-assembly, 2) steady growth, 3) density decay, and 4) termination. Thus, it is necessary to develop a decoupled understanding of impact of moisture on each different phase during the growth process. The motivation of

research in Section 4.1 is to reveal the specific function of water during different growth phases. Utilizing the moisture control module from the integrated CVD system (Section 2.2.3), the moisture level can be varied and the sample can be introduced to this stable moisture level. The moisture concentration can also be varied during different phases in growth stage without changing the ratio of growth gases (He, H_2 and C_2H_4), so that the role of moisture during different phases can also be studied.

4.1.2 Method: moisture assisted recipe

All samples produced in Section 4.1 follow the same recipe called "Moisture Assisted Recipe" (Figure 4.1):

Step 1: The catalyst coated substrate is placed onto the quartz boat and transferred to the load lock chamber in transfer arm system. Then the whole system is sealed and pumped down with a vacuum pump (DS 302, Varian). Pump is turned off after reading of pressure in the system is below 1 Torr, and the system is filled with Helium (99.999% Cryogenic Gases). The pump-fill is repeated for two more cycles.

Step 2: The furnace is then heated to 775 ℃ over 10 minutes with He (100 sccm, 99.999% Cryogenic Gases) and H_2 (400 sccm, 99.99%, Cryogenic Gases).

Step 3: The flow is held the same as described in step 2 for another 5 minutes to avoid overshoot of temperature after ramping up.

Step 4: The transfer arm is used to send the sample from the load lock chamber to the sweet spot of the furnace (7 cm from center of furnace, downstream). The flow is still held the same as described in the previous step for 10 minutes. During this stage, the catalyst film is chemically reduced and dewets into nanoparticles.

Step 5: The transfer arm is again used to move the sample from the sweet spot of the furnace to the load lock chamber. The same flow from step 4 is held for another 2 minutes in order to let the hot sample cool down in the same atmosphere as it was annealed.

Step 6: The flow is then switched to 500 sccm He and 100 sccm H_2 for 16 minutes. After that, flow of He is decreased to 400 sccm and another 100 sccm of C_2H_4 (150 sccm, 99.5%, Cryogenic Gases) is introduced into system and held for an additional 7 minutes. From the beginning of this step, if the growth is designed to start with moisture assisted condition, 14 sccm out of the total He flow will be driven through the water bubbler and provide approximately 370 ppm moisture to the system.

Step 7: Sample is sent to the reaction spot again by the transfer arm. The flow is held the same as in step 6 for 3 minutes. This step covers the activation/self organization phase of

growth, and also the beginning of steady growth.

Step 8: The same flow is held for another 2 to 17 minutes, according to the desired recipe. Also, the 14 sccm out of the total He flow can be again routed through water bubbler, or not, at the beginning of this step. Step 8 covers growth phases including steady state, density decay and termination.

Step 9: Upon completion of the growth duration, the furnace cover is lifted quickly, and the transfer arm is used to move the sample out of the furnace. This ensures the sample cools rapidly, while the same gas flow is maintained for an additional 5 minutes. Flow through the water bubbler will be turned off at the beginning of this step if there were any.

Step 10: The flow is switched to He only (1000 sccm). The system is unsealed and the sample is removed after it has cooled below 100 ℃.

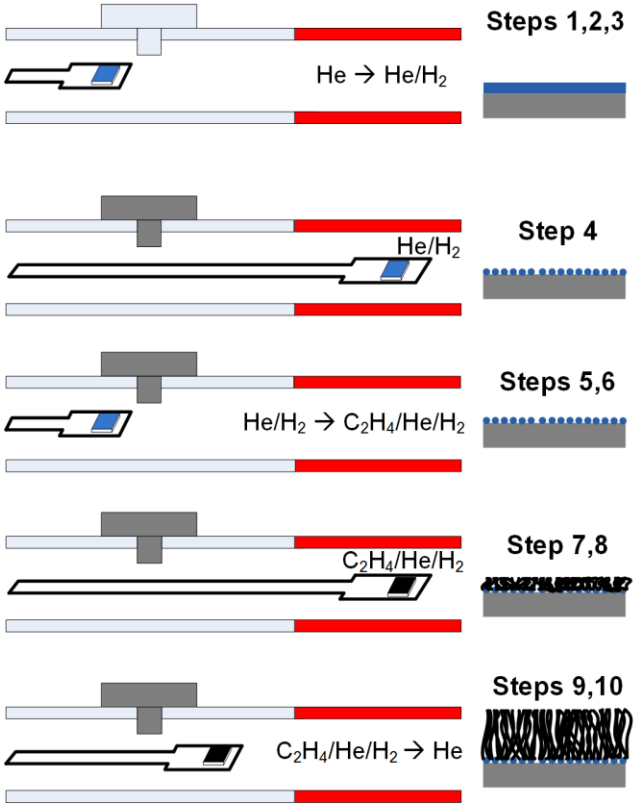

Figure 4.1 Schematic sequences of moisture assisted recipe. The transfer arm moves inward from left to right and is sitting at the downstream direction of furnace.

As mentioned above in step 6 and 7, according to the requirement of study, some samples are produced without the presence of moisture during these two steps. For the convenience of discussion, I call this modified recipe the “Baseline recipe”.

As mentioned in Chapter 3, to prevent contamination from batch to batch, oxidation is carried

out at elevated temperature (875 ℃) in the presence air flow (100 sccm, extra dry air, Cryogenic Gases), for a period of 30 minutes.

Catalyst samples used in Chapter 4 are prepared with the same recipe as introduced in Chapter 3.

4.1.3 Impact of moisture during activation/self organization phase

A series of experiments is designed to study the impact of moisture during different phases in growth stage, and the supply of moisture is shown in Table 4.1. For all the 4 samples in this section, step 8 is chosen to be 7 minutes, so the duration of the entire growth stage was 10 minutes.

Table 4.1 Experiment design: revealing the role of moisture during different phases of growth stage.

Supply of moisture		Sample			
		A	B	C	D
Step	7	No	No	Yes	Yes
	8	No	Yes	No	Yes

In Figure 4.2a a typical record of moisture evolution during the entire synthesis process is shown. This is a record for sample D, which is annealed with no moisture supply (step 4, 15-25 minutes, shown in Figure 4.2b) and grown with about 375 ppm of moisture from the start to the end of hydrocarbon exposure (step 7 and 8, 50-60 minutes, shown in Figure 4.2c). As mentioned in Chapter 3, due to the way of controlling moisture supply and the delay from hygrometer reading, it takes time for moisture concentration to rise up or drop down during the experiment. For all of these 4 samples compared in this section, the inputs of moisture during anneal are similar, as shown in Figure 4.2b. There is a few ppm of run-to-run difference during this stage, and I suggest this is due to the lag of reading from hygrometer, which can be affected by the final state from the previous run. For the moisture levels during growth stage (Figure 4.2c), significant change of moisture concentration can be observed from sample B and C a few seconds after the 53^{th} minute, which is the starting of step 8. It takes about 5 seconds for the digital MFCs to reach the new input levels, and then the

hygrometer would detect the change of moisture in the system. Again, due to the lag of reading from hygrometer, the actual moisture level in growth environment may change faster than as shown here.

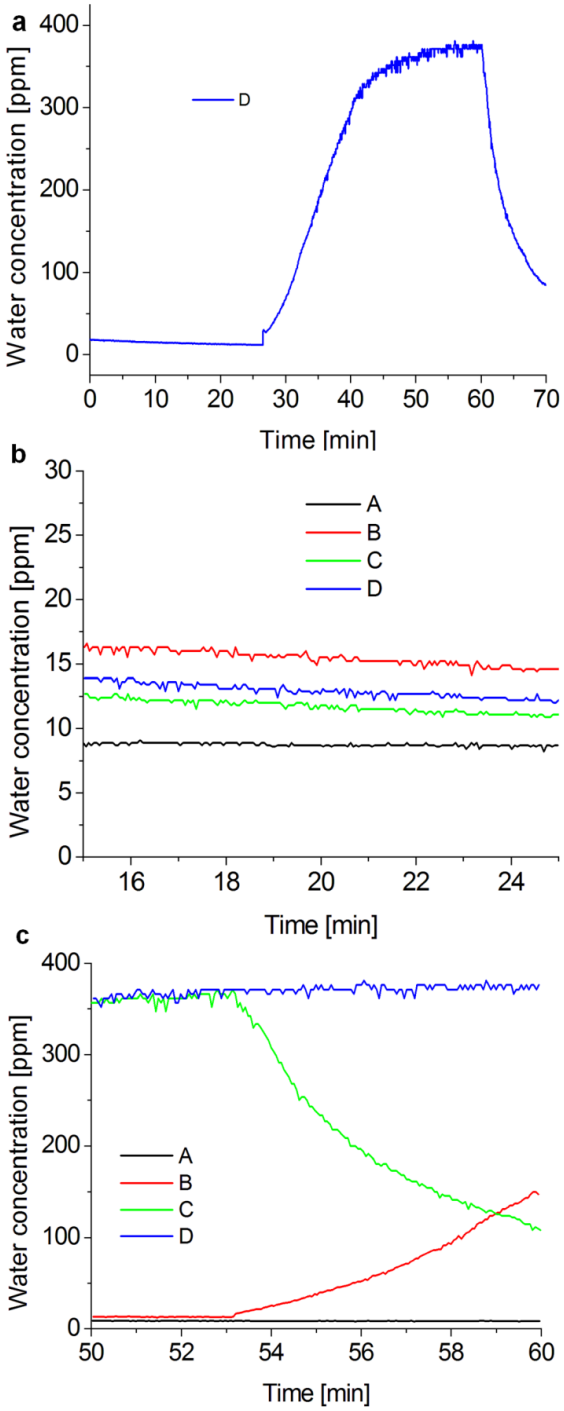

Figure 4.2 Record of moisture: (a), variation of moisture during the entire synthesis process of sample D. Annealing happened during 15-25 minutes and growth took place during 50-60 minutes. (b), moisture level during annealing stages. (c), moisture level during growth stages.

SEM images of the corresponding CNT growth results can be found in Figure 4.3. The left

column of images are obtained by growths start with no moisture input (baseline recipe, sample A and B), and they only show tangled CNTs on substrate. The right column ones are prepared with approximately 370 ppm moisture at the beginning of hydrocarbon exposure (moisture assisted recipe, sample C and D), aligned CNT forests are observed. Such distinguished result suggests that the presence of moisture is essential to the activation of catalyst particles at the beginning of CNT forest growth. After the nucleation and initiation of CNT growth, the addition of moisture in the growth system is not sufficient to help achieve aligned CNT forest.

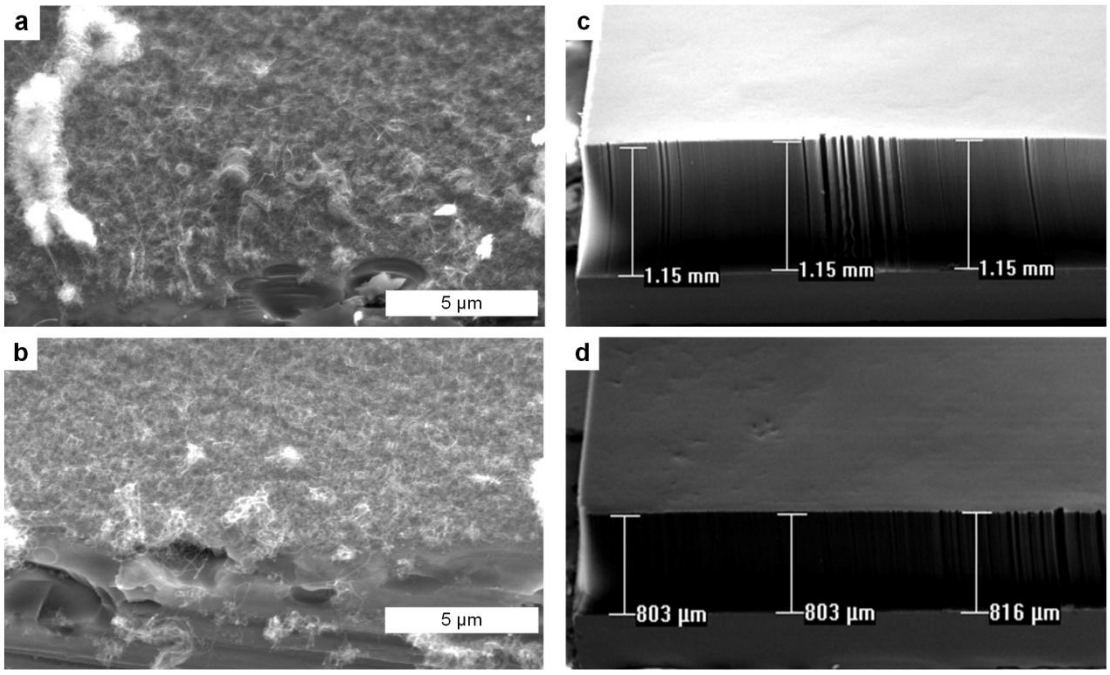

Figure 4.3 SEM images of CNT growth results generated from different moisture supply conditions. Images a, b, c and d correspond to samples A, B, C and D listed on Table 4.1.

Furthermore, there is an interesting difference between sample C and D. Both these samples had a moisture supply of approximately 370 ppm at the beginning of growth. According to the SEM images, the height of sample D is about 800 µm, which is about 300 µm shorter than sample C. The only difference between these two samples is that moisture supply of sample C is cut off after the initial three minutes of growth. This result suggests that the presence of moisture after the nucleation/self organization phase reduces the subsequent CNT growth rate and/or the lifetime of the catalyst population. In order to verify this hypothesis, another series of experiments are carried out to study the kinetics of moisture assisted CNT growth.

4.1.4 Influence of moisture during steady state and density decay phases

Two groups of experiments with different growth times are carried out for the study of this section: one group follows the recipe for sample C, in which the supply of moisture is cut off after the first 3 minutes of growth (Group 0-3 min). The other group follows the recipe for sample D, which the supply of moisture is held constant from the beginning to the end of growth stage (Group 0-end). Growth times of 3, 5, 7, 10, 15 and 20 minutes are carried out for each group. Noticing the difference of moisture supply starts from the 4^{th} minute between these two groups, there is only one run of experiment carried out for 3 minutes of growth.

The height, mass and volumetric density versus time, measured and calculated from the series of samples is plotted in Figure 4.4, and the numerical data are listed on Table 4.2. The difference of height is apparent from samples that produced with 5 minutes of growth, which suggests the moisture had a sustained influence on the kinetics of forest growth during the entire growth stage. As shown in Figure 4,4a, regardless of whether moisture is cut off after the first 3 minutes or not, the forest height increases with time for the first 10 minutes of hydrocarbon exposure. After that, there is a decay of forest height for both groups. Similar trend can be also observed from the mass evolution according to growth time, as shown in Figure 4.4b. From the evolution of forest height and mass shown in Figure 4.4, the catalyst lifetime is similar for both groups. This result suggests the change of moisture supply after the nucleation/self organization phase doesn't lead to a substantial difference in the lifetime of catalyst particles based on macroscopic observation.

Table 4.2 Height, mass and volumetric density of forests produced by moisture assisted recipe.

		Growth time [min]	3	5	7	10	15	20
Moisture supply	0-3 minutes	Height [μm]	-	576	763	1150	1092	875
		Mass [μg]	-	270	310	460	430	350
		Density [μg/mm^3]	-	14.65	12.69	12.50	12.31	12.49
	0-end	Height [μm]	326	545	654	829	691	571
		Mass [μg]	180	210	290	440	390	210
		Density [μg/mm^3]	17.27	12.04	13.85	16.58	17.64	11.49

The "shrink" of forest after termination is very sensitive to the purity of gases delivered to CNT manufacturing environment. It can be only observed with pump down of CVD system

at the beginning of the synthesis process (Section 4.1.2), and addition to regular pump down and refill gas deliver lines, which was one of the techniques reported by Oliver et al [39] to help achieve better consistency of forest fabrication. If the CVD system was left alone without running any experiments for more than one week, this shrinkage of forest will no longer appear until a thorough pump down and refill for all gas lines used for CVD process. It is possible that the shrink of forest was caused by the elimination of residue oxygen in the CVD system.

Furthermore, a forest obtained with moisture supply only for 0-3 minutes growth is always taller than forest obtained with moisture supply during the entire growth stage for the same growth time. And this difference in forest height between Group 0-3 min and Group 0-end is becomes greater as growth time increases before the termination. The control of moisture supply during growth stage was a gradual change as shown in Figure 4.2c, and the difference of moisture concentration between Group 0-3 min and Group 0-end would become greater and greater as growth time increases. Comparing with the height difference of forest between these two groups, which was also getting bigger and bigger as growth time increases, it is clear that the presence of moisture after nucleation/initiation phase led to a slower growth rate of forests.

The mechanism that causes this slower growth rate is not totally clear yet, and needs further research to reveal. The absence of moisture after the nucleation phase might lead to change on kinetics of hydrocarbon decomposition, and/or catalytic behavior, and this topic can be a future direction of research.

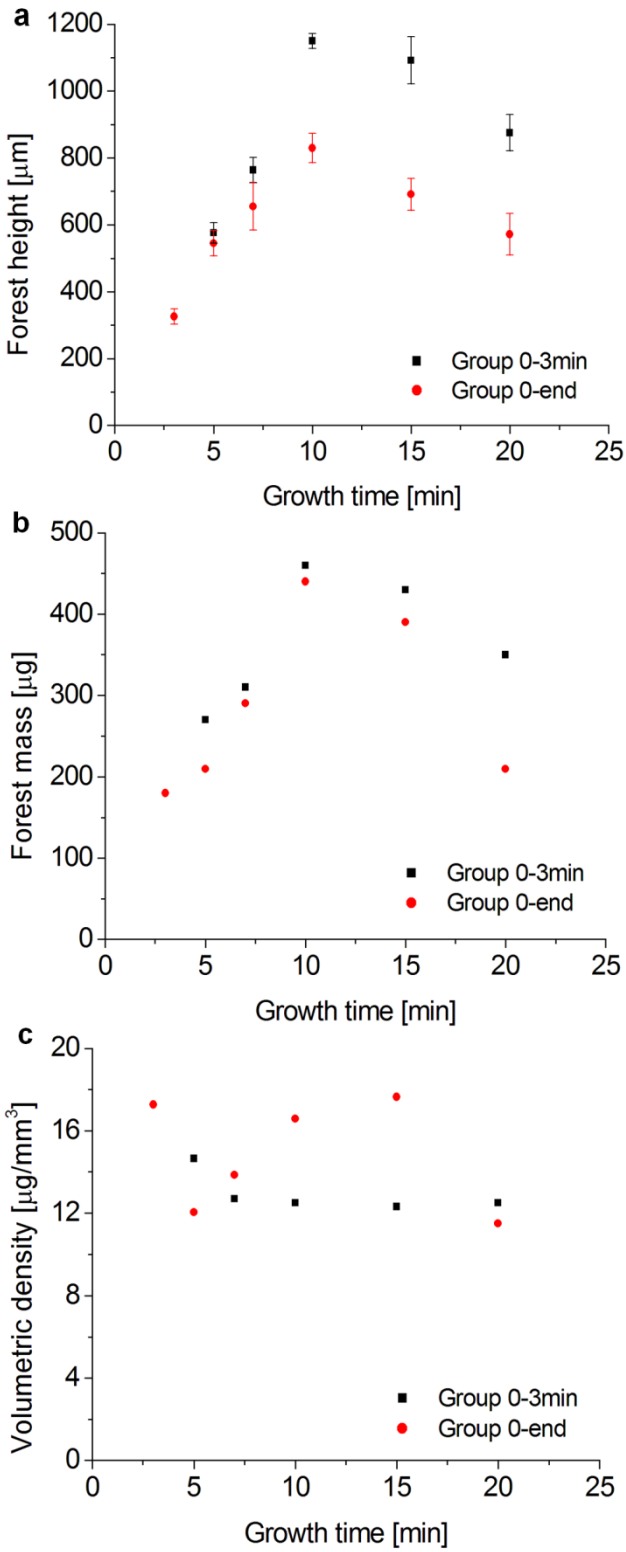

Figure 4.4 Kinetics of forests produced by moisture assisted recipe with different control of water supply. (a), forest height versus growth time. (b), forest mass versus growth time. (c), volumetric density calculated from height and mass.

4.2 Carbon preloaded catalyst film annealing

4.2.1 Background and Introduction

Hydrocarbon gases used in the CVD process will decompose and be deposited on the wall of the reactor during CNT growth. And for the CVD system used in this study, the reactor wall means the inside wall of the 1" quartz tube. Presence of carbon deposits on reactor wall had been noticed to have significant impact to CNT growth results since a few years ago. Liu et al [52] had reported a solid characterization on the carbon deposits on reactor wall, and suggested that these deposits would release hydrocarbon species (possibly CH_2) and further facilitate the formation of catalyst particles and benefit CNT growth. My colleges Bedewy et al also noticed the improvement of CNT growth due to carbon deposits on reactor wall also [67]. Oshima et al [74] studied the evolution of Fe catalyst during CNT synthesis , and ex-situ conversion electron Mössbauer spectroscopy indicated there was small amount of Fe_3C formed during heat up process due to residual hydrocarbon in the reactor tube, and the amount of Fe_3C would increase as CNT growth continues. Furthermore, studied by Wirth et al [75], the main active phase of catalyst could be different due to the crystal structure of Fe: for α-rich Fe particles, Fe_3C is the dominant component that constitutes CNT growth, while for γ-rich iron particles, the metallic iron is the main catalyst phase. But even for the case that iron carbide takes an important role for the catalytic process, it's not always the case that the rich carbon phase is better. Mazzucco et al [76] studied the phase transition of catalyst particles during CNT synthesis process, and reported the more carbon rich phase Fe_5C_2 is less active for CNT formation compared to the less carbon rich phase Fe_3C. The improvement of CNT growth caused by carbon deposition on reactor wall can be quantitatively controlled by using the sample loading module. Substrate can be held in the load-lock chamber while the reactor chamber is heated with controlled amount of hydrocarbon, and then the system is purged with reduced gas atmosphere (He, H_2) used for catalyst anneal. The substrate is then inserted to reactor chamber after the purging, and is annealed in the reactor that has carbon deposited on its inner wall. This process is defined as 'carbon preload'. Combined with the moisture control module, the integrated CVD system is able to take advantage from both carbon preload and moisture assisted growth together. Research indicates these two activations improved CNT growth from different aspects, and they can be integrated together for CNT forest production without disturbing each other.

4.2.2 Method: carbon preload recipe and combined recipe

To study the effect of carbon exposure prior to CNT growth, there are two groups of samples

produced in Section 4.2: forest produced by carbon preload annealing, and forest produced by a combination of carbon preload annealing and water assisted growth.

Carbon Preload Recipe:

Step 1: The catalyst coated substrate is placed onto the quartz boat and transferred to the load lock chamber in the transfer arm system. Then the whole system is sealed and pumped down with a vacuum pump (DS 302, Varian). The pump is turned off after the reading of pressure in the system is below 1 Torr, and the system is filled with Helium (99.999% Cryogenic Gases). The pump-fill is repeated for two more cycles.

Step 2: The furnace is then heated to 775 ℃ over 10 minutes with He (100 sccm, 99.999% Cryogenic Gases) and H_2 (400 sccm, 99.99%, Cryogenic Gases).

Step 3: 100 sccm of C_2H_4 (150 sccm, 99.5%, Cryogenic Gases) is then added to the flow for 3 minutes. After those 3 minutes, the C_2H_4 flow is shut off, and the total flow returns to 100 sccm of He and 400 sccm of H_2 for another 7 minutes. A visible opaque layer of carbon deposits is formed on the wall of quartz tube, as shown in Figure 4.5a. There is photo of clean quartz tube without carbon preload shown in Figure 4.5b.

Step 4: The transfer arm is used to send the sample from load lock chamber to reaction spot of the furnace (7 cm from center of furnace, downstream). The flow is still held the same as described in the previous step for 10 minutes. During this stage, it is expected that the catalyst film is chemically reduced and dewets into nanoparticles.

Step 5: The transfer arm is again used to move the sample from the reaction spot of the furnace to load lock chamber. The same flow from step 4 is held for another 2 minutes in order to let the hot sample to cool down in the same atmosphere as it was annealed.

Step 6: The flow is then switched to 400 sccm He and 100 sccm H_2 for 1 minute. After that, another 100 sccm of C_2H_4 is introduced into system and held for an additional 7 minutes.

Step 7: Sample is sent to the reaction spot again by the transfer arm. The flow is held the same as in step 6 for 10 minutes. This is the growth step and the duration of this step can be adjusted according to experiment design.

Step 8: Upon completion of the growth duration, the furnace cover is lifted quickly, and the transfer arm is used to move the sample out of the furnace. This ensures the sample cools rapidly, while the same gas flow is maintained for an additional 5 minutes.

Step 9: The flow is switched to He only (1000 sccm). System is unsealed and the sample is removed after it has cooled below 100 ℃.

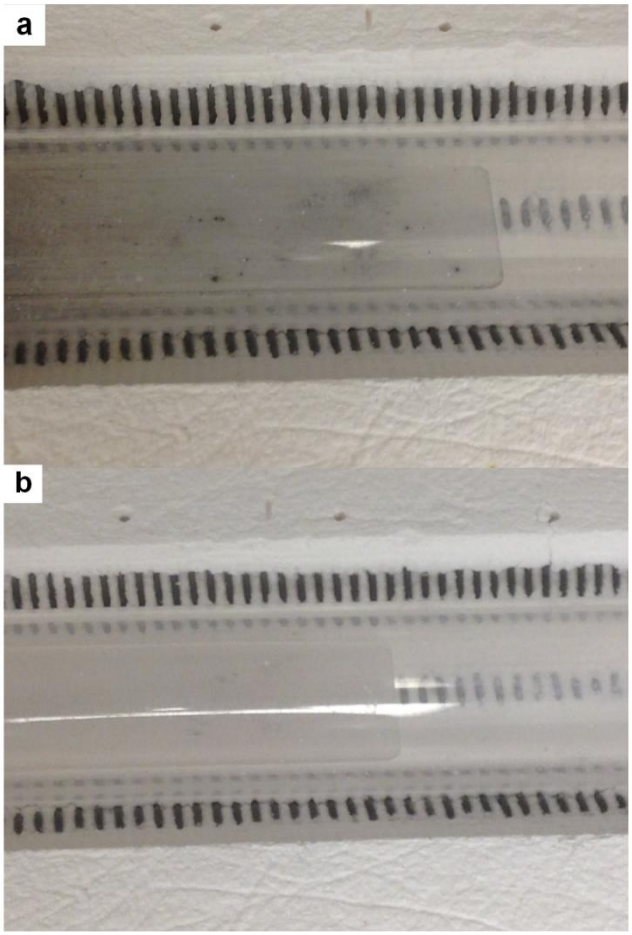

Figure 4.5 Reactor wall with and without carbon deposition. (a), Quartz tube after carbon preload. (b), 'cleaned' quartz tube after air baking, as a comparison.

Combined recipe with carbon preload annealing and moisture assisted growth:

This recipe starts with steps 1-4 from carbon preload recipe, and then followed by step 5-10 from moisture assisted recipe.

Again, in order to prevent contamination from batch to batch, oxidation is carried out at elevated temperature (875 ℃) in the presence air flow (100 sccm, extra dry air, Cryogenic Gases), for a period of 30 minutes.

4.2.3 Kinetics: Improvement from carbon preload and assistance of moisture

First, a series of CNT growth experiments is performed where growth time is gradually increased until the termination of forest height and mass is observed. A group of 6 samples are produced by carbon preload recipe, with hydrocarbon exposure of 5, 7, 10, 15, 20 and 30 minutes. Similarly, another series of samples is produced by the combined recipe, with growth time of 5, 10, 15, 20, 30 and 40 minutes. Later, to gain further information on how the

density evolution happened, another set of experiments with shorter growth time (20, 40, 60 seconds and 2, 3, 4 minutes) is also carried out with the carbon preload recipe and combined recipe.

In Figure 4.6, the relationship between CNT forest height, mass, volumetric density and growth time is shown for forests obtained from moisture assisted recipe (series 1, Group 0-3 min from Section 4.1), carbon preload recipe (series 2) and the combined recipe (series 3). The data from these plots are listed on Table 4.3.

Table 4.3 Height, mass and volumetric density of forests produced by carbon preload recipe and combined recipe, compared with moisture assisted recipe (0-3 minutes).

Growth time [min]	Moisture assisted			Carbon preload			Combined		
	Height [μm]	Mass [μg]	Density [μg/mm^3]	Height [μm]	Mass [μg]	Density [μg/mm^3]	Height [μm]	Mass [μg]	Density [μg/mm^3]
1/3				2.39			3		
2/3				11.8	80	212	18	80	137
1				25.7	130	158	55	210	119
2				97.4	300	96.3	142	360	79.0
3	326	180	17.3	182	450	77.3	264	590	70.0
4				287	570	62.1	408	830	63.6
5	576	270	14.6	401	680	52.9	542	900	51.9
7	763	310	12.7	614	850	43.3			
10	1150	460	12.5	931	920	30.9	1205	1340	34.8
15	1092	430	12.3	1257	920	22.9	1696	1500	27.6
20	875	350	12.5	1372	990	22.6	2070	1560	23.6
30				1362	990	22.7	2289	1740	23.8
40							2265	1820	25.1

Figure 4.6a shows the kinetics of forest height versus time for all the 3 series. Series 1 shows a faster growth rate of forest height compare to series 2, but the height of series 1 terminates at about 1200 μm after 10 minutes of growth, which is shorter and terminated faster than that for series 2 (about 1350 μm, 20 minutes of growth). On the other hand, series 1 and series 3 show very similar growth rate of height from 3 to 10 min of growth time. The growth rates of height from 3 to 10 minutes for both series are also similar to the growth rate from 10 to 20 min of series 3. So the moisture assisted growth can still improve the growth kinetics of height when carbon preload annealing is applied to the CVD process.

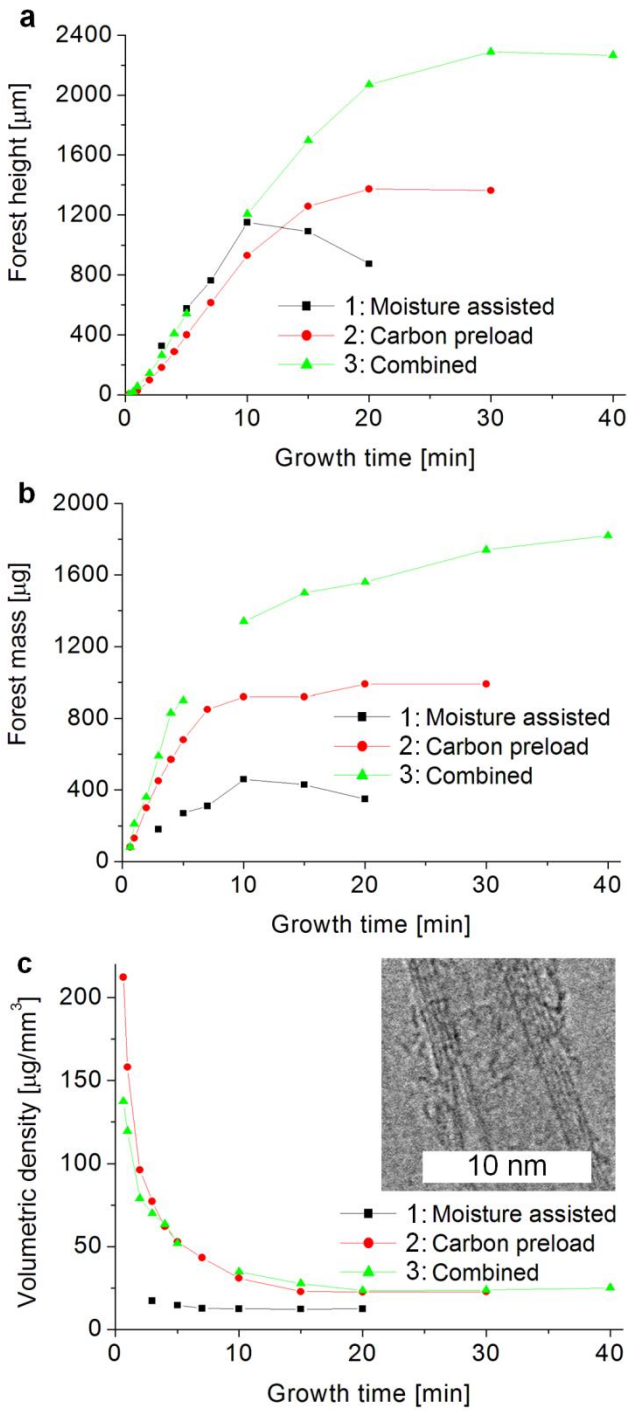

Figure 4.6 Kinetics of forests produced by carbon preload recipe and combined recipe. Data from moisture assisted recipe (0-3 minutes) is also listed for comparison. (a), forests height versus growth time. (b), forest mass versus growth time. (c), volumetric density versus calculated from height and mass. The inset in (c) is a TEM image of CNT produced by the combined recipe.

The kinetics of mass for all 3 series is shown in Figure 4.6b, and series 2 always has a greater mass compare to series 1 at the same growth time. The kinetic of forest mass for series 3, which is the combined recipe, shows the greatest mass among all three series. Combined the

kinetics of forest height and mass versus time for series 1 and 2, it is reasonable to consider that moisture assisted growth can lead to a faster growth rate of forest height, while carbon preload anneal can lead to a greater density of forest growth.

Furthermore, the volumetric density of forests calculated from height and mass is shown on Figure 4.6c. The initial density of forest obtained from carbon preload recipe (series 2) is even greater than the combined recipe (series 3) for growth time from 40 seconds to 3 minutes, but as growth goes on the density of forest obtained from series 2 and 3 are very similar (3~30 minutes). The forests produced by combined recipe and carbon preload recipe showed a very high density at the beginning of growth. Recorded in Table 4.3, the volumetric density during the first minute is approximately 100-150 $\mu g/mm^3$ for combined recipe and 160~210 $\mu g/mm^3$ for carbon preload recipe. But even during the first 3 minutes of growth, combined recipe always produced CNT forest with taller height and greater mass compare to carbon preload recipe. This data of density states that the improvement of growth rate of forest height in series 3 led by moisture assisted growth was achieved while still maintaining the high density forest led by the carbon preload anneal. These two techniques that improve the yield of CNT forest can be used in sequence with the integrated CVD system.

The density data at 20 seconds of growth is not very reliable due to the limit of electronic balance: it was measured at 0.01 mg mass increase after growth compared to raw catalyst (for both carbon preload recipe and combined recipe), but this 0.01 mg is within the accuracy limit of the measurement device. So in Table 4.3 and Figure 4.6 I only reported the height of forests grown for 20 seconds, but didn't include data of mass and density for this growth time.

Measurement from TEM provides the outer diameter of CNTs produced by the combined recipe is 7.9 ± 1.1 nm. A TEM image of an individual CNT obtained from the combined recipe is shown in the inset image of Figure 4.6c. The average number of walls for the CNTs counted from TEM images is 4.9 ± 1.1. The area density of forest can be then calculated by the method provided by Esconjauregui et al [77]:

Assume all the CNTs from a forest have identical mass (m) and the same height (l). The mass of the forest (M) can be assumed as:

$$M = mN \qquad \text{(Equation 4.1)}$$

Here N is the number of CNTs in the forest. Assuming all the CNTs are vertically aligned over the substrate with area A, the area density can be calculated as:

$$\frac{\mathrm{N}}{\mathrm{A}} = \frac{\mathrm{M/Al}}{m/l} \qquad \text{(Equation 4.2)}$$

Here N/A is the area density, M/Al is the mass density, and m/l is the weight gain per unit length of one CNT. This weight gain m/l is derived from the average nanotube diameter (d) and number of walls (n). SWNTs are rolled tubes of graphene, whose area per unit mass is 1315 m^2/g [78], so m/l can be expressed as:

$$\frac{\mathrm{m}}{\mathrm{l}} = \frac{\pi \mathrm{d}}{1315} \qquad \text{(Equation 4.3)}$$

When calculating MWNTs, all walls contribute to m/l. The diameters of the inner walls (d_i) can be given by the following equation assuming the spacing between the walls is 0.34 nm [79].

$$\mathrm{d_i} = \mathrm{d} - 0.68(\mathrm{i} - 1) \qquad \text{(Equation 4.4)}$$

Then the aggregate diameter (D) of all n walls with units in nm [80] is found as:

$$\mathrm{D} = \sum_{1,\mathrm{n}}[\mathrm{d} - 0.68(\mathrm{n} - 1)] = [\mathrm{nd} = 0.34\mathrm{n}(\mathrm{n} - 1)] \qquad \text{(Equation 4.5)}$$

So the weight gain for MWNTs can be calculated as:

$$\frac{\mathrm{m}}{\mathrm{l}} = \pi \mathrm{D}/(1315 \times 10^{18}) \qquad \text{(Equation 4.6)}$$

Here the unit of m/l is g/nm when D is in nm. Since the area density of forest is changing during the growth, a series of area densities is calculated using samples with different growth times from 40 seconds to 20 minutes. It is assumed that all forests produced with different growth times have exactly the same and repeatable kinetics. $(N/A)_i$ stands for the average area density of the forest from time t_{i-1} to time t_i, as well as the average area density of the forest between height l_{i-1} to l_i:

$$\left(\frac{\mathrm{N}}{\mathrm{A}}\right)_\mathrm{i} = \frac{(\mathrm{M_i} - \mathrm{M_{i-1}})/\mathrm{A}(\mathrm{l_i} - \mathrm{l_{i-1}})}{m/l}, \text{ for i>1} \qquad \text{(Equation 4.7)}$$

$$\left(\frac{\mathrm{N}}{\mathrm{A}}\right)_1 = \frac{(\mathrm{M_1})/\mathrm{A}(\mathrm{l_1})}{m/l} \qquad \text{(Equation 4.8)}$$

And the result is shown in Figure 4.7. The highest area density obtained at 40 seconds of growth is $1.8 \times 10^{11}/cm^2$. The decay of area density versus growth time looks roughly linear on the logarithm plot, and the reason of the imperfectness is the kinetics of growth can not be repeated exactly the same from run to run. The decay of area density versus growth time suggests the deactivation rate of forest growth is exponential to growth time.

The best volumetric density from series 3 (137 $\mu g/mm^3$) is about one magnitude lower compare to the ultrahigh density growth from Sugime et al [81], which is the highest density

reported so far and obtained by using Mo-Co co-catalyst. But forests produced from in Sugime's study were in the height of less than 1 μm, while the forest produced by my recipe is 18 μm. Furthermore, techniques used to improve the forest growth are different. Sugime's ultrahigh density growths were achieved by engineering the composition of catalyst and enhancing the interaction between catalyst particles and support substrate, while my recipe improved the yield of CNT forest by better activating catalyst particles using carbon preload annealing and moisture assisted growth.

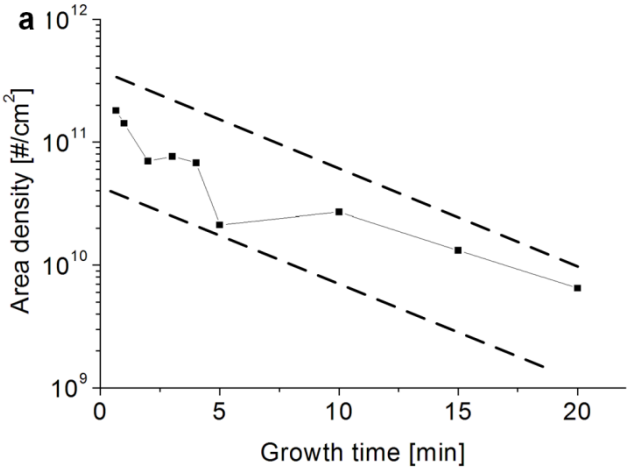

Figure 4.7 Area density of CNT versus growth time. The area density of CNT decreases exponentially as growth time increases.

Although density of forests still decreases with time, forest produced by combined recipe is 4 times as great as the density obtained from moisture assisted growth at even 3 minutes. When the growth time increased to 10 minutes, the combined recipe is still 2.8 times as good as moisture assisted recipe.

A series of characterizations was then carried out on the catalyst particles prepared by the combined recipe to provide an explanation of possible mechanisms caused by carbon preload.

4.3 Impact of carbon preload on Catalyst film

Because the substrate is heated to 775 ℃ during annealing, and this is the same as the temperature for growth, it's reasonable to consider if any CNTs formed during the carbon preload annealing. Carbon preload catalyst chips are prepared following step 1-4 from carbon preload recipe as described in Section 4.2.2, and then rapidly removed from heated zone, then cooled down to room temperature in same atmosphere as applied for annealing step. Regular

annealed catalyst chips are also prepared following step 1-4 from moisture assisted recipe, then also quickly pulled out of the heated zone and cooled to room temperature in the same atmosphere as applied for the annealing step. The major difference between these two procedures is there is controlled input of carbon preload step for regular annealed catalyst. Although trace amount of carbon can still exist in the CVD system due to the random contamination from the surrounding environment, the amount of carbon supply during regular anneal is much less than that during carbon preload anneal.

4.3.1 Surface morphology characterization

High resolution SEM images are taken from regular annealed catalyst and carbon preload annealed catalyst by FEI Nova 200 Nanolab SEM, and there is no difference detected between these two samples. Figure 4.8a shows SEM image taken from carbon preload chip, while Figure 4.8b shows the SEM image taken from regular annealed chip. Unlike the extended time period for carbon preload and annealing from Liu et al [52], 3 minutes of carbon preload, followed by 10 minutes of annealing doesn't lead to any detectable features under high resolution SEM. Furthermore, measurement of chip mass before and after anneal also indicates there is no detectable change of weight during this annealing process.

The carbon preload chip and regular annealed chip are then taken to AFM, scanned by a Bruker Dimension Icon in Scan Assist mode. AFM images of carbon preload chip and regular annealed chip are shown as Figure 8c&8d, respectively. The AFM results suggest number density of catalyst particles is 3.02×10^{11} per cm^2 on carbon preload substrate, which is a 29.74% improvement compared to 2.33×10^{11} per cm^2 from regular annealed substrate. Increase of catalyst particle density due to addition of carbon source during annealing process was also reported by Chen et al [82], while they were using small flow rate of hydrocarbon during annealing instead of pre-exposure of the quartz tube to a brief flow of hydrocarbon prior to insertion of the sample for annealing.

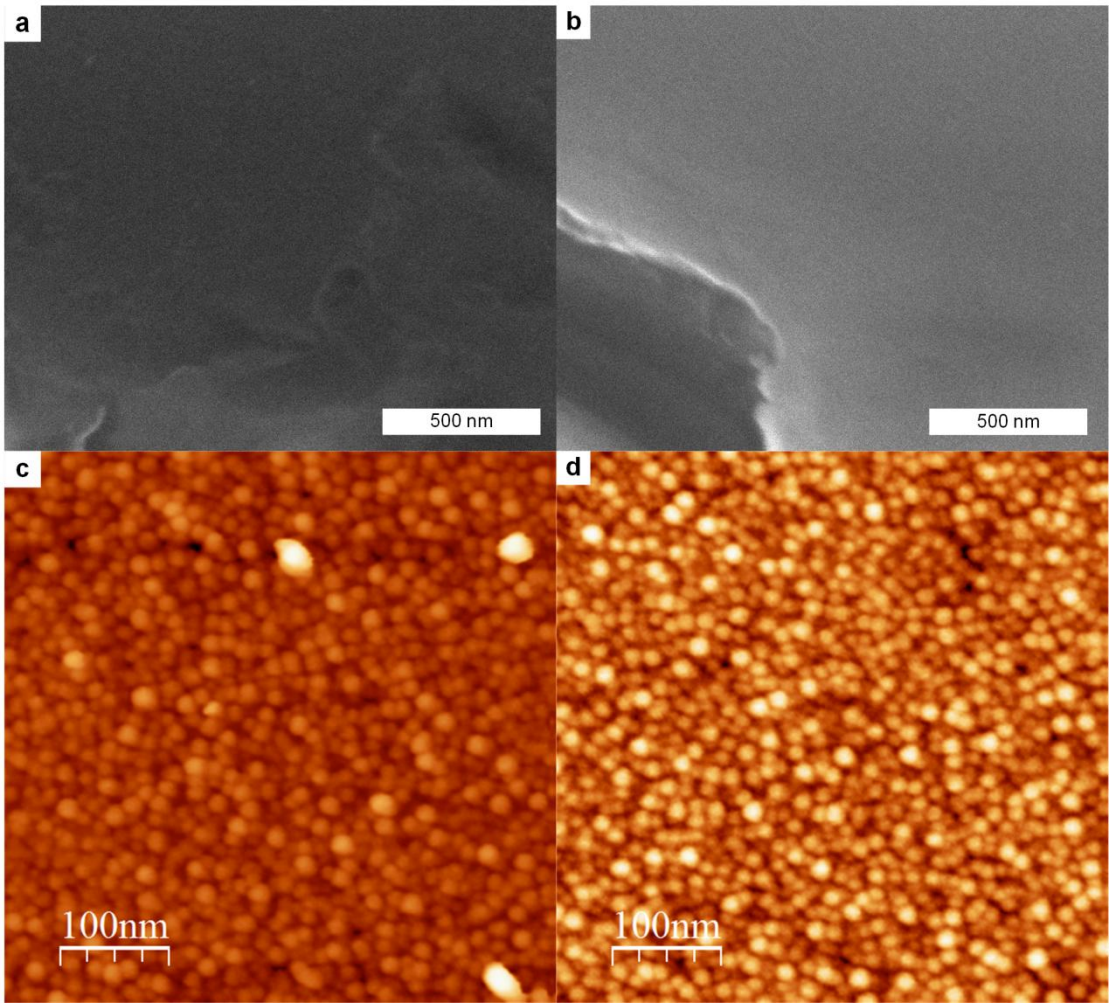

Figure 4.8 Surface characterizations on carbon preload annealed catalyst and regular annealed catalyst. Image a and c are SEM and AFM images from carbon preload catalyst chip, and image b and d are SEM and AFM images from regular annealed catalyst chip.

4.3.2 XPS study of surface chemistry

The 30% improvement of particle density from regular anneal (used for moisture assisted growth) to carbon preload anneal (carbon preload recipe and combined recipe) is not enough to explain a four times difference in forest density between moisture assisted growth and carbon preload/ combination growth. In order to further reveal the activation mechanism for carbon preload treatment, X-ray photoelectron spectroscopy (XPS) analysis is performed. The XPS study is performed by a Kratos Axis Ultra XPS with Al mono source. In order to get a comprehensive understanding of composition and chemistry on the catalyst chips, depth profile is generated by Argon plasma. Both broad survey scan that generates elemental composition and core scan of Carbon 1s and Fe 2p peaks are applied to samples before the plasma etch and after 20, 40 and 60 seconds of plasma etch. Scans are calibrated according to Au 4f 7/2 peak at 84.0 eV.

The major components on surface of these two catalyst chips are Al, C, Fe, O, and Si. The detailed compositions of these elements are listed on Table 4.4. The concentration of Al, Fe and O are similar for regular annealed catalyst and carbon preload catalyst with the same duration of plasma etch, so I only show a plot with composition of C and Si on Figure 4.9a. It is interesting that there is no Si signal detected from the surface of carbon preload annealed catalyst chip before plasma etching. According to the nature of XPS, signal of elemental composition are usually detected from a depth within 10 nm below the solid surface [83, 84]. The thickness of Al_2O_3 support layer is also about 10 nm, and there could be pores formed during annealing on this support layer. It could be that the deposition of carbon layer obtained from carbon preload annealing is thick enough to shield on top of the catalyst and support layer to prevent collecting signal from Si, or the deposition of carbon blocked the pores in the Al_2O_3 layer that could enable receiving scattering from Si.

Table 4.4 Elemental composition at surface of catalyst chips with different plasma etching time. Numbers in table stand for percentage of atomic composition.

Element		Al 2p	C 1s	Fe 2p	O 1s	Si 2p
Regular annealed	0s	23.78	14.51	5.79	39.69	15.29
	20s	32.66	1.02	9.64	41.84	14.61
	40s	34.29	0.94	9.48	41.68	13.61
	60s	35.85	0.96	8.49	41.24	13.46
Carbon preload	0s	24.34	32.57	5.23	37.86	0.00
	20s	29.13	11.00	9.40	35.83	14.31
	40s	31.45	6.55	10.08	38.07	13.85
	60s	34.10	4.57	9.20	39.64	12.50

The evolution of composition along plasma etching suggests the carbon signal from regular annealed catalyst is random contamination from surrounding environment, and this fact is then further stated by results from core scans, which will be discussed in later paragraph. Prior to the plasma etching, there is about 15% of carbon on regular annealed sample, but after even 20 seconds of etching, the composition of carbon is decreased to about 1% (loss of 93.3%). This remaining one percent is almost constant during the rest of etching, and I suggest such signal of carbon residue is due to the roughness of substrate surface. The hemispherical catalyst particles with uneven heights will lead to incompletion of carbon etching on the surface, as shown on Figure 4.9b. On the other hand, 33.8% of carbon still

remains on carbon preload sample after 20 seconds of plasma etching (total composition decreased from 32.6% to 11.0%).

Core scan of carbon 1s peak also indicates the majority of carbon signal from regular annealed substrate is just random contamination from surrounding environment as shown on Figure 4.9c. The C-C, C-O and C=O peaks shown on the figure stand for very typical random carbon contaminations and/or graphene like carbon [85, 86]. The C-C peak is a mixture of sp2 and sp3 carbon. The reason is that after 20 seconds of plasma etching, both C-O and C=O peaks are removed, leaving a much weaker C-C peak that is also shifted 0.24 eV towards higher binding energy. Combined with the 93.3% of loss in elemental composition shown in Figure 4.9a, it is clear that the 20 seconds plasma etching removed the majority of random carbon contamination that contains more reactive bonds such as C=O and C-O, and only remaining peak is the C-C peak.

Carbon 1s peak from carbon preload annealed catalyst are also analyzed. The peak before plasma etching is plotted on Figure 4.9d (red), along with the peak after plasma etching for 20 seconds (green) and peak before etching from regular annealed substrate (black). The C-O and C=O peaks from carbon preload sample before etching has a similar height compare to regular annealed sample, which indicates the adventitious contamination is obtained due to the same source: contamination from environment during sample storage and transportation. Again, the peaks of C-O and C=O bonds disappeared after plasma etching, and only left one peak for C-C bonds. But the signal of C-C peak from carbon preload substrate after 20 seconds of plasma etching was much stronger than that for regular annealed catalyst. It's reasonable to consider there are two sources of carbon signal contribution to the carbon preload sample: 1), random carbon contamination from the environment, 2), carbon features formed on or with Fe catalyst particles during annealing step. Since all the carbon related peaks here are all much greater than 283 eV, there can't be any iron carbide formed on catalyst prepared by carbon preload recipe, nor regular annealed recipe. Plot of core scans for Fe 2p peaks shown on Figure 4.9e also suggested the chemistry of Fe on the substrate is not iron carbide. Fe 2p 3/2 peaks from both samples are about 711eV, which could be Fe_2O_3 [83, 87] or Fe_3O_4 [87, 88]. The catalyst particles didn't experience the transformation process to cementite (Fe_3C) as mentioned by Mazzucco et al [76] at least during the carbon preload annealing stage. In this case, the carbon 1s peak in Figure 4.7d looks more like a mixture of CNT and/or graphene fragments, formed during annealing due to the released CH_x species

from carbon deposits on reactor wall. In order to confirm this feature, further characterizations are carried out in the next section.

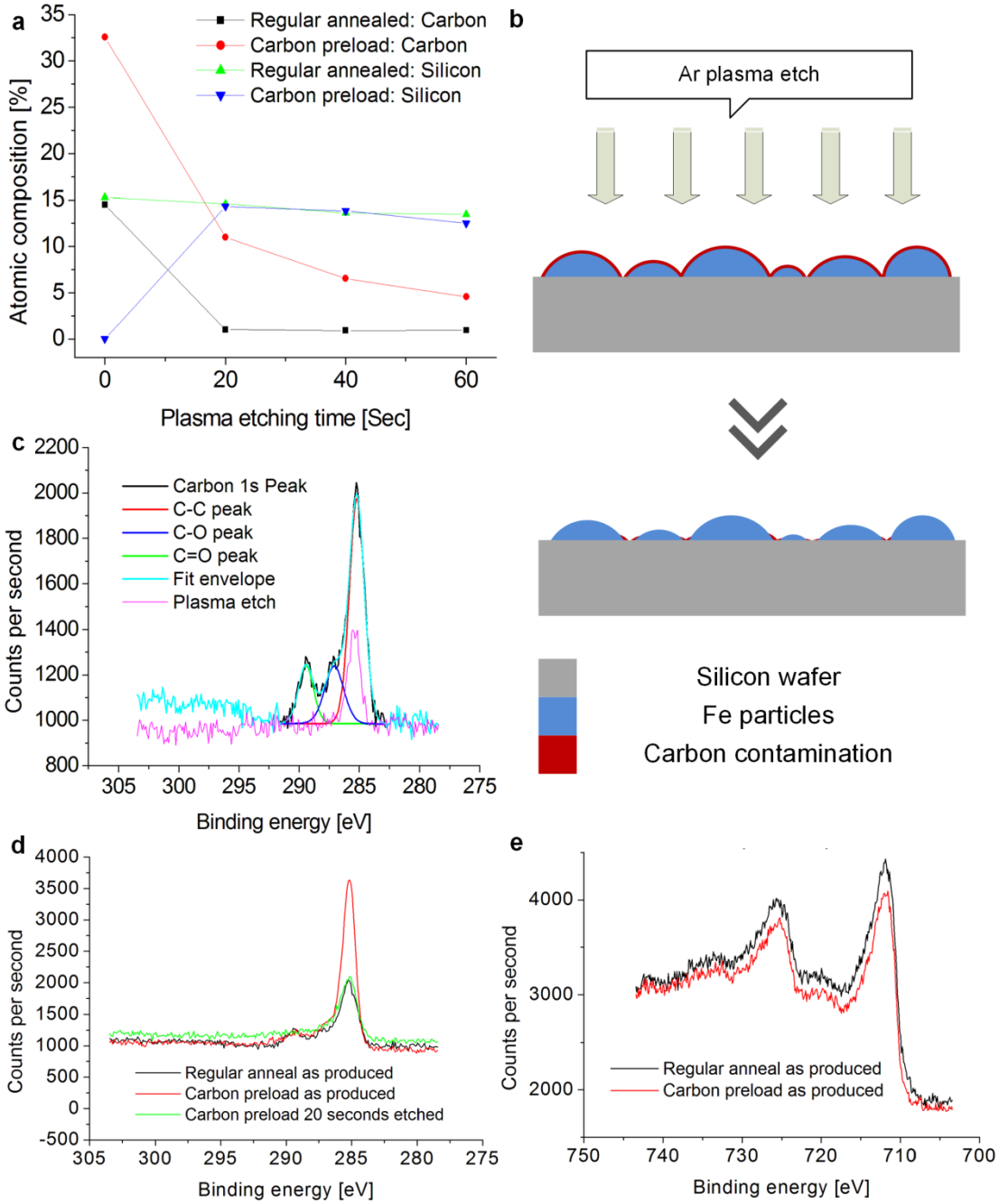

Figure 4.9 XPS analysis on as annealed catalyst chips. (a), evolution of atomic composition of C and Si elements. (b), schematic of incomplete plasma etching on carbon due to roughness of catalyst surface. (c), adventitious carbon contamination observed on surface of regular annealed chip. "Carbon 1s peak" stands for signal generated before plasma etching, and the fittings are modeled based on this non-etched signal. The "Plasma etch" curve is the signal of carbon 1s peak after 20 seconds of plasma etching. (d), Carbon 1s peak from carbon preload and regular annealed substrate. (e), Fe 2p peak from carbon preload and regular annealed substrate.

4.3.3 Graphene formed on top of catalyst particle

Raman spectroscopy is performed on both catalyst substrates using a WITec alpha 500 system (532nm laser) and the results are shown in Figure 4.10a. Spectra from both substrates are collected using an integration of 10 scans, and each scan was 0.5 seconds. It is very clear that there is no peak shown from regular annealed sample in the range of 1100 to 3500 cm^{-1}, while G, D and 2D peaks are observed from the carbon preload sample. The peaks from carbon preload annealed catalyst suggest there should be graphene layer or caps of CNTs on the catalyst particles.

In order to investigate the form of carbon that is introduced by the preload step, TEM samples are prepared from carbon preload annealed chip. Glass microscope slides are used to scratch on the surface of catalyst chip, so that nano particles can be taken off from the catalyst chip. Then the Glass slides are rinsed with alcohol and the particles are transferred to TEM grids. TEM image shown in Figure 4.10b demonstrate fragments of single layer graphene coated on catalyst particles, and the ring pattern of diffraction from the graphene layer is shown in Figure 4.10c.

Based on all characterizations described above, I suggest a pre-activation mechanism on catalyst particles caused by carbon preload. The schematic of this mechanism is shown on Figure 4.11. During catalyst film dewetting process, the CH_x species released from carbon deposits on quartz tube will react with catalyst particles, and form fragments of graphene structure, which may later turn to cap of CNTs during growth. It is also possible that the catalyst particle becomes saturated with carbon and then the graphene structure is formed. The effect of carbon preload here is brining nucleation of CNTs from the beginning of growth stage to the annealing stage. Since the amount of carbon released during the annealing process from reactor wall is much less comparing to the carbon supply during CNT growth, the catalyst particles can react with carbon at a much slower rate and would not be poisoned. The nucleated particles will be “frozen” after annealing stage, taken out of the reactor and waiting until the moisture-rich growth environment is ready.

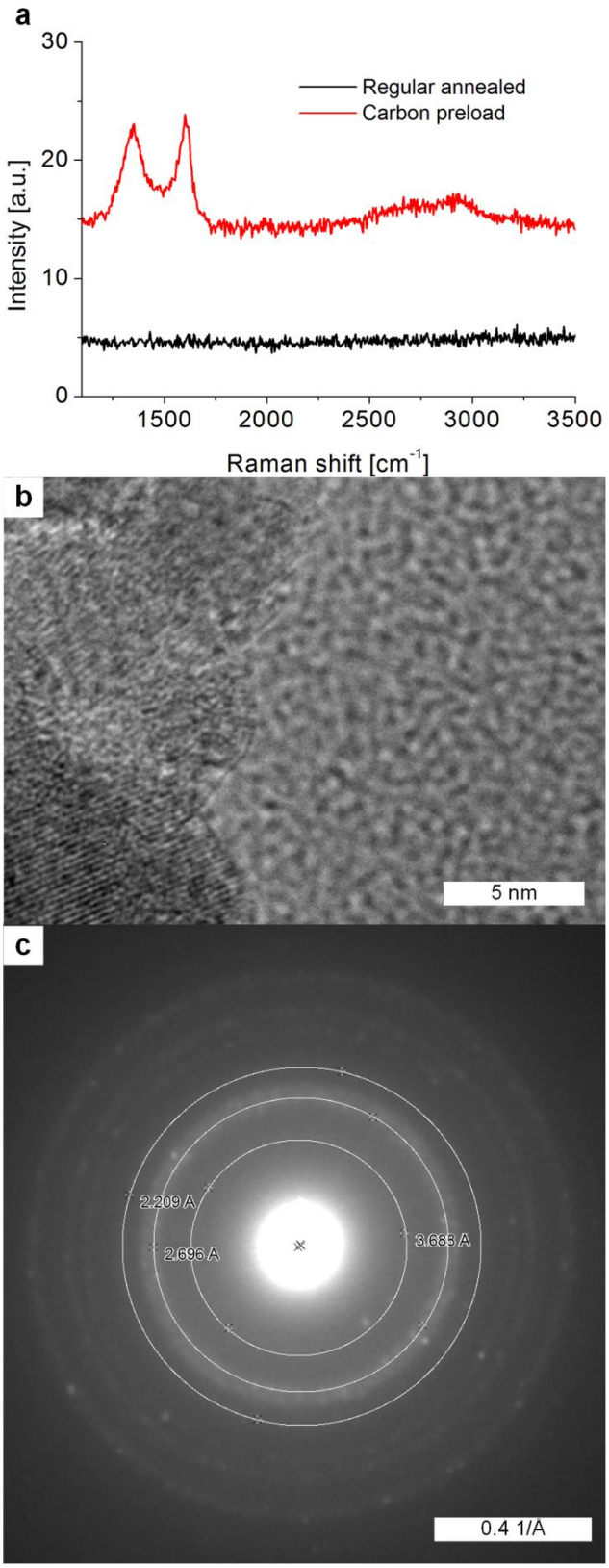

Figure 4.10 Conformation of graphene layer on catalyst particle by Raman and TEM characterization. (a), D and G peaks observed by Raman on carbon preload chip. (b), high resolution TEM image shows the single layer of graphene covers on top of catalyst particle. (c), diffraction pattern of graphene.

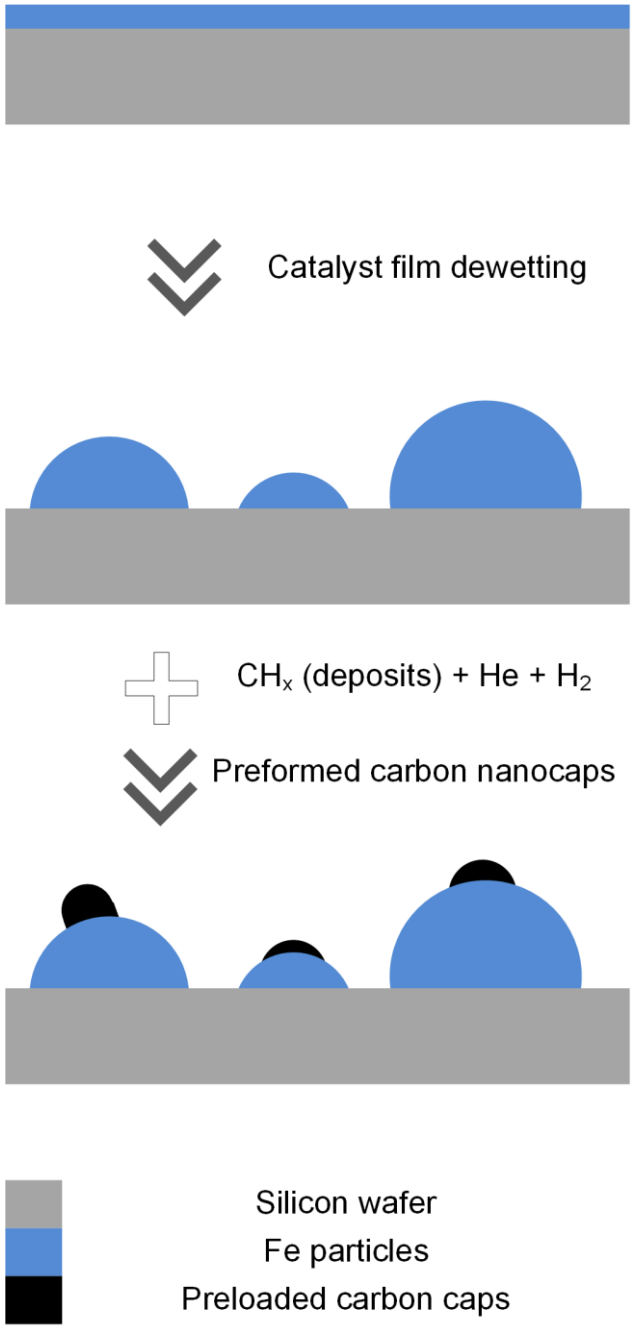

Figure 4.11 Schematic of catalyst particles activated by carbon preload. Carbon deposits preloaded to reactor wall will release CH_x species during anneal step. These hydrocarbon species will react with catalyst and start to form caps of CNTs. In this way the catalysts are "pre-activated" before the formal hydrocarbon exposure (growth step).

4.4 Conclusion and future directions

In this chapter, the different role of moisture during nucleation/self-organization phases and steady-state phase of growth is revealed, and it is demonstrated the activation of catalyst particles due to moisture is only valid at the beginning of growth (nucleation/self organization phase). Then with carbon preload integrated to CNT forest manufacturing

process, the volumetric density of forest achieved as high as 137 μg/mm^3 whiling give better kinetics of height and mass compared to carbon preload recipe and moisture assisted recipe. The presence of moisture from combined recipe helps increase the growth rate of forest compared to carbon preload only recipe, while maintaining the same level of volumetric density for CNT growth greater than 3 minutes. Finally, a series of characterization are carried out to reveal the mechanism of carbon preload activation and the "pre-activation" mechanism is discussed.

Although a lot of evidences had been shown in this study to support the pre-activation mechanism, the conversion from graphene fragments to CNTs is still not clearly understood and observed yet. Further study is still needed to understand the details of nucleation of carbon nanotubes, in order to better optimize the process of catalyst particle activation and improve the lifetime of catalyst.

CHAPTER 5
GROWTH OF ALIGNED CARBON NANOTUBES FROM THE NATIVE SURFACE OF HAYNES556 ALLOY

This chapter reports the synthesis of aligned CNTs on the native surface of Haynes556 alloy. This project was motivated by collaboration with Pall Corporation, who had interest in CNTs grown on Haynes 556 for filtration applications. First, characterization of the surface chemistry is carried out to show the feasibility of growing CNTs on the native surface of Haynes556 alloy, and then direct growth of CNT forests is achieved when composition of Fe on the surface is increased to 5.94% by heat treatments. After that, a discussion of consistency of forest growth reveals that the presence of moisture during growth stage is necessary for aligned CNT growth. Finally, it is shown that forests can be regrown after removal, along with a short discussion about the impact of heat treatment before growth.

5.1 Background and introduction

Growth of CNTs on bulk metals attracts researchers' interests due to the less expensive cost compares to traditional methods studied over the past two decades [43-47]. Furthermore, growth of CNTs on metal substrates is also important for the applications requires direct and firm contact between CNTs and substrates, such as MEMS devices, thermal conductors and probes [24, 26, 29, 89]. Enhanced by microwave hot-filament deposition in a low pressure environment, Miao et al [90] were able to achieve various sizes and shapes of CNTs on 20-30nm thick layer of nickel/iron alloy. They deposited the nickel/iron alloy on a silicon substrate by thermal evaporation, and demonstrated a different base growth mechanism on transition metals. After that, Parthangal et al [91] achieved aligned forests growth on various of metal substrate such as SS foil, titanium nitride, and aluminium, etc. Similar to Miao et al, they deposited these alloys on top of a silicon dioxide wafer. And addition to the metal substrates, another layer of iron based catalyst was prepared from aqueous solution. Lepro et al [92] obtained aligned forest on type 321 stainless steel foil without extra catalyst, but their technique required electron beam deposited Al_2O_3 as a buffer layer. Similar results were also achieved by other groups: Kim et al [93] achieved aligned forests growth on stainless steel

304 substrate with additional support layer, while Pal et al [94] required external catalyst source such as xylene-ferrocene. On the other hand, Cole et al [95] and Shin et al [96] chose no additional catalyst but surface treatment prior to growth, and Cole et al obtained vertically aligned carbon fibers while Shin et al obtained tangled CNT growth.

Our group had a collaboration with Pall Company which focused on the direct growth of carbon nanotubes on the native surface of different metal and metal alloys. As one of those projects, Pall requested that we attempt to grow aligned CNT forests on the native surface of micro fiber meshes made of Haynes556 alloy. Among all the previous studies, Pal et al [94] demonstrated aligned forest could be obtained from some of the Inconel™ and Haynes™ superalloys with floating catalyst CVD process, and also demonstrate the formation of Cr_2O_3 layer in these superalloys would help to form suitable catalyst and then improve growth results. But in their studies, Haynes 556 showed low density and non-aligned CNT growth even with help from external catalyst sources. A thick layer of crust (about 100 μm) was observed on top of substrate surface, while low density and non-aligned CNTs were grown among the crust.

5.2 Methods and experiments

5.2.1 Substrate treatment and forest synthesis

Large pieces of Haynes 556 fiber mesh (fiber diameter: 20-30 μm) is obtained from Pall Company, and then cut into 5mm by 5mm small pieces by hard duty scissors. Flat Haynes 556 alloy sheet (0.12-0.13 by 12.00 by 12.00 inches) is obtained from Haynes International and then cut into 5mm by 5mm squares (still 0.12-0.13 inches thick) using an abrasive waterjet machine (OMAX). After cutting, these substrates are rinsed by 2-propanol (IPA, >99.7%, Sigma-Aldrich) and dries by a gentle flow of dry air.

All growths are carried out with the sample loading module as described in Chapter 2. The growth recipes are described below.

Standard Haynes recipe

Step 1 (oxidation): Haynes 556 substrates are loaded 7cm downstream from the center of furnace. Substrates are oxidized in air (100 sccm, extra dry air, Cryogenic Gases) at 825 ℃ over 60 minutes, and then the flow is switch to He (1000 sccm, 99.999% Cryogenic Gases)

for 1 minute.

Step 2 (reduction): The substrate is reduced in He (400 sccm) and H_2 (100 sccm, 99.99%, Cryogenic Gases) for another 70 minutes at 775 ℃.

Step 3 (growth): C_2H_4 (100 sccm, 99.5%, Cryogenic Gases) is introduced to the tube furnace for 15 minutes for CNT growth.

Step 4 (cool down): At the end of growth, heat is shut off and the furnace cover was opened. The substrate is then transferred out of the heated region. The same flow as in the growth stage is kept for another 5 minutes, and then switched to 1000 sccm of He until the sample is cooled down.

He/H_2O tank assisted Haynes recipe

This recipe follows exactly the same procedure as the standard Haynes recipe; the only difference is that the He flow for this recipe is supplied from a calibrated He/H_2O tank (A31 100 ppm H_2O in Helium, certified mixture, CGA 580 top pressure 500 psi, CryogenicGases).

Decoupled Haynes recipe

Step 1 (oxidation): Haynes 556 substrates are loaded at 7cm downstream from the center of the furnace. Substrates are oxidized in air (100 sccm, extra dry air, Cryogenic Gases) at 825 ℃ over 60 minutes, and then the flow was switch to He (1000 sccm, 99.999% Cryogenic Gases) for 1 minute.

Step 2 (reduction): The substrate is reduced in He (400 sccm) and H_2 (100 sccm, 99.99%, Cryogenic Gases) for another 30 minutes at 775 ℃.

Step 3 (decouple): At the end of the reduction stage, substrate is transferred out of the heated region, and then same flow as during the reduced stage is kept for another 2 minutes.

Step 4 (preparation): C_2H_4 (100 sccm, 99.5%, Cryogenic Gases) is introduced to the tube furnace for 18 minutes.

Step 5 (growth): The substrate is again transferred back to the same spot as it was oxidized and reduced. The same flow is kept over another 10 minutes for growth.

Step 6: At the end of growth, heat is shut off and the cover of furnace is opened. Substrate is then transferred out of the heated region. The same flow as in the growth stage is kept for another 5 minutes, and then switched to 1000 sccm of He until the sample is cooled down.

Moisture can be added during anytime of the entire synthesis process depends on the requirement of study. If moisture is present during both reduction and growth stages (Step

2-5), the recipe is called *moisture assisted Haynes recipe*, and similarly, if moisture is only present during reduction stage (Step 2), it is *Haynes recipe with moisture assisted reduction*; if moisture is only present during the hydrocarbon exposure stages (Step 4-5), it is *Haynes recipe with moisture assisted growth*.

Again, as mentioned in Chapter 3, to prevent contamination from batch to batch oxidation is carried out at elevated temperature (875 ℃) in the presence air flow, for a period of 30 minutes.

5.2.2 Material characterization

Scanning Electron Microscopy (SEM) images of the CNT forests are taken by using a Philips XL30 FEG SEM with a working distance of 10 mm and electron beam voltage of 10 kV, and FEI Nova 200 Nanolab SEM with a working distance of 5 mm and electron beam voltage of 10 kV. Transmission Electron Microscopy (TEM) images are taken using a JEOL 3011 at 300 kV and 113 mA. X-ray photoelectron spectroscopy (XPS) study is performed by a Kratos Axis Ultra XPS with Al mono source with current of 8 mA and voltage of 14 kV. The data generated from XPS are processed by CasaXPS software, which allows calculating the atomic concentration of elements from the surface of sample substrate.

5.3 Feasibility of grown CNTs on native Haynes556 surface

From the bulk composition provided by Haynes International, it seems that the Haynes 556 alloy itself should be sufficient to support CNT growth, even if not aligned. As listed in Table 5.1, Haynes 556 alloy comprises Fe, Ni, Co and Cr, which are known catalytic elements (Fe, Ni and Co) and support layer elements (Cr) for CNT growth. However, as characterized by XPS, the elemental composition on the surface of as arrived Haynes 556 alloy reports the majority of the surface is composed of carbon (72.5%) and oxygen (26.7). These results indicate the surface of Haynes556 alloy is not only oxidized, but also heavily contaminated by carbon. This may be attributed to the transportation and storage process prior to XPS analysis, and the spectra generated from XPS only penetrated about 10 nm from the surface of substrate [83, 84], . This result is also illustrated in Figure 5.1a.

Table 5.1 Elemental composition of Haynes 556 alloy

	C	Co	Cr	Fe	Mn	Ni	O
Bulk composition	0.49	18.01	24.95	32.73	1.07	20.10	0.00
Surface composition	72.45	0.22	0.29	0.30	0.00	0.0	26.74

Numbers are in percentage (%). Bulk composition obtained from official data sheet of Haynes International. Surface composition stands for the as arrived status.

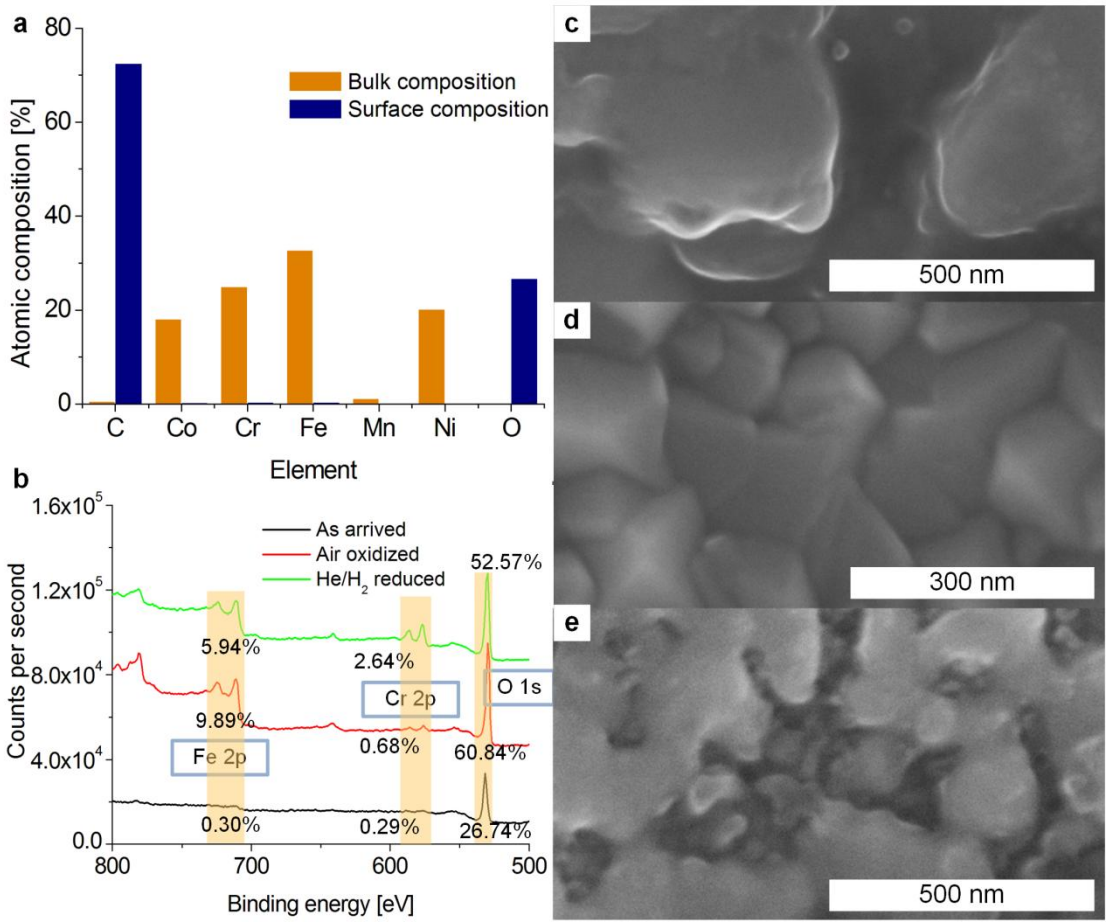

Figure 5.1: Elemental composition of Haynes 556 alloy. (a), bulk composition of Haynes 556 provided by Haynes International shows this alloy is rich in catalytic and support elements for CNT growth, while surface composition of as arrived Haynes 556 alloy suggests the majority of elements on surface is not suitable for CNT growth. (b), elemental composition on surface treated by air oxidation and He/H_2 reduction. Treatment of oxidation and reduction provides a surface more suitable for CNT growth. (c), (d) and (e), High resolution SEM images of as arrived, air oxidized and He/H_2 reduced Haynes 556 substrate surfaces.

In order to make the surface suitable for CNT growth, substrates are taken to a furnace and processed through air oxidation and He/H_2 reduction, as described in Section 5.2.1

(Decoupled Haynes recipe Step 1 and 2). XPS characterization is also performed on air oxidized and air oxidized plus He/H_2 reduced substrates. The results are plotted on Figure 5.1b. Compares to the untreated substrate, once oxidized by air, a significant increase in Fe concentration (from 0.30% to 9.89%) is observed from the XPS analysis. At the same time, due to the continuous hour of oxidation, the presence of oxygen is also increased by a factor of 2.3. Furthermore, with an additional 30 minutes of reduction by He and H_2, there is loss of concentration in Fe but another gain of Cr, which is an important element that can form support layer and enhance CNT growth [94]. Detailed compositions of all elements are shown in Table 5.2. It is interesting that the major metal elements on the surface after both heat treatments are Fe, Cr and Co, while the presents of Ni is almost negligible. Such results may be due to the difference of migration speed among different elements.

Table 5.2 Elemental composition of treated Haynes 556 alloy

	C	Co	Cr	Fe	Mn	Ni	O
Air oxidized	21.35	5.07	0.68	9.89	1.69	0.47	60.84
He/H2 reduced	35.57	2.44	2.64	5.94	0.77	0.07	52.57

High resolution SEM images of untreated, air oxidized and He/He reduced Haynes 556 substrate surface are also shown in Figure 5.1c, d, and e, respectively. It appears that re-crystallization happens during these heat treatment steps. The untreated surface shows very random features on a scale of hundreds of nanometers, and after oxidized in air at 825 ℃, new grains formed on the surface, on a scale of a few tens of nanometers up to about a hundred nanometers. Then the substrate is further reduced by He and H_2, and much smaller nano-features were formed on the surface.

After oxidation and reduction, catalytic (Fe) and supportive (Cr) elements are brought to the surface of substrate. At the same time, the geometry of nano-features on surface is seen to be more suitable for CNT growth. Much smaller features, including particle structures ranging from 10-100 nm are observed after heat treatments, whereas the untreated surface is consisted of random features with a diameter on the order of hundreds of nanometers. These smaller features show a similar scale when compared to CNTs obtained from Haynes 556 alloy. In the next section, CNT growth will be processed on these heat treated substrates.

5.4 Aligned and consistent forest growth on Haynes 556 alloy

In this section, the initial successful growth of aligned CNT forests is first demonstrated. Then, the inconsistency of CNT growth during long term study is brought up, and the role of moisture during forest production is revealed.

5.4.1 Consistency of aligned forest growth on Haynes 556 fiber mesh

After air oxidation and He/H_2 reduced, vertically aligned CNT forests can be obtained directly from native surface of Haynes556 alloy, without any additional support layer or external supply of catalyst. Figure 5.2a and b show the SEM images of Haynes 556 fiber mesh before and after CNT growth. TEM images of CNTs are also shown in Figure 5.2e&f. The CNTs grown from Haynes 556 alloy are found to be multi-walled with approximately 10-15, with diameter of 20-30 nm. Some of the CNTs are found to have an empty cap (Figure 5.2e), while for some cases catalyst particle is also captured in the cap of CNTs (Figure 5.2f). These TEM images suggest the CNT growth mechanism on Haynes 556 alloy is a mixture of tip growth and base growth.

This growth is carried out with the standard Haynes recipe, and at this point of research, the presence of moisture in the system had not been addressed by researchers in our group. As a result, the standard Haynes recipe was later realized not always working: The aligned forests shown in Figure 5.2b are obtained during the humid seasons of a year, such as spring and summer. furthermore, the gas delivery system in our lab was soft tygon tubing. With such setup the moisture from ambient could diffuse into the gases used for growth compared to impermeable stainless steel tubing, which was later used in the lab and led to the growth result shown in Figure 5.2c.

Inspired by the work from my colleagues Ryan Oliver and Erik Polsen [39], and also my work introduced in Chapter 3, control and recording of moisture is then enabled in the furnace. Using the calibrated He/H_2O tank, now aligned forest can be consistently obtained from the native surface of Haynes 556 alloy. The record of moisture concentration during synthesis process is plotted on Figure 5.2g. Although the He/H_2O assisted Haynes recipe provided consistent growth of aligned forests, the exact role of moisture during the entire synthesis process is not clearly understood yet. In order to further study the importance of moisture for different stage during synthesis process, a group of experiments is carried out using decoupled Haynes recipe.

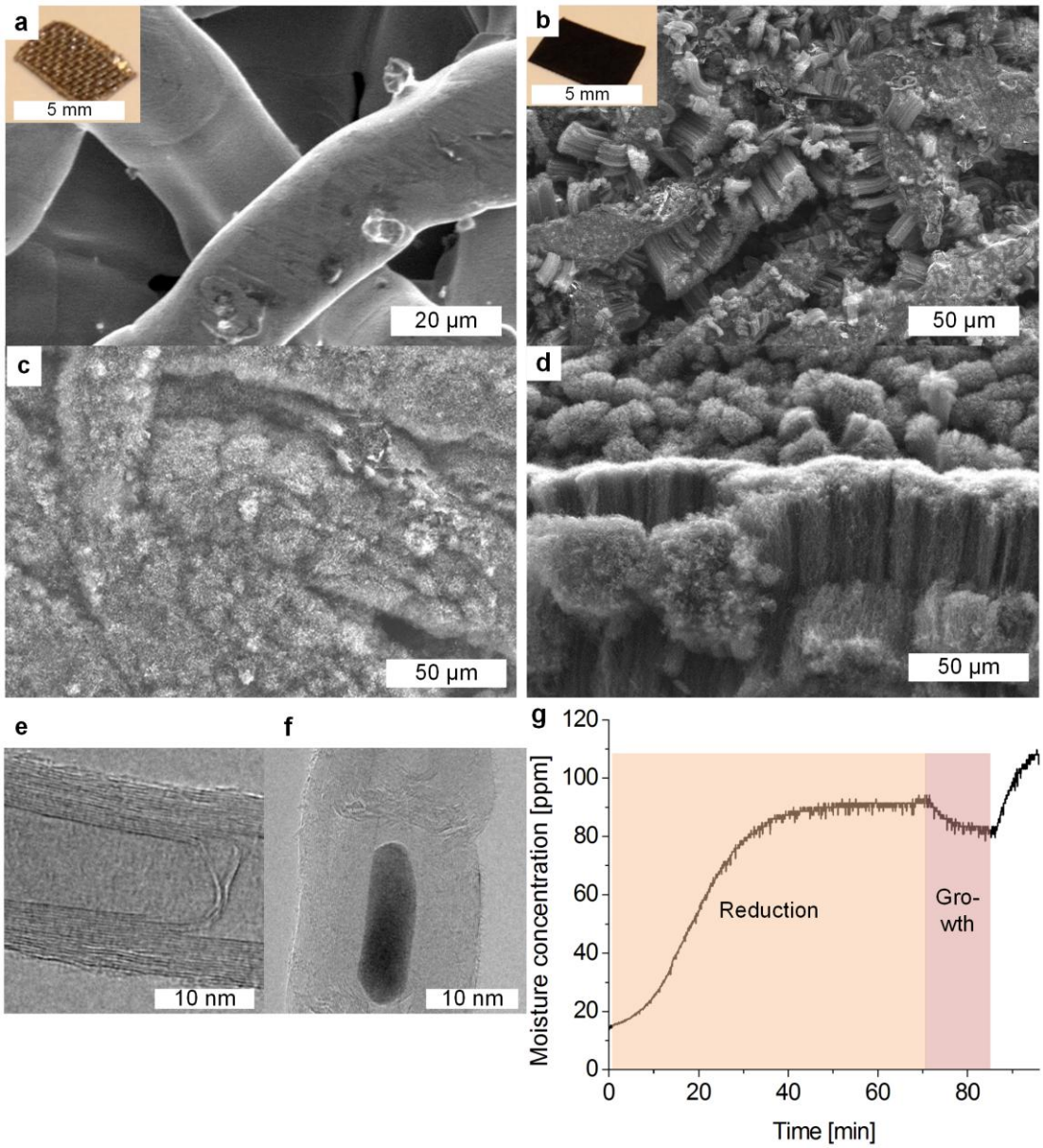

Figure 5.2: Direct growth of aligned forests achieved on native surface of Haynes 556 fiber mesh. (a), as arrived Haynes 556 fiber mesh. (b), aligned forests obtained from native surface of Haynes 556 fiber mesh by standard Haynes recipe. (c), Inconsistent growth result: a few months later, aligned forest no longer showed up with standard Haynes recipe. (d), Consistent growth of aligned forests guaranteed by He/H_2O tank assisted Haynes recipe. (e), (f), TEM images of CNTs grown from Haynes 556 alloy. (g), Record of moisture level during reduction stage and growth stage when using He/H_2O tank assisted Haynes recipe.

5.4.2 Impact of moisture at different stages during synthesis process

Moisture concentration in the growth system can be adjusted by driving a small portion of He flow through the water bubbler, as introduced in Chapter 2. A series of 3 experiments are then designed to have rich moisture concentration (~400ppm) during reduction stage, growth stage, or both reduction and growth stages. Substrates used in this section are 5mm by 5mm square samples cut from the flat Haynes 556 alloy sheet (0.12-0.13 by 12.00 by 12.00 inches).

Applying the decoupled Haynes recipe, the reduction stage and growth stage can be operated with different moisture concentration without crosstalk. The records of moisture concentration for these three trials are plotted on Figure 5.3a, and the growth results of these three experiments are showing on Figure 5.3b-g.

The Haynes recipe with moisture assisted reduction doesn't provide aligned forests. Zoomed in SEM image (Figure 5.3c) shows there are tangled CNTs grown around micro/nano clusters on the substrate surface. These clusters may be a mixture of amorphous carbon along with metal/metal oxides on the sample surface. On the other hand, the remaining two experiments both show successful growth of aligned forests. Images from Figure 5.3d&e demonstrate aligned forest grown by Haynes recipe with moisture assisted growth, and so did images from Figure 5.3f&g for moisture assisted Haynes recipe. Such results indicate the present of moisture during the CNT synthesis on Haynes556 alloy is similar to regular CNT forest growth on Si substrate (introduced in Chapter 3&4). Presence of moisture at the beginning of hydrocarbon exposure can possibly help etch amorphous carbon deposited on catalyst particles, thus improving activation. Considering the very high carbon concentration on He/H_2 reduced Haynes 556 surface (35.57%, atomic ratio), the presence of water becomes necessary for CNT forest growth on Haynes 556 alloy.

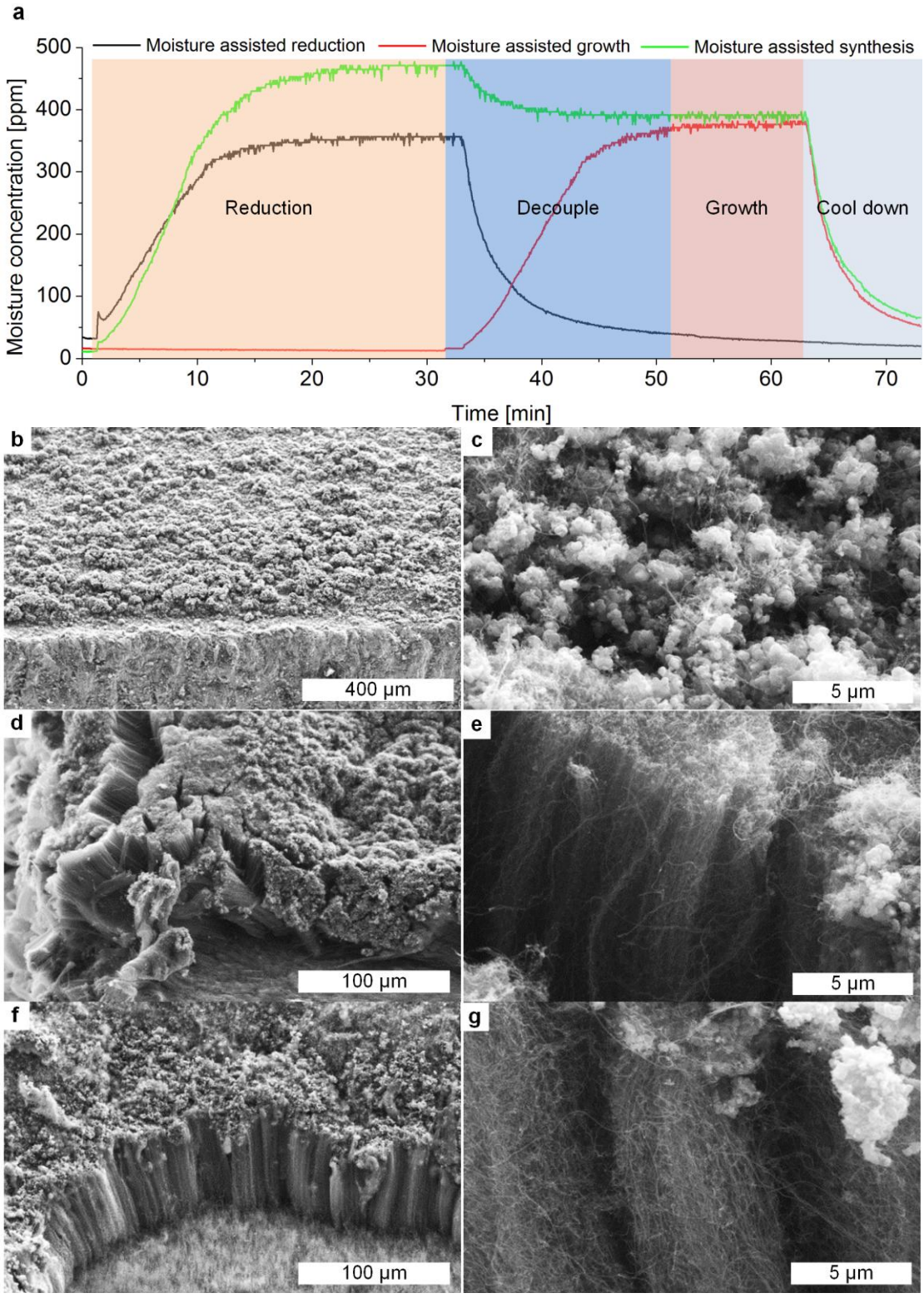

Figure 5.3 Importance of moisture during reduction and growth stages. (a), record of moisture concentration after oxidation stage. (b), (c), SEM images of as grown sample produced by Haynes recipe with moisture assisted reduction. (d), (e), SEM images of as grown sample produced by Haynes recipe with moisture assisted growth. (f), (g), SEM images of as grown sample produced by moisture assisted Haynes recipe.

5.5 Restore of CNT forest on previously grown substrates

Direct growth of aligned forest on native surface of Haynes 556 alloy can be considered as a cost-effective manufacturing process. Furthermore, it is also important to think about recycling and refurbishment of the CNT-Haynes 556 alloy hybrid product. Haynes 556 alloy could be used in high temperature and chemically harsh environments due to its high melting temperature and good resistance to carbon/acid corrosion. On the other hand, the CNTs grown on Haynes 556 surface may not last as long as the Haynes556 media. Although Pall Corporation did not provide detailed directions for future application, it is still important for us to consider the case that the CNTs could be worn out due to certain application uses. In the practical applications, CNT forests grown on the surface can be worn out in many different ways, including but not limited by mechanical damage, high temperature oxidation, and chemical corrosion. Considering Haynes 556 alloy itself is a relatively expensive material, an economic solution will be to re-grow aligned CNT forest on old Haynes 556 samples whose forests have been damaged.

To test whether CNTs can be grown again after removal from the metal surface, as grown samples are sonicated in 2-propanol to remove the CNTs (Crest Ultrasonics Model 1100D, 10 minutes, power setting 9). The majority of CNTs are taken off during the sonication, but there are still remaining tangled CNTs attached with surface of substrate (Figure 5.4a). Such a substrate treated by sonication is called a “worn out” substrate. The remaining CNTs will be cleaned off during the air oxidation stage for the subsequent growth process (Figure 5.4b, sample baked in air at 875 ℃ for 5 minutes). The “worn out” substrate is then sent to the furnace for refurbishing and follows the Haynes recipe with moisture assisted growth, resulting in re-grown CNTs as shown in Figure 5.4e&f. Comparing with forests grown from a brand new substrate (Figure 5.4c&d), the height of the “refurbish” forest is slightly shorter, and the alignment of CNTs also looks worse for the refurbish sample.

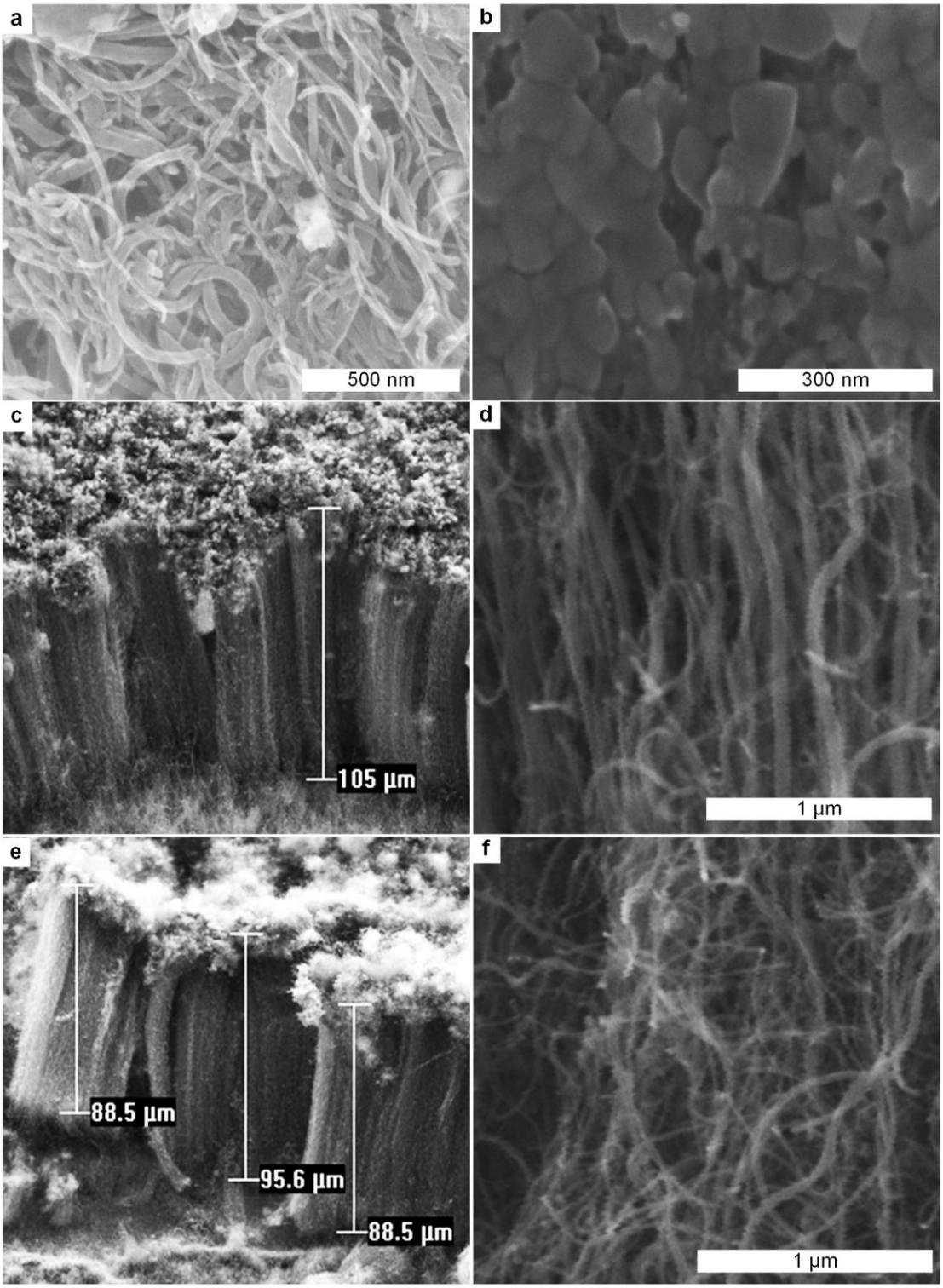

Figure 5.4 Restore of CNT forests on a piece of as grown substrate. (a), SEM images of as grown substrate after sonication. (b) sonicated sample after short baking in air. (c), (d), CNT forest grown from a brand new Haynes556 substrate. (e), (f), CNT forest grown from a "worn out" Haynes556 substrate.

One reason for the degradation of growth results could be the loss of catalyst particles. As shown in Section 5.4.1, a portion of the CNTs grown from Haynes 556 alloy is due to the tip-growth mechanism. Catalyst particles will be kept in the cap of CNTs when growth followed such a mechanism. Then after the CNT forest are "worn out", the catalyst particle density on surface of Haynes 556 substrate is going to be lower. For the refurbish process starts on a degraded surface, it is reasonable to expect the quality of CNT forest will be poorer. The change of elemental composition on substrate surface could be another reason for the growth degradation. As listed on Table 5.2, concentration of Fe is decreasing from air oxidation to He/H_2 reduction, while the concentration of Cr is increasing. The refurbishment process will repeat the Haynes recipe with moisture-assisted growth again, which may cause a further decay of Fe concentration on the substrate surface.

5.6 Impact of heat treatment on forest growth kinetics

Previous study on refurbished substrates indicates the duration of heat treatment has significant impact on growth results. In order to further explore the impact of heat treatments prior to CNT growth, a series of experiments are performed using the Haynes recipe with moisture assisted growth. Results in Figure 5.5 show that the duration of heat treatment significantly affects the height of forests. Detailed data are also shown in Table 5.3.

Growth results from no oxidation and no reduction show there is any forest grown on Haynes 556 alloy. This agrees with the discussion about feasibility of growing aligned forest on native Haynes 555 surface, as mentioned in Section 5.3.

Aligned forests are found with 30 minutes oxidation only recipe, which indicated the reduction of metal oxides can also happen during hydrocarbon exposure. On the other hand, short but aligned forests are also observed from samples treated only with 30 minutes of reduction but no oxidation. The existence of aligned forest indicates that a sufficient amount of Fe and Cr to support aligned forest growth is brought onto the surface of substrate during the 30 minutes of He/H_2 annealing. Then the presence of moisture helps to etch off the carbon contamination on substrate surface and activate catalyst particles for forest growth.

Furthermore, when both oxidation and reduction are performed before hydrocarbon exposure, there are always aligned forests grown on the Haynes 556 alloy. As heat treatment duration

increases, taller and taller forests can be obtained. Since all experiments are carried out with the same 10 minutes of growth time, the increased heat treatment duration is suggesting faster growth rate of forests.

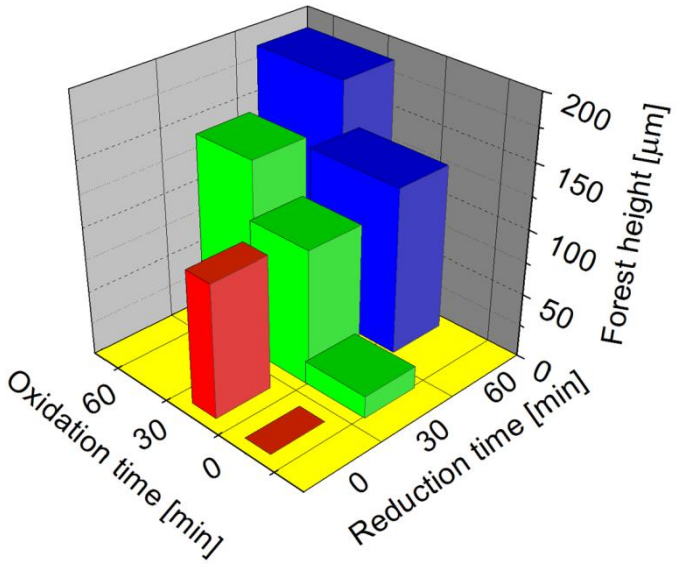

Figure 5.5 Forest height affected by heat treatment. For the forests grown on brand new Haynes 556 substrates, increased heat treatment duration from 0-60 minutes will help to obtain taller forests.

Table 5.3 Impact of heat treatment duration on forest height

Forest height (μm)		He/H2 reduction time (min)		
		0	30	60
Air oxidation time (min)	0	0.00	17.43	N/A
	30	103.77	105.00	129.33
	60	N/A	150.67	189.50

5.7 Conclusion and future directions

In this study, direct growth of aligned forest is first proved to be possible on native surface of Haynes 556 alloy, without deposition of support layer or external source of catalyst. Study on controlled supply of moisture then reveals the present of water during growth stage is critical to obtain aligned forests. This growth technique is also able to re-grow aligned forest again on a previously grown substrate, after the CNT forests are removed by sonication. Considering Haynes 556 based product may be used in harsh environments that lead to etching of CNTs, re-growth of CNTs on a previously worn out Haynes 556 substrate is a cost-effective solution in large scale manufacturing. Finally, a study related with heat

treatment is carried out, showing that it's necessary to provide heat treatments before hydrocarbon exposure in order to obtain aligned forest. Within the studied time frame of 0-60 minutes, increased heat treatment duration for either oxidation or reduction can both improve the growth rate of CNT forest.

Although a simple technique is developed to grow aligned forest on Haynes 556 alloy in this study, there are still things to be discovered in the future. The issue of degradation of catalyst density after growth needs to be solved, in order to provide consistent quality of products even after refurbishment. This topic can be studied together with the impact of heat treatment on growth behavior. The growth kinetics affected by heat treatments can be related with the evolution of elemental composition on surface of Haynes 556 alloy, and provide further feedback to improve the forest manufacturing technique on Haynes 556.

CHAPTER 6
CARBON NANOTUBE ENHANCED POROUS STAINLESS STEEL FILTER FOR GAS PURIFICATION

Work described in this chapter seeks to improve the particle capture efficiency of commercial stainless steel filter (Pall Corporation) by direct growth of carbon nanotubes. The project sponsor, Pall Corporation, stated the goals as maximizing particle capture efficiency while limiting the pressure drop across the enhanced filter to be less than 15-20 psi. In order to achieve the goal of this project, tangled CNTs are grown from the native surface of sintered porous stainless steel material. Uniform synthesis of CNTs throughout a centimeter-scale filter assembly is first demonstrated. Then, it is found that the pressure drop is related to the CNT synthesis conditions, including growth time and moisture concentration. After that, retention tests are applied to the CNT enhanced porous filter and demonstrate the particle capture efficiency can be improved up to 8 orders of magnitude. Finally, a model showing relationship between pressure drop, particle capture efficiency and CNT packing ratio is established, and provides an analytical explanation about the behavior of particle capture.

6.1 Background and introduction

Particle capture and filtration technology is widely used in nowadays industrial applications [97, 98], such as water purification [99, 100], gas coalescing [101], and exhausts gas treatment [102, 103]. Among all different materials used to make filtration deceives, stainless steel is one of the most attractive choice due to its inexpensive price.

This project was motivated by Pall Corporation, seeking to improve the performance of their existing stainless steel micro porous filter. These filters are called ‘PSP cups’, and are made of sintered micro-scale stainless steel powder. The picture of PSP cup and its microstructure can be found in Figure 6.1a&b. The body of the PSP cup filter includes two parts: a closed piece of porous media and a circular holder plate. This PSP filter is used to capture particles from high-purity gas streams, as schematically shown in Figure 6.1c. This device can be used to remove solid impurities from gas steam, such as suction flange of rotary pump, filter media

of air conditioner, exhaust gas treating apparatus. According to the information provided by Pall Corporation, when tested with aerosol of 20 nm in diameter, only about 10% of solid particles are remaining in the gas stream after passing through the PSP filter, and the pressure drop across the filter is less than 1 psi (details will be described in Section 6.2, Methods and experiments). My project aims to improve the performance of PSP filter, by maximizing the particle capture efficiency, while remaining the pressure drop across the enhanced filter to be less than 15~20 psi.

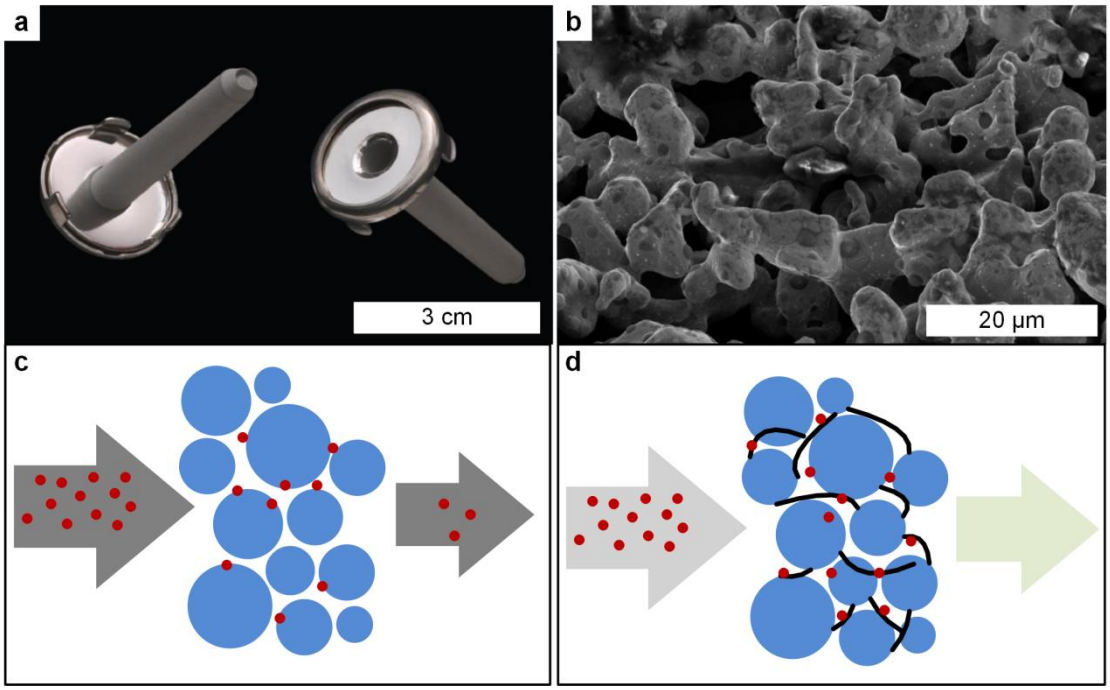

Figure 6.1: Micro porous filter provided by Pall Corporation (a), photo image of micro porous filter. (b), SEM image of micro porous filter surface. The filter is made of sintered SS micro particles, with an average diameter about 20 µm. (c), sketch of filtration process. Stream of gas with solid particles is driven through the micro porous filter, and about 90% of the particles will be captured by this micro porous filter. (d), goal of this project: enhance the filtration performance by integrating tangles CNTs to original micro porous filter.

In order to improve the performance of the filter, a smaller pore size and higher packing fraction is demanded. Because the original PSP filter is made of sintered micro SS powder, the pore size can be decreased to nanometer scale by growing CNTs on the original filter. Tangled CNTs will fill into the micro pores on the PSP cup filter, and form 3D nano-porous structures. Considering the filter was operated at a pressure about 40-50 psi, strong adhesion between CNTs and the porous filter is required, in order to avoid CNTs coming off the SS substrate during particle capture process. Furthermore, limited by the cost of product, the manufacturer also required the CNT growth technique to be as cost-effective as possible.

Taking advantage of SS powder material, which is a good source of catalyst for CNT growth, the best way to achieve strong adhesion between CNTs and the filter with a low cost manufacturing process is to grow CNTs directly on the native surface of PSP filter without external catalyst.

Growth of CNTs on SS substrates has been extensively studied by previous researchers. CNTs can be grown from SS substrate with external support and /or catalyst [92, 104-107]. For example, Lee et al reported aligned CNTs grown from SS mesh with electron beam deposited Al_2O_3 support and Fe catalyst [104]. Masarapu et al [105, 108] achieved multi-wall CNTs using ferrocene and xylene on SS foil with surface cleaned by sulfuric acid. Lepro et al [92] didn't use external catalyst but they deposited thin SiO_x on SS foil as buffer layer. On the other hand, direct growth of CNTs without any external catalyst or support can still be achieved with various different conditions. Yuan [109], Park [110], Vander [111] and Baddour [112] demonstrated CNT growth on SS 304 substrates without external catalyst. Karwa et al [113] reported aligned CNT forest growth on SS 316 tubing, using C_2H_4 at pressure of 275 kPa. Camilli et al [114] also reported CNT growth on SS 316 substrate, but they chose to supply C_2H_2 at 12 torr (1.6 kPa) and obtained tangled CNT growth. The PSP cup filters are made of 316L stainless steel, which is very similar compared to the SS substrates that had been studied in the past. Integrating CNTs on the native surface of PSP cup body is not the most challenging aspect of this project. Rather, controlling of CNT morphology which influences the relationship between filtration performance and pressure drop is most critical. As described earlier, this project aims to tangled CNT growth on porous media instead of aligned forest growth, so C_2H_2 is chosen to be the hydrocarbon source instead of C_2H_4.

In this study, tangled CNTs are directly grown uniformly throughout the entire porous filter, without requiring any external catalyst or support layer. In order to achieve such growth results, additional oxidation/reduction on porous media is required prior to CNT growth. In this chapter, a design of quartz holder is first introduced for PSP cups, which provided non-contact alignment of the cup body in the CVD system and enabled uniform growth. Then the fabrication process is introduced, along with a demonstration of uniform growth. After that, a series of study related with pressure drop across the enhanced filter is carried out. This study indicates the proper growth time and moisture concentration that would meet Pall's requirements. Later, retention tests are performed CNT enhanced PSP cup filters, showing

that the filtration performance of the original filter could be improved by CNTs as high as 8 orders of magnitude. But the greater improvement of filtration performance is always accompanied by greater pressure drop. Finally, an analytical model is developed, and explains why it is not possible to achieve great improvements of filtration performance while maintaining relatively low pressure drop.

6.2 Methods and experiments

6.2.1 Design of sample holder

As shown in Figure 6.1a, the porous filter is welded on the holder plate, and the whole body of PSP filter becomes a "T" shape. When laying this T-shape body on a typical flat quartz boat (Shown in Chapter 2), there is always going to be a spot on the porous media that direct contacts with the quartz boat, and further leads to uneven growth around that spot. Such defect growth effect can be observed in Figure 6.2a, labeled with red circle. It is clear that the contacting spot showed a much lighter color compare to surroundings, which suggested much less dense of CNT growth. Furthermore, in such an orientation, the whole filter is going to experience uneven flow and temperature distribution through its own body, which may cause non-uniform CNT growth.

In order to achieve uniform growth on this porous media, a specialized quartz holder is designed for PSP filter, as shown in Figure 6.2b. During the growth process, the holder plate is sitting in a pair of slots on the holder, and keeps the porous media lying parallel to the direction of flow. Because the porous media would have no physical contact with the quartz holder, gas stream is going to flow all the way around the porous media, and then uniform growth of CNTs could be achieved.

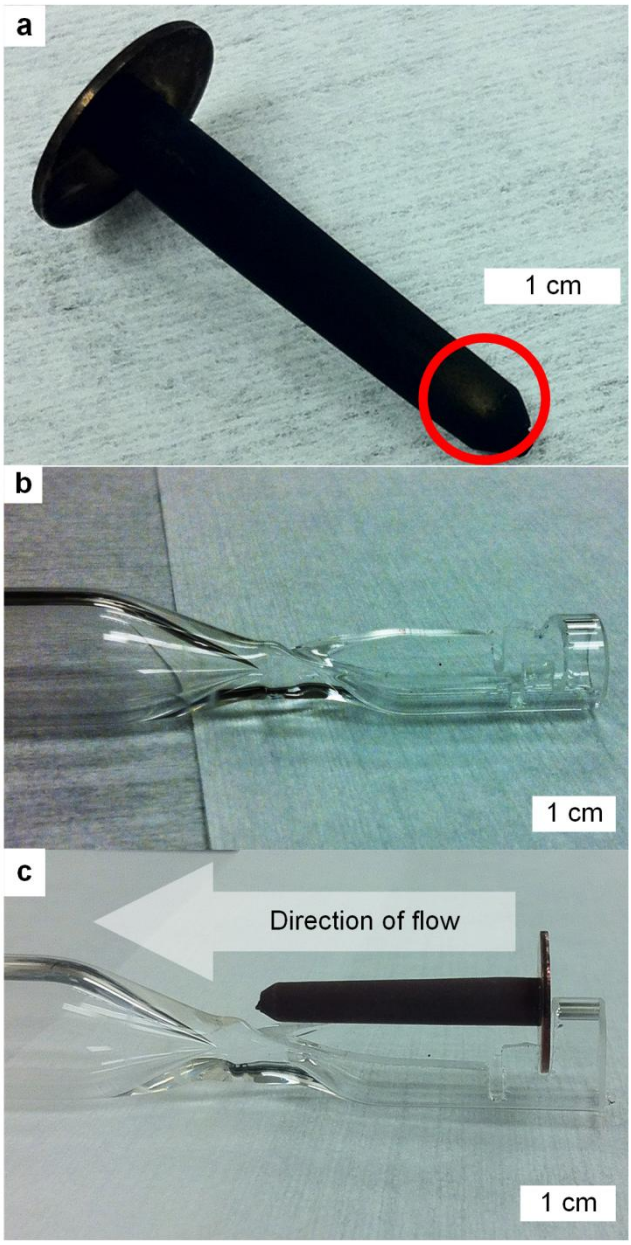

Figure 6.2: Design of PSP filter holder. (a), defect detected from as grown PSP filter if the substrate is laid down directly to a typical flat quartz holder. (b), specialized quartz holder for PSP filter. (c), alignment of PSP cup on special holder.

6.2.2 Growth recipe

All growths were carried out with the transfer arm system as described in Chapter 2. The experiments generally followed the same style of recipe as shown below, and in some cases the recipe is adjusted according to specific requirements of study:

Step 1 (oxidation): PSP filter is loaded at 7cm downstream from the center of the furnace. It is oxidized in air (100 sccm, extra dry air, Cryogenic Gases) at 500 ℃ over 60 minutes, and cools down to room temperature.

Step 2 (purge): Sample still sits at the same spot as previous step. He (1000 sccm, 99.999% Cryogenic Gases), C_2H_2 (50 sccm, grade AA acetylene, dissolved, Cryogenic Gases) and CO_2 (50 sccm, carbon dioxide USP grade 2.2, Cryogenic Gases) are used to purge the system for 5 minutes at room temperature.

Step 3 (reduction): After that, the flow is switched to He (100 sccm) and H_2 (400 sccm, 99.99%, Cryogenic Gases) for another 5 minutes. The furnace is then heated to 775 ℃ over 10 minutes with the same flow. After the temperature reaches 775 ℃, the temperature and flow are both held the same for another 10 minutes.

Step 4 (decouple): At the end of the reduction stage, substrate is transferred out of the heated region, and then same flow as during the reduced stage is kept for another 2 minutes. Then, 20 sccm of C_2H_2 and 20 sccm of CO_2 are also added to the system. 1 minute later, H_2 is shut off and the flow rate of He is increased to 560 sccm. This flow is kept for another 7 minutes.

Step 5 (growth): Sample is then transferred to the same spot as it was oxidized and reduced. Same flow is kept over another 3 minutes for growth. The duration of growth can be adjusted according to requirement of study.

Step 6 (post-treatment): At the end of growth, power to the furnace is shut off and the cover of furnace is opened. Substrate is then transferred out of the heated region. The same flow as in the growth stage is kept for another 5 minutes, and then switches to 1000 sccm of He until the sample is cooled down.

Growth on the PSP filter can also be assisted by the present of moisture. In order to introduce a controllable amount of moisture to the growth system, the regular He tank is replaced by a calibrated He/H_2O tank (A31 100 ppm H_2O in Helium, certified mixture, CGA 580 top pressure 500 psi, Cryogenic Gases).

Furthermore, the concentration of carbon source can also be adjusted depending on the objective of study. The flow rate of C_2H_2 and CO2 is always kept as 1:1 in this study, and the total flow rate during growth is always 600 sccm. So the concentration of hydrocarbon can be defined as flow rate of C_2H_2 over total flow rate. In this study, 3.3% (20 sccm) and 1.7% (10 sccm) of C_2H_2 concentrations was used for CNT growth.

Again, as mentioned in Chapter 3, to prevent contamination from batch to batch, oxidation is carried out at elevated temperature (875 ℃) in the presence air flow, for a period of 30 minutes.

6.2.3 Characterization

Scanning Electron Microscopy (SEM) images of the CNT forests are taken by using a Philips XL30 FEG SEM with a working distance of 10 mm and electron beam voltage of 10 kV, and FEI Nova 200 Nanolab SEM with a working distance of 5 mm and electron beam voltage of 10 kV.

Pressure drop across the CNT-enhanced PSP filter was generated by a flow cell setup. The layout the flow cell setup is shown in Figure 6.3. The PSP filter is installed in the holder cell provided by Pall Corporation. There is a pair of pressure transducers before and after the PSP filter, in order to record the pressure drop across the filter. The flow through this filter cell can be controlled either by the manual flow controller or digital flow controller. A pair of three-way valves is also installed before and after each flow controller, so the controllers can be enabled or bypassed.

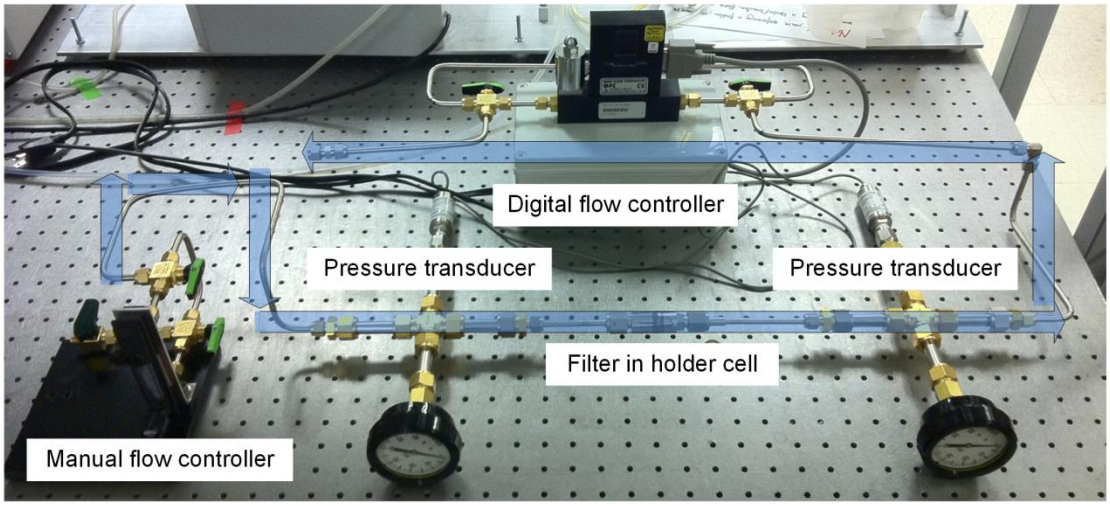

Figure 6.3 Setup of flow cell used to test pressure drop across PSP filter.

The pressure drop test follows the procedure below:

Step 1: The as grown CNT-PSP filter is installed in the holder cell. Manual flow controller is enabled and digital flow controller is bypassed. Inlet pressure is set to 50 psi. 5 L/min of air flow is processed through the filter for half an hour. Then the air flow is stopped.

Step 2: Manual flow controller is bypassed and digital flow controller is enabled. 6 L/min of air flow is processed through the filter for half an hour, and readings from pressure transducers are recorded by a Labview program.

Step 3: The air flow is shut off, and both manual and digital flow controllers were bypassed.

The system is left standing by for another 10 to 15 seconds so that the remaining pressure built up in the holder cell is released. Then the holder cell is unfastened and the filter was taken out.

The pressure drop across the filter is obtained from an average of data recorded from the 24^{th} minute to 26^{th} minute.

Retention (particle capture) test is carried out by Pall Corporation at Cortland, NY. NaCl aerosol particles are generated with air flow, and then driven through the enhanced filter at a flow rate of 5 L/minute with a head pressure of 50 psi. The diameter of NaCl particles is about 20 nm, and the concentration of NaCl particles in the air flow is $7.8x10^7$ particles/L. There is a particle detector downstream to count the concentration of particles after the enhanced filter. The performance of enhanced filter is described by retention rate, which is upstream the concentration of NaCl particles over the downstream concentration of NaCl particles. The whole retention test takes 15 minutes, and the final retention rate is the average of the record from the entire 15 minutes.

6.3 CNT growth results on PSP cups

At the starting stage of this project, growths were carried out when the PSP cup directly laid on the inner wall of quartz tube or sit on top of a flow quartz boat. As introduced in Section 6.2.1, non-uniform growth of CNTs can even be observed by eye. So a specialized quartz holder shown on Figure 6.2b&c is designed to provide uniform growth of CNTs on PSP filters. Uniform and tangled CNTs are obtained throughout the entire body of porous media with this holder, as shown in Figure 6.4. Figure 6.4a is a photo picture of cracked PSP porous media before growth, and this picture is used to show the spots that were going to be taken SEM images after CNT growth. Here the photo picture was taken on a different filter before growth because the CNT enhanced porous media is too dark to provide a detailed photo image. The enhanced filter is grown for 5 minutes, and then cracked for SEM imaging. Three spots are chosen here in order to demonstrate the uniformity of CNT growth: Figure 6.4b stands for the growth on outer surface of the filter, Figure 6.4c stands for the growth penetrated into the body of the filter, and Figure 6.4d stands for the growth on the inner surface of the filter.

From Figure 6.4b, c and d, it is clear that the densities of tangled CNTs are similar among all these spots. More spots through the wall of this hollow cylindrical filter are also examined,

and the growth turns out to be very uniform from the top to the end of the porous filter, as best as can be determined from SEM images.

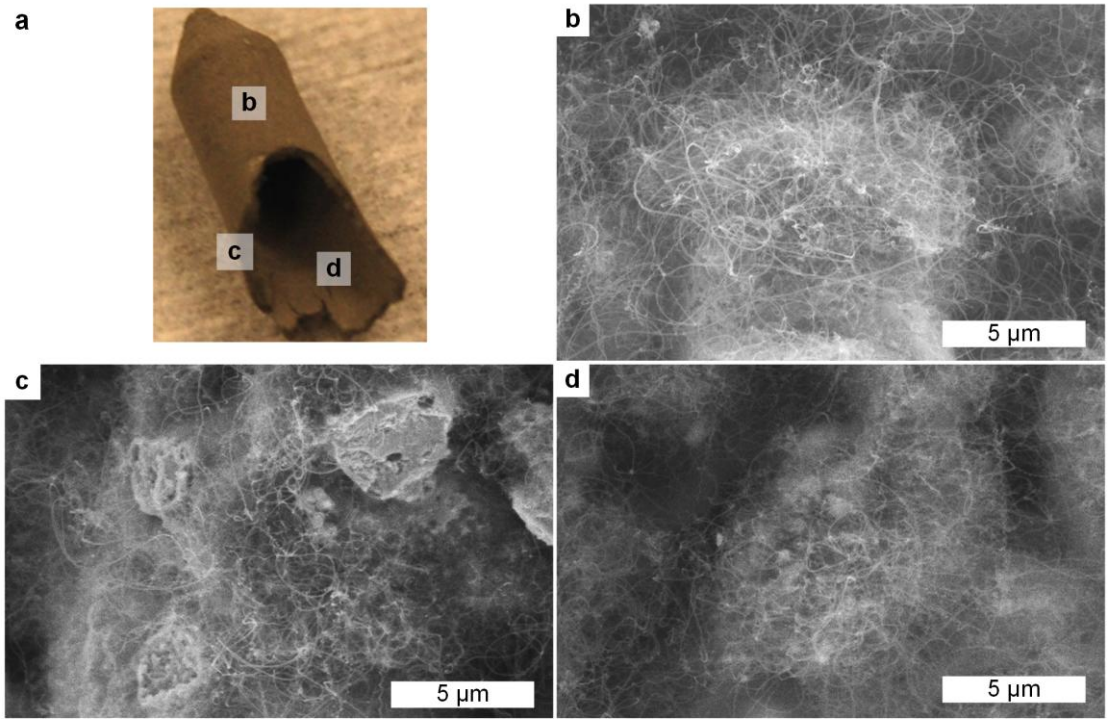

Figure 6.4 Uniform growth of tangled CNTs achieved through the entire porous media. (a), photo picture of a cracked filter before growth. The picture is taken to demonstrate the spots that are going to be examined for uniformity of growth. Labels b, c and d stands for the spots where SEM images in b, c and d are taken. (b), (c), and (d), SEM images of as grown sample. The density of tangled CNTs looks similar at each different spot.

6.4 Pressure drop across the enhanced filter

6.4.1 Evolution of pressure drop according to growth time

The density of CNTs grown in micro porous between sintered SS powder is going to change according to growth time, and density (packing ratio) of CNTs in porous media is going to determine the pressure drop across the filter and the particle capture efficiency of the filter. It is necessary to understand the impact of growth time on pressure drop in order to manufacture the enhanced filter that meets the requirements from Pall. A group of experiments with different growth time from 30 seconds to 7 minutes is carried out, and the result is shown on Figure 6.5a. The pressure drop of the enhanced filter increases according to growth time for the first 5 minutes, and then decreases for the growth time greater than 5 minutes. Figure 6.5b shows a record from the 30 minutes pressure drop test on an enhanced filter grown for 3 minutes.

The pressure drop of the enhanced filter had a relatively small increase for growth time less or equals 2 minutes. Less than 5 psi of pressure drop is observed for enhanced filters with growth time of 1 and 2 minutes, while pressure drop for filters grown for 3 minutes or more is above 15 psi. This is due to the warm up of the porous media. As mentioned in Section 6.2.2, samples at room temperature are going to be transferred into furnace for growth. Unlike the 8mm by 4mm by 0.5mm silicon chips studied in Chapter 3&4, the PSP filters in this project take much more time to heat up due to their much heavier mass (~40 mg for Si chips and ~800 mg for PSP cups). According to the pressure drop from Figure 6.5a, it might take about 2 minutes for the temperature of the PSP filter to rise from room temperature to growth temperature. The decay of pressure drop after 5 minutes indicates the growth of CNTs is terminated, and the existing CNTs will be destroyed in the growth atmosphere after catalyst is deactivated for growth.

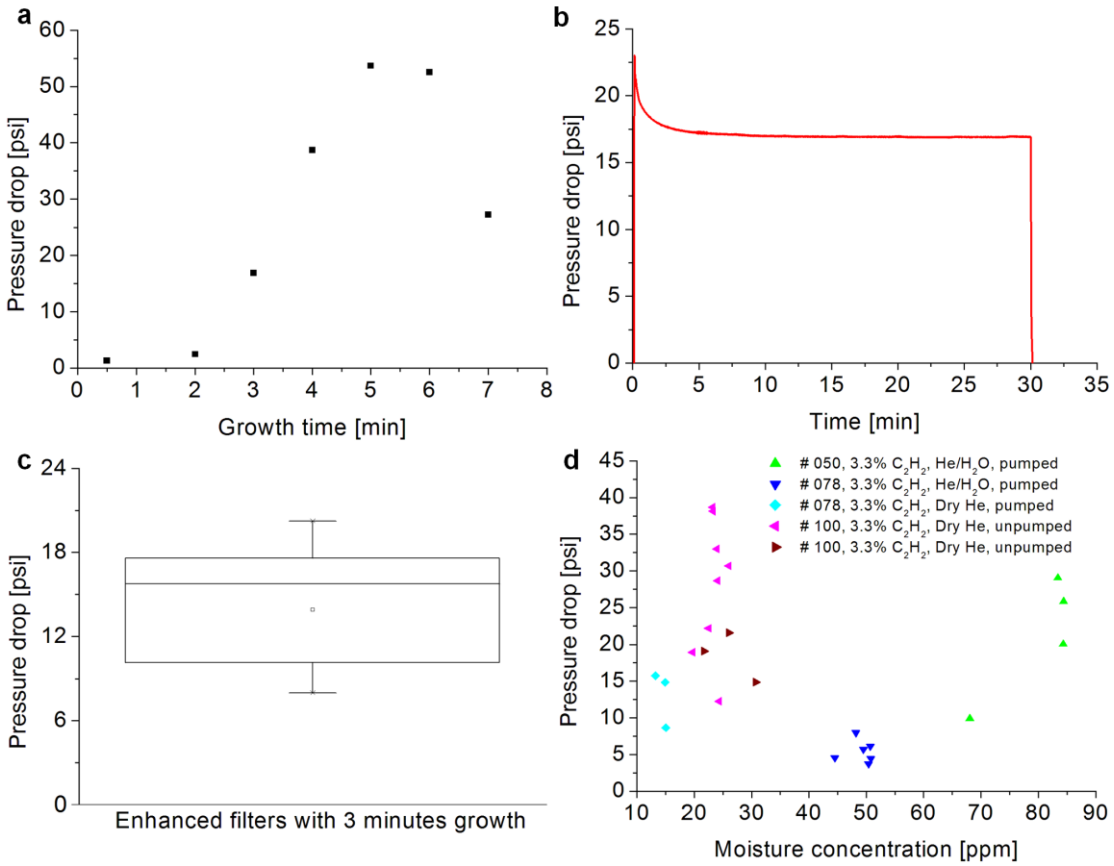

Figure 6.5 Pressure drop across enhanced filter affected by growth time, moisture concentration and hydrocarbon concentration. (a), Pressure drop according to different growth time. (b), record of pressure drop collected from an enhanced filter grown for 3 minutes. (c), variance of pressure drop among repeated experiments with the same condition. (d), pressure drop affected by moisture and gas delivery control.

6.4.2 Consistency of production

From the study of different growth time, 3 minutes of growth looked like the most appropriate growth time in order to improve the performance of PSP filter while keeping the pressure drop still below 20 psi. So another series of repeat study is carried out to test the reliability of this technique. Unfortunately, the performance of pressure drop is very inconsistent according to repeat experiments. As plotted in Figure 6.5c, 10 repeat experiments are taken during one month of study with the same growth conditions, but the pressure drop varies from about 8 psi to 22 psi, with a mean value about 15psi. Such fluctuation will not be acceptable in industrial production, and further study is necessary to understand the possible factors that cause the huge fluctuation.

6.4.3 Impact of moisture and residue impurities in CVD system on pressure drop

Similarly as the study mentioned in Chapter 5, the collaboration with Pall was initiated earlier than the study of growth consistency (Chapter 3). So at the beginning of this study, the importance of moisture in growth system was not addressed, and the work of consistency improvement in our lab [39] had not yet completed. Going along with other studies that improves the general consistency of experiments in our lab, enhanced PSP filters are produced in varies condition during the 1.5 years of study, and the results are shown in Figures 6.5d. For the discussion in this section, it is assumed that higher pressure drop is caused by higher packing fraction of CNTs. The analytical model that is going to be introduced in Section 6.6 states this assumption is correct.

The #050, #078 and #100 stand for the different batches of raw PSP filters provided by Pall Corporation, and the concentration of C_2H_2 indicates composition of gases supplied during growth, as introduced in Section 6.2.2. At the beginning of this study, regular He supply (dry He) is used for CNT growth. And as study goes on, the importance of moisture is noticed, and calibrated He/H_2O tank is used in order to obtain different moisture concentration during growth.

The pumped/unpumped label states the status of common gas delivery system in our lab. As introduced in Section 6.2.2, the flow rate of C_2H_2 and CO_2 is low compare to other gases, and these two gases are seldom used for other projects in our lab (10~20sccm and 100~1000 sccm). As a result, moisture and other residues from the ambient could diffuse into the gas delivery lines, which then cause unpredictable fluctuation of growth results. Furthermore,

since the C_2H_2 and CO_2 lines are rarely used, the contamination from ambient is going to cumulate even more significant compare to He or H_2 lines which are frequently used at a relatively high flow rate. The pumped label indicates the gas delivery lines are regularly pumped down every two weeks, so that the gases in delivery lines could be regularly vented and then refilled with gas tanks. The unpumped experiments (#100 batch samples) were completed before the pump down policy is established in our lab, which suggests the gas composition in C_2H_2 and CO_2 lines could be very random.

As shown on the left part of Figure 6.5d, the unpumped experiments lead to a pressure drop from 12 psi to 40 psi. Such huge fluctuation may be contributed by the residues and impurities in C_2H_2 and CO_2 lines. Gases delivered through these lines might bring unstable levels of oxygen caused by the diffusion from ambient air to the growth system. Presence of oxygen will not be detected by the hydrometer, but will take an important role during CNT growth. Comparing the samples produced with and without regular pump down, it is clear that for the same moisture concentration, the regularly pumped down lines can provide much better consistency with respect of pressure drop for enhanced PSP filters.

Then looking at the samples produced with pumped lines only. A "U-shaped" relationship between pressure drop and moisture concentration is observed. Pressure drop across the enhanced filter is about 10-15 psi with less than 20 ppm of moisture during growth. As moisture concentration increased to about 40-50 ppm, the pressure drop of the samples decreases below 10 psi. Then as moisture increases to 70-90 ppm, another significant increase of pressure drop is observed. The detailed reason of such trend between pressure drop and moisture level is not clearly understood yet. My hypothesis is the presence of moisture can impact the CNT growth via multiple mechanisms during the CVD process, and some of the mechanisms may have opposite response as the concentration of moisture increases.

Besides the data plotted on Figure 6.5d, there are also samples from batch #078 and #050 that are prepared with 40-50 ppm moisture and 1.7% of C_2H_2. The pressure drop of these samples was about 2-4 psi, slightly lower than 5-8 psi that obtained from #078, 3.3% C_2H_2 and 40-50ppm of moisture. The data obtained from 1.7% C2H2 was not plotted on Figure 6.5d since the trend was straight forward: diluted supply of hydrocarbon during growth would lead to less intense growth of tangled CNTs and lower pressure drop across the CNT enhanced

PSP filter. From the record of repeat experiments, fluctuation still exists even with pump down of gas delivery system and control of moisture between 40-50 ppm. The remaining fluctuation might be due to the following reasons: First, the fluctuation came from the raw PSP filters. The raw filters have a pressure drop about 0.5-0.6 psi, which is a much narrower distribution. But such fluctuation in pressure drop is based on micrometer scale features, and could be scaled up after grown with tangled CNTs. Second, human error introduced during synthesis. The current design of transfer arm is operated manually, which would introduce a batch to batch error when transferring samples in and out during synthesis process. Growth kinetics could be very different with different temperature that the filter arrives at the growth spot, and this arrival temperature could be significantly affected by the transfer in speed before growth stage.

6.5 Particle capture performance of enhanced filter

Enhanced PSP filters with different pressure drops are taken to Pall Corporation for retention test. Although the final product requires an operation pressure drop no greater than 15-20 psi, it is still valuable to study the retention property at different pressure drops. Several tests are taken with enhanced filters with a pressure drop from 2 psi to about 50 psi, and the results are shown on Figure 6.6 along with the performance of raw PSP filters.

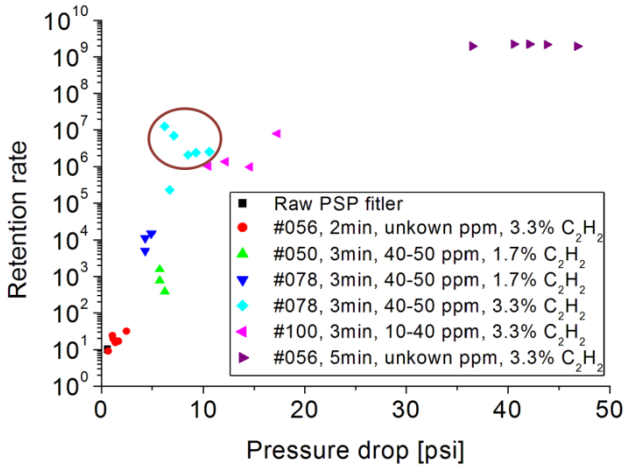

Figure 6.6 Retention rate of enhanced PSP filter versus pressure drop. Retention rate always increases with increased pressure drop across enhanced filter, but the improvement of retention is most significant during the first 10 psi.

As explained in Section 6.2.3, the retention rate is calculated by the concentration of particles in upstream over that in downstream. From Figure 6.6 it is clear that the raw PSP filter has a retention rate about 10, which means 90% of the particles are captured. The performance of

enhanced filter grown for 2 minutes is closed to the raw filter, which indicates the amount of CNTs grown on this filter might be very limited. On the other hand, PSP cups from the same batch (#056) grown for 5 minutes show incredible improvement of retention performance. Although the pressure drop of the 5 minutes #056 group is too high to meet the requirement for this project, it is still stating tangled but dense CNTs are very good material to capture particles about 20 nm in diameter.

Generally, an increased retention rate is demonstrated along with increased pressure drop of enhanced filter. But the improvement of retention performance is more significant during the first 10-20 psi of pressure drop. Pall Corporation is satisfied with the enhanced filter produced by 3.3% C_2H_2 with 40-50 ppm of moisture, which provides a retention rate about 10^5~10^7 while only have a pressure drop around 10 psi (labeled with red circle in Figure 6.6). In order to further understand the limit of this improvement, an analytical model is established to describe the behavior of pressure drop and retention performance based on CNT packing ratio in the enhanced filter.

6.6 Modeling of pressure drop and particle capture

The retention test is completed with an air flow that contained NaCl aerosol. There are no additional electrical or magnetic fields applied during the test, so the model is established based on particle capture by mechanical means. Single fiber efficiency is used to connect the relationship between CNT packing ratio and pressure drop and particle capture efficiency [115].

Since the model is not established for a precise prediction for the exact performance of the CNT enhanced PSP filter, but just an analytical explanation about why it is not possible to achieve high particle capture efficiency and low pressure drop at the same time, some simplifications are applied to the model in order to reduce the complexity. Both CNTs and NaCl aerosols are assumed to be monodisperse. The diameter of CNTs is assumed to be 30 nm, while the NaCl particles are assumed to be 20 nm. The dimension of raw PSP cup is measured by a digital caliper. The filter has a length of 31.0 mm, wall thickness of 0.4 mm and inner diameter of 2.1 mm. The concentration of NaCl aerosol is 7.8×10^7 particles/L, which equals to 1.3×10^{-16} mol/L. Such low concentration will not affect too much on the density of air steam flowed through the CNT-PSP filter, so I assume the density of air remained the same.

The model assumes CNTs are grown uniformly across the entire filter, which agrees with the results shown in Section 6.3. The pressure drop is calculated by the following equation, which considers the air flow met the CNTs at arbitrary inclination:

$$\Delta p = \frac{2\eta chU}{R^2[-\frac{1}{2}\ln(c)-0.75+c-\frac{c^2}{4}]} \quad \text{(Equation 6.2)}$$

Here η is the viscosity of air, c is the packing fraction of CNTs in porous filter, h is the thickness of filter, U is the velocity of air when entered the filter, and R is the radius of a CNT (assumed to be constant). Pressure drop of the CNT enhanced filter is calculated when the CNT packing fraction is varied from 0.00001 to 0.02, and then normalized at the end of calculation.

The particle capture by mechanical means had three mechanisms: interception, inertial impaction and diffusional deposition, as shown in Figure 6.7a. Interception happens when a particle follows the flow stream around the fiber and then touches the fiber. Impaction happens when a particle goes on a straight path and impacts with the fiber. The diffusional deposition happens when a particle is not tightly held by the flow stream and diffuses through a random path to the fiber. Detailed description of the three mechanisms are described by Brown et al [115].

In this model, diffusional deposition is obtained by the following equation:

$$E_D = 2.32\zeta^{-\frac{1}{3}}Pe^{-\frac{2}{3}} \quad \text{(Equation 6.3)}$$

The ζ is also called hydrodynamic factor, and in this model I chose to use Kuwabara's theory. So ζ is calculated by:

$$\zeta = \frac{-0.5\ln(c)-0.75+c+\frac{c^2}{4}}{1-c} \quad \text{(Equation 6.4)}$$

Pe stands for Peclet number, which is:

$$Pe = \frac{2UR}{D} \quad \text{(Equation 6.5)}$$

And D is the coefficient of diffusion:

$$D = \mu k_B T \quad \text{(Equation 6.6)}$$

T is temperature in Kelvin, and k_B is the Boltzmann constant. μ is the mobility of particles, which is:

$$\mu = \frac{Cn}{3\pi\eta d_p} \quad \text{(Equation 6.7)}$$

Here d_p is the diameter of particles that will be captured, and Cn is the Cunningham correction factor:

$$Cn = 1 + \frac{2A\lambda}{d_p} + \frac{2Q\lambda}{d_p} e^{-\frac{Bd_p}{2\lambda}} \quad \text{(Equation 6.8)}$$

Where A=1.246, Q=0.42, B=0.87 and λ , the mean free path of molecues at normal temperature and pressure, is 0.065 μm.

The capture mechanism of interception and inertial impaction is calculated together:

$$E_{IR} = E_R + 2\zeta^{-2} J S_t \quad \text{(Equation 6.9)}$$

$$S_t = \frac{{d_p}^2 \rho U}{18\eta d_f} \quad \text{(Equation 6.10)}$$

$$J = (29.6 - 28c^{0.62})N_R - 27.5{N_R}^{2.8} \quad \text{(Equation 6.11)}$$

$$N_R = \frac{d_p}{d_f} \quad \text{(Equation 6.12)}$$

Here d_f is the diameter of CNTs, and ρ is the density of air. E_R is the particle capture by direct interception:

$$E_R = \frac{(1-c){N_R}^2}{Ku(1+N_R)^m} \quad \text{(Equation 6.13)}$$

$$Ku = -\frac{1}{2}\ln(c) - 0.75 + c + \frac{c^2}{4} \quad \text{(Equation 6.14)}$$

$$m = \frac{2}{3(1-c)} \quad \text{(Equation 6.15)}$$

Finally, the total particle capture efficiency calculated by the single fiber theory is a sum up from all three mechanisms:

$$E = E_D + E_{IR} \quad \text{(Equation 6.16)}$$

Since interception and inertial impaction capture are more significant as particle size increases, and the aerosol used in this study is nano particles, the capture efficiency contributed by diffusional deposition is more significant than that by interception and inertial impaction. As CNT packing fraction increases, the contribution to particle capture efficiency by interception and inertial impaction also increases. As a result, diffusional deposition contributes to 91.4% of the of total particle capture efficiency at packing ratio of 0.00001, and 67.8% at packing ratio of 0.02 (Figure 6.7b). The capture efficiency is also normalized at the end of calculate, in order to compare with the trend from pressure drop. The result was plotted on Figure 6.7c.

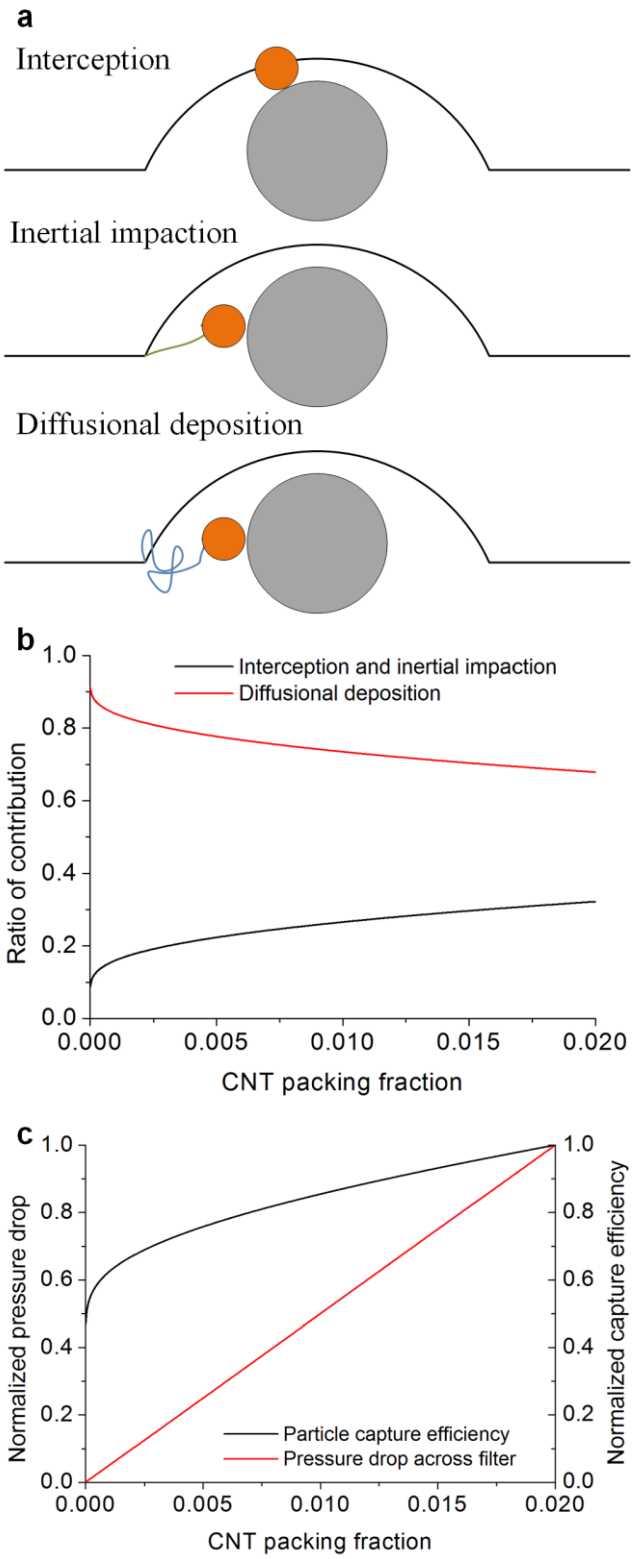

Figure 6.7 Analytical modeling on CNT enhanced PSP cup filter. (a), three capture mechanisms by mechanical means. (b), contribution to particle capture efficiency by different mechanisms. (c), pressure drop across the enhanced filter and particle capture efficiency related with CNT packing fraction in the micro porous filter.

From the normalized plot, it is predicted that the pressure drop across the enhanced filter increases almost linearly according to CNT packing fraction. On the other hand, particle capture efficiency starts to increase as an exponential curve when the CNT packing fraction is very low (less than 0.0025). And then as more and more CNTs are filled in the porous filter, the slope of capture efficiency becomes much smaller compared with that at low CNT packing fraction. Such modeling result qualitatively explains the retention test: when a small amount of CNTs is grown on the PSP cup, the pressure drop increased due to the CNTs is also at a relatively low level (from <1 psi to about 10 psi, Figure 6.6). And due to the significant improvement of particle capture efficiency at low CNT packing fraction, the retention rate increases from 10^1 to 10^7. But when much more CNTs is grown on the PSP cup (pressure drop reaches 40-50 psi), the additional improvement on retention rate is much limited (from 10^7 to 10^9).

The model also suggests the filter design for future applications: at the same level of CNT packing fraction, in order to obtain better particle capture performance, the CNTs grown on the porous filter should be relatively loose but long, instead of short and dense. Because when the total length of CNTs is kept as constant (same overall packing fraction), short and dense CNTs mean a much higher local packing fraction, which will be an optimal case to aim for high particle capture efficiency while keeping pressure drop at relatively low level.

There are also limitations of the model. Both pressure drop and particle capture efficiency are derived from CNT packing fraction in the model, but the actual CNT packing fraction of as produced enhanced filter is unknown. The model describes the ability of particle capture in unit less numbers, but due to the missing information of CNT packing fraction on as produced enhanced filters and the physical properties of particle and fiber, the particle capture efficiency can not be converted to quantitative prediction of retention rate of an enhanced filter. For example, there is no data obtained for the pressure drop between 20 and 35 psi on Figure 6.6, and the model can not predict the corresponding retention rate for that range of pressure drop. Addition to pressure drop and retention rate, the CNT packing fraction of enhanced filter also needs to be evaluated in order to provide quantitative prediction on the performance of enhanced filter.

6.7 Conclusion and future work

In this chapter, uniform growth of dense tangled CNTs is demonstrated on the native surface

of PSP porous filters without external catalyst. A specialized quartz holder is designed in order to achieve this uniform growth. Possible factors that affect the pressure drop of enhanced filter are studied such as growth time, residue in gas lines, and moisture during growth. Performance of the enhanced filter can be adjusted by these factors according to requirement from real applications. The pressure drop across enhanced filter produced with 3 minutes of CNT growth is found to achieve the minimum value with 40-50 ppm of moisture during growth, and this group of enhanced filter can improve the retention performance by 4~6 orders of magnitude while maintaining the pressure drop only about 10 psi. The results of study satisfy the sponsor of this project. Finally, an analytical model is established to explain the behavior of pressure drop and retention rate based on packing ratio of CNTs in the enhanced filter. This model also explains why the improvement of retention is much more significant in the regime of low pressure drop, and suggests the CNTs grown on filter should be long and loose instead of short and dense. In the future, a continuous manufacturing prototype can be further designed in order to transfer the technique from lab scale study to industrial production. The batch to batch consistency of the enhanced filter would also benefit from the continuous production, since the gas supply would be more stable during continuous operation compare to lab scale production.

CHAPTER 7
CONTRIBUTIONS AND OUTLOOK

7.1 Contributions of this thesis

This thesis has presented an understanding of how fluctuations of moisture transients influence the consistency of CNT forest growth, and adapted this understanding to a new process that achieves highly consistent high density CNT forest production. In parallel, and with benefit of the above understanding, processes were developed for CNT synthesis directly on bulk Haynes 556 alloy without external source of catalyst. Furthermore, uniform coating of tangled CNTs can be achieved on a commercially produced stainless steel micro porous filter and the particle capture efficiency of this filter can be improved for several orders of magnitude.

The major contributions of this thesis include:

- The design and fabrication of a transfer arm assisted CVD system, which allows rapid insertion and removal of the substrate from the heated zone of the furnace. This capability enables separation of catalyst annealing and CNT growth steps while the furnace atmosphere is interchanged.

- The understanding of influence of moisture transients on CNT growth consistency and height kinetics:

    - The decoupled method reduced the run-to-run variance of forest height by 76% compared to reference process. The improvement on consistency was achieved by decreasing the transient of moisture concentration during 10 minutes of CNT growth stage from 100 ppm to 15 ppm.

    - The decoupled method improved the growth kinetics of forest height by 21%~63% compared to reference process, under different moisture conditions.

- When substrate was annealed with moisture level less than 15 ppm, kinetics of forest height was similar for growths at moisture level from 40 to 450 ppm. These kinetics of heights were 30% greater than growth with moisture level less than 15 ppm.

- Developed a method significantly increased CNT forest density by carbon preload annealing and moisture assisted growth:

  - Moisture was necessary during catalyst activation phase of CNT growth, but presence of moisture after activation was negative on kinetics of forest height.

  - Density of CNT forests produced with carbon preload annealing was 3~4 times as much as that produced without preloading of carbon.

  - Raman spectroscopy and TEM showed graphitic structures were formed on catalyst particle after carbon preload annealing.

- Developed a process for direct synthesis of CNT forest on the native surface of Haynes 556 alloy, which is used for filtration applications by Pall Cooperation.

  - Growth was enabled by air oxidation at 825 ℃ and He/H2 reduction at 775 ℃ on substrate surface before hydrocarbon exposure.

  - Consistent aligned forest was achieved by supplying 300-400 ppm of moisture during CNT growth stage.

  - Demonstrated that forests can be regrown after previously grown CNTs were removed.

- Established a process for growth of a uniform tangled CNT coating on stainless steel porous filter.

  - Novel design of sample holder that provides uniform CNT growth throughout the entire body of stainless steel micro porous filter.

- Demonstration of growth consistency improved by moisture and residue control in the gas delivery system

- Demonstration of particle capture efficiency of the CNT enhanced filter performs as high as 8 orders of magnitude compared to the original uncoated SS filter. 6 orders of magnitude of improvement achieved on CNT enhanced filter with a pressure drop less than 15 psi, as required by Pall cooperation.

- Established an analytical model shows pressure drop across the filter increases almost linearly with CNT packing fraction, while particle capture efficiency increases much faster at lower CNT packing fraction, and explained the retention test results.

In addition to work presented in this thesis, I have also contributed to the following collaborative projects during my PhD studies at the University of Michigan:

- In collaboration with postdoctoral associate Dr. Sudhanshu Srivastava, I proposed and led the study that demonstrated fabrication of multidirectional and hierarchical carbon nanotube (CNT) films on diverse substrates, using nanocomposite catalyst films prepared by layer-by-layer (LBL) assembly [116].

- In collaboration with visiting scholar Dr. Weipeng Lv, I contributed to CNT synthesis on inorganic anisotropic nanospheres. The successful growth of MWNTs on the Janus micro and nanoparticles may be useful to produce a wide range of heterogeneous catalyst systems and catalytic supporters [117].

- In collaboration with postdoctoral associate Dr. Sebastian Pattinson, I shared my past experience and understanding of CNT growth on stainless steel micro fiber substrates, demonstrated the surface evolution of this material during heat treatment prior to hydrocarbon exposure, and provided an optimized recipe to fabricate tangled CNTs on native surface of this material. This was used in an environmental transmission electron microscopy study that showed how surface restructuring upon oxygen exposure at elevated temperatures enables CNT growth from bulk stainless steel substrate [118].

7.2 Key questions and future directions

In spite of the accomplishments of this thesis, the following questions are identified for further work on this topic:

- Further understanding of how the carbon exposure influences the chemistry and phase of the catalyst, and what causes the high activation rate of catalyst with carbon preload anneal.

- Improve catalyst lifetime: the work from this dissertation provided a novel method to help activate catalyst particles in several different aspects, which naturally improves catalyst lifetime compare to the reference process. But, further study can still be carried out after CNT nucleation. The forests obtained from combined recipe (Chapter 4) with carbon preload annealing and moisture assisted growth achieves a density as high as 137 $\mu g/mm^3$ for the first minute of growth, but then decays exponentially as growth time/forest height increases. Further study is still needed to keep catalyst activated in order to obtain high density and tall forests.

- Application on small feature devices: All samples demonstrated in this thesis for lab scale study are plain catalyst without any patterns. But based on the study during the past few years, it is known that the combined recipe (Chapter 4) can provide much better growth on small patterned features (i.e. less than 10 μm) compare to the reference process. Such improvement can contribute to a better activation of catalyst particles caused by the combined recipe. Future research can take this advantage and enable applications including microstructured surfaces and MEMS devices that require fine features.

- Optimized synthesis technique on Haynes alloy: study of CNT growth on Haynes 556 alloy had already demonstrated growth of aligned forests, but it is noticed that the quality of CNT forest obtained from re-growth is worse than the first run of growth. As discussed in Chapter 5, such degradation can be closely related to the evolution of elemental composition on surface of substrate. Combined with the impact of heat treatment on growth results, the evolution of elemental composition and its impact on CNT forest growth needs to be further studied, in order to achieve an optimal fabrication process that reduces the degradation of CNT forest as

re-growth cycles continue.

- Consistent production of CNT enhanced micro porous SS filters: at the end of previous study, noticeable amount of batch to batch fluctuation is still observed. Besides the fluctuation inherited from raw filters, the lab scale manufacturing process contributed to a significant portion of the fluctuation. For future applications with industrial scale production, the manufacturing process needs to be re-designed in order to enable large scale production, so that the batch to batch fluctuation due to impurity residues in gas delivery systems caused by low flow rate of C_2H_2 and CO_2 can be eliminated.

BIBLIOGRAPHY

[1] Iijima S. HELICAL MICROTUBULES OF GRAPHITIC CARBON. Nature. 1991;354(6348):56-8.

[2] Yu MF, Files BS, Arepalli S, Ruoff RS. Tensile loading of ropes of single wall carbon nanotubes and their mechanical properties. Physical Review Letters. 2000;84(24):5552-5.

[3] Dulinska-Molak I, Mao HL, Kawazoe N, Chen GP. Variation of Mechanical Property of Single-Walled Carbon Nanotubes-Treated Cells Explored by Atomic Force Microscopy. Journal of Biomedical Nanotechnology. 2014;10(4):651-9.

[4] Gao Y, Zong GY, Bai HW, Fu Q. Combined effects of stretching and nanofillers on the crystalline structure and mechanical properties of polypropylene and single-walled carbon nanotube composite fibers. Chinese Journal of Polymer Science. 2014;32(2):245-54.

[5] Coleman JN, Khan U, Blau WJ, Gun'ko YK. Small but strong: A review of the mechanical properties of carbon nanotube-polymer composites. Carbon. 2006;44(9):1624-52.

[6] Coleman JN, Khan U, Gun'ko YK. Mechanical reinforcement of polymers using carbon nanotubes. Advanced Materials. 2006;18(6):689-706.

[7] Chen GH, Futaba DN, Kimura H, Sakurai S, Yumura M, Hata K. Absence of an Ideal Single-Walled Carbon Nanotube Forest Structure for Thermal and Electrical Conductivities. Acs Nano. 2013;7(11):10218-24.

[8] Berber S, Kwon YK, Tomanek D. Unusually high thermal conductivity of carbon nanotubes. Physical Review Letters. 2000;84(20):4613-6.

[9] Biercuk MJ, Llaguno MC, Radosavljevic M, Hyun JK, Johnson AT, Fischer JE. Carbon nanotube composites for thermal management. Applied Physics Letters. 2002;80(15):2767-9.

[10] Che JW, Cagin T, Goddard WA. Thermal conductivity of carbon nanotubes. Nanotechnology. 2000;11(2):65-9.

[11] Du CS, Yeh J, Pan N. High power density supercapacitors using locally aligned carbon nanotube electrodes. Nanotechnology. 2005;16(4):350-3.

[12] Du CS, Pan N. High power density supercapacitor electrodes of carbon nanotube films by electrophoretic deposition. Nanotechnology. 2006;17(21):5314-8.

[13] Ebbesen TW, Lezec HJ, Hiura H, Bennett JW, Ghaemi HF, Thio T. Electrical conductivity of individual carbon nanotubes. Nature. 1996;382(6586):54-6.

[14] Yao Z, Kane CL, Dekker C. High-field electrical transport in single-wall carbon nanotubes. Physical Review Letters. 2000;84(13):2941-4.

[15] Sandler J, Shaffer MSP, Prasse T, Bauhofer W, Schulte K, Windle AH. Development of a dispersion process for carbon nanotubes in an epoxy matrix and the resulting electrical properties. Polymer. 1999;40(21):5967-71.

[16] Dai HJ, Wong EW, Lieber CM. Probing electrical transport in nanomaterials: Conductivity of individual carbon nanotubes. Science. 1996;272(5261):523-6.

[17] Durkop T, Getty SA, Cobas E, Fuhrer MS. Extraordinary mobility in semiconducting carbon nanotubes. Nano Letters. 2004;4(1):35-9.

[18] Chen GH, Futaba DN, Sakurai S, Yumura M, Hata K. Interplay of wall number and diameter on the electrical conductivity of carbon nanotube thin films. Carbon. 2014;67:318-25.

[19] Terranova ML, Sessa V, Rossi M. The world of carbon nanotubes: An overview of CVD growth methodologies. Chemical Vapor Deposition. 2006;12(6):315-25.

[20] Fidelus JD, Wiesel E, Gojny FH, Schulte K, Wagner HD. Thermo-mechanical properties of randomly oriented carbon/epoxy nanocomposites. Composites Part a-Applied Science and Manufacturing. 2005;36(11):1555-61.

[21] Huang SM, Cai XY, Liu J. Growth of millimeter-long and horizontally aligned single-walled carbon nanotubes on flat substrates. Journal of the American Chemical Society. 2003;125(19):5636-7.

[22] Zhang M, Atkinson KR, Baughman RH. Multifunctional carbon nanotube yarns by downsizing an ancient technology. Science. 2004;306(5700):1358-61.

[23] Fung CKM, Zhang MQH, Chan RHM, Li WJ, Ieee. A PMMA-BASED micro pressure sensor chip using carbon nanotubes as sensing elements. 18th IEEE International Conference on Micro Electro Mechanical Systems (MEMS). Miami Beach, FL; 2005; p. 251-4.
[24] Varadan VK. Nanotechnology, MEMS and NEMS and their applications to smart systems and devices. In: Mohan S, Dattaguru B, Gopalakrishnan S, eds. Smart Materials, Structures, and System, Pts 1 and 2 2003, p. 20-43.
[25] He JH, Sun SQ, Ye JS, Lim TM. Self-Assembly Carbon Nanotubes on Cantilever Biosensor for Sensitivity Enhancement. International Mems Conference 2006. 2006;34:423-8.
[26] Marconnett AM, Yamamoto N, Panzer MA, Wardle BL, Goodson KE. Thermal Conduction in Aligned Carbon Nanotube-Polymer Nanocomposites with High Packing Density. Acs Nano. 2011;5(6):4818-25.
[27] Kim B, Chung H, Kim W. Supergrowth of Aligned Carbon Nanotubes Directly on Carbon Papers and Their Properties as Supercapacitors. Journal of Physical Chemistry C. 2010;114(35):15223-7.
[28] Challa SK, Harris B, Hiestand JW, Asme. Preliminary Study of the Effects of Carbon Nanotubes on Cpu Cooling. Proceedings of the Asme International Mechanical Engineering Congress and Exposition 2010, Vol 4. 2012:17-22.
[29] Baughman RH, Zakhidov AA, de Heer WA. Carbon nanotubes - the route toward applications. Science. 2002;297(5582):787-92.
[30] Fan SS, Chapline MG, Franklin NR, Tombler TW, Cassell AM, Dai HJ. Self-oriented regular arrays of carbon nanotubes and their field emission properties. Science. 1999;283(5401):512-4.
[31] Fang WL, Chu HY, Hsu WK, Cheng TW, Tai NH. Polymer-reinforced, aligned multiwalled carbon nanotube composites for microelectromechanical systems applications. Advanced Materials. 2005;17(24):2987-+.
[32] Jiang YQ, Zhou Q, Lin L, Ieee. PLANAR MEMS SUPERCAPACITOR USING CARBON NANOTUBE FORESTS. 22nd International Conference on Micro Electro Mechanical Systems (MEMS). Sorrento, ITALY: Ieee; 2009; p. 587-90.
[33] Bedewy M, Meshot ER, Guo HC, Verploegen EA, Lu W, Hart AJ. Collective Mechanism for the Evolution and Self-Termination of Vertically Aligned Carbon Nanotube Growth. Journal of Physical Chemistry C. 2009;113(48):20576-82.
[34] Treacy MMJ, Ebbesen TW, Gibson JM. Exceptionally high Young's modulus observed for individual carbon nanotubes. Nature. 1996;381(6584):678-80.
[35] Frank S, Poncharal P, Wang ZL, de Heer WA. Carbon nanotube quantum resistors. Science. 1998;280(5370):1744-6.
[36] Esconjauregui S, Fouquet M, Bayer BC, Ducati C, Smajda R, Hofmann S, et al. Growth of Ultrahigh Density Vertically Aligned Carbon Nanotube Forests for Interconnects. Acs Nano. 2010;4(12):7431-6.
[37] Xu M, Futaba DN, Yumura M, Hata K. Alignment Control of Carbon Nanotube Forest from Random to Nearly Perfectly Aligned by Utilizing the Crowding Effect. Acs Nano. 2012;6(7):5837-44.
[38] Yamada T, Maigne A, Yudasaka M, Mizuno K, Futaba DN, Yumura M, et al. Revealing the Secret of Water-Assisted Carbon Nanotube Synthesis by Microscopic Observation of the Interaction of Water on the Catalysts. Nano Letters. 2008;8(12):4288-92.
[39] Oliver CR, Polsen ES, Meshot ER, Tawfick S, Park SJ, Bedewy M, et al. Statistical Analysis of Variation in Laboratory Growth of Carbon Nanotube Forests and Recommendations for Improved Consistency. Acs Nano. 2013;7(4):3565-80.
[40] Sakurai S, Inaguma M, Futaba DN, Yumura M, Hata K. Diameter and Density Control of Single-Walled Carbon Nanotube Forests by Modulating Ostwald Ripening through Decoupling the Catalyst Formation and Growth Processes. Small. 2013;9(21):3584-92.
[41] Hata K, Futaba DN, Mizuno K, Namai T, Yumura M, Iijima S. Water-assisted highly efficient synthesis of impurity-free single-waited carbon nanotubes. Science. 2004;306(5700):1362-4.
[42] Meshot ER, Plata DL, Tawfick S, Zhang YY, Verploegen EA, Hart AJ. Engineering Vertically Aligned Carbon Nanotube Growth by Decoupled Thermal Treatment of Precursor and Catalyst. Acs Nano. 2009;3(9):2477-86.
[43] Iijima S, Ajayan PM, Ichihashi T. GROWTH-MODEL FOR CARBON NANOTUBES. Physical Review Letters. 1992;69(21):3100-3.
[44] Hofmann S, Sharma R, Ducati C, Du G, Mattevi C, Cepek C, et al. In situ observations of catalyst dynamics during surface-bound carbon nanotube nucleation. Nano Letters. 2007;7(3):602-8.
[45] Meyyappan M, Delzeit L, Cassell A, Hash D. Carbon nanotube growth by PECVD: a review. Plasma Sources Science & Technology. 2003;12(2):205-16.
[46] Guo T, Nikolaev P, Thess A, Colbert DT, Smalley RE. CATALYTIC GROWTH OF SINGLE-WALLED NANOTUBES BY LASER VAPORIZATION. Chemical Physics Letters. 1995;243(1-2):49-54.
[47] Hart AJ, Slocum AH. Rapid growth and flow-mediated nucleation of millimeter-scale aligned carbon

nanotube structures from a thin-film catalyst. Journal of Physical Chemistry B. 2006;110(16):8250-7.
[48] Kataura H, Kumazawa Y, Maniwa Y, Ohtsuka Y, Sen R, Suzuki S, et al. Diameter control of single-walled carbon nanotubes. Carbon. 2000;38(11-12):1691-7.
[49] Li Y, Liu J, Wang YQ, Wang ZL. Preparation of monodispersed Fe-Mo nanoparticles as the catalyst for CVD synthesis of carbon nanotubes. Chemistry of Materials. 2001;13(3):1008-14.
[50] Cantoro M, Hofmann S, Pisana S, Scardaci V, Parvez A, Ducati C, et al. Catalytic chemical vapor deposition of single-wall carbon nanotubes at low temperatures. Nano Letters. 2006;6(6):1107-12.
[51] Li QW, Zhang XF, DePaula RF, Zheng LX, Zhao YH, Stan L, et al. Sustained growth of ultralong carbon nanotube arrays for fiber spinning. Advanced Materials. 2006;18(23):3160-+.
[52] Liu K, Liu P, Jiang K, Fan SS. Effect of carbon deposits on the reactor wall during the growth of multi-walled carbon nanotube arrays. Carbon. 2007;45(12):2379-87.
[53] Liao HW, Hafner JH. Low-temperature single-wall carbon nanotube synthesis by thermal chemical vapor deposition. Journal of Physical Chemistry B. 2004;108(22):6941-3.
[54] Finnie P, Li-Pook-Than A, Lefebvre J, Austing DG. Optimization of methane cold wall chemical vapor deposition for the production of single walled carbon nanotubes and devices. Carbon. 2006;44(15):3199-206.
[55] Meshot ER, Verploegen E, Bedewy M, Tawfick S, Woll AR, Green KS, et al. High-Speed in Situ X-ray Scattering of Carbon Nanotube Film Nucleation and Self-Organization. Acs Nano. 2012;6(6):5091-101.
[56] Weisenberger MC, inventor WEISENBERGER M C (WEIS-Individual) UNIV KENTUCKY RES FOUND (KENT-C), assignee. Producing aligned carbon nanotube tape for increasing unidirectional heat conduction from a work piece involves preparing strips of aligned carbon nanotube; and splicing strips of carbon nanotube together end-to-end on a flexible support patent US2009266477-A1; US8632879-B2 US2009266477-A1 29 Oct 2009 B32B-037/12 200974 Pages: 11 English US8632879-B2 21 Jan 2014 C09J-009/00 201407 English.
[57] Huang H, Liu CH, Wu Y, Fan SS. Aligned carbon nanotube composite films for thermal management. Advanced Materials. 2005;17(13):1652-+.
[58] Ashrafi B, Hubert P, Vengallatore S. Carbon nanotube-reinforced composites as structural materials for microactuators in microelectromechanical systems. Nanotechnology. 2006;17(19):4895-903.
[59] Zhang M, Fang SL, Zakhidov AA, Lee SB, Aliev AE, Williams CD, et al. Strong, transparent, multifunctional, carbon nanotube sheets. Science. 2005;309(5738):1215-9.
[60] Stadermann M, Sherlock SP, In JB, Fornasiero F, Park HG, Artyukhin AB, et al. Mechanism and Kinetics of Growth Termination in Controlled Chemical Vapor Deposition Growth of Multiwall Carbon Nanotube Arrays. Nano Letters. 2009;9(2):738-44.
[61] Hasegawa K, Noda S. Millimeter-Tall Single-Walled Carbon Nanotubes Rapidly Grown with and without Water. Acs Nano. 2011;5(2):975-84.
[62] In JB, Grigoropoulos CP, Chernov AA, Noy A. Hidden role of trace gas impurities in chemical vapor deposition growth of vertically-aligned carbon nanotube arrays. Applied Physics Letters. 2011;98(15):3.
[63] Wyss RM, Klare JE, Park HG, Noy A, Bakajin O, Lulevich V. Water-Assisted Growth of Uniform 100 mm Diameter SWCNT Arrays. ACS applied materials & interfaces. 2014;6(23):21019-25.
[64] Hasegawa K, Noda S. Moderating carbon supply and suppressing Ostwald ripening of catalyst particles to produce 4.5-mm-tall single-walled carbon nanotube forests. Carbon. 2011;49(13):4497-504.
[65] Wang BN, Bennett RD, Verploegen E, Hart AJ, Cohen RE. Characterizing the morphologies of mechanically manipulated multiwall carbon nanotube films by small-angle X-ray scattering. Journal of Physical Chemistry C. 2007;111(48):17933-40.
[66] Wang BN, Bennett RD, Verploegen E, Hart AJ, Cohen RE. Quantitative characterization of the morphology of multiwall carbon nanotube films by small-angle X-ray scattering. Journal of Physical Chemistry C. 2007;111(16):5859-65.
[67] Bedewy M, Meshot ER, Reinker MJ, Hart AJ. Population Growth Dynamics of Carbon Nanotubes. Acs Nano. 2011;5(11):8974-89.
[68] Pillai SK, Ray SS, Moodley M. Purification of single-walled carbon nanotubes. Journal of Nanoscience and Nanotechnology. 2007;7(9):3011-47.
[69] Hou PX, Liu C, Cheng HM. Purification of carbon nanotubes. Carbon. 2008;46(15):2003-25.
[70] Meshot ER, Bedewy M, Lyons KM, Woll AR, Juggernauth KA, Tawfick S, et al. Measuring the lengthening kinetics of aligned nanostructures by spatiotemporal correlation of height and orientation. Nanoscale. 2010;2(6):896-900.
[71] Hermans PH. Contribution to the physics of cellulose fibres; a study in sorption, density, refractive power and orientation: Elsevier Pub. Co. Amsterdam; 1946.
[72] Futaba DN, Hata K, Yamada T, Mizuno K, Yumura M, Iijima S. Kinetics of water-assisted single-walled

carbon nanotube synthesis revealed by a time-evolution analysis. Physical Review Letters. 2005;95(5):4.
[73] Oliver CR, Westrick W, Koehler J, Brieland-Shoultz A, Anagnostopoulos-Politis I, Cruz-Gonzalez T, et al. Robofurnace: A semi-automated laboratory chemical vapor deposition system for high-throughput nanomaterial synthesis and process discovery. Review of Scientific Instruments. 2013;84(11):14.
[74] Oshima H, Shimazu T, Siry M, Ko MB. Analysis of Fe Catalyst during Carbon Nanotube Synthesis by Mossbauer Spectroscopy. Journal of Physical Chemistry C. 2009;113(43):18523-6.
[75] Wirth CT, Bayer BC, Gamalski AD, Esconjauregui S, Weatherup RS, Ducati C, et al. The Phase of Iron Catalyst Nanoparticles during Carbon Nanotube Growth. Chemistry of Materials. 2012;24(24):4633-40.
[76] Mazzucco S, Wang Y, Tanase M, Picher M, Li K, Wu ZJ, et al. Direct evidence of active and inactive phases of Fe catalyst nanoparticles for carbon nanotube formation. Journal of Catalysis. 2014;319:54-60.
[77] Esconjauregui S, Xie RS, Fouquet M, Cartwright R, Hardeman D, Yang JW, et al. Measurement of area density of vertically aligned carbon nanotube forests by the weight-gain method. Journal of Applied Physics. 2013;113(14):7.
[78] Dijon J, Fournier A, Szkutnik PD, Okuno H, Jayet C, Fayolle M. Carbon nanotubes for interconnects in future integrated circuits: The challenge of the density. Diamond and Related Materials. 2010;19(5-6):382-8.
[79] Chiodarelli N, Richard O, Bender H, Heyns M, De Gendt S, Groeseneken G, et al. Correlation between number of walls and diameter in multiwall carbon nanotubes grown by chemical vapor deposition. Carbon. 2012;50(5):1748-52.
[80] Zhong GF, Warner JH, Fouquet M, Robertson AW, Chen BA, Robertson J. Growth of Ultrahigh Density Single-Walled Carbon Nanotube Forests by Improved Catalyst Design. Acs Nano. 2012;6(4):2893-903.
[81] Sugime H, Esconjauregui S, Yang JW, D'Arsie L, Oliver RA, Bhardwaj S, et al. Low temperature growth of ultra-high mass density carbon nanotube forests on conductive supports. Applied Physics Letters. 2013;103(7):5.
[82] Chen ZM, Kim DY, Hasegawa K, Noda S. Methane-Assisted Chemical Vapor Deposition Yielding Millimeter-Tall Single-Wall Carbon Nanotubes of Smaller Diameter. Acs Nano. 2013;7(8):6719-28.
[83] C.D. W, W.M. R, L.E. D, J.F. M, G.E. M. Handbook
of X-Ray Photoelectron Spectroscopy: Perkin-Elmer Corporation; 1979.
[84] Powell CJ. ATTENUATION LENGTHS OF LOW-ENERGY ELECTRONS IN SOLIDS. Surface Science. 1974;44(1):29-46.
[85] Weckhuysen BM, Rosynek MP, Lunsford JH. Characterization of surface carbon formed during the conversion of methane to benzene over Mo/H-ZSM-5 catalysts. Catalysis Letters. 1998;52(1-2):31-6.
[86] Shchukarev AV, Korolkov DV. XPS study of group IA carbonates. Central European Journal of Chemistry. 2004;2(2):347-62.
[87] Allen GC, Curtis MT, Hooper AJ, Tucker PM. X-RAY PHOTOELECTRON SPECTROSCOPY OF CHROMIUM-OXYGEN SYSTEMS. Journal of the Chemical Society-Dalton Transactions. 1973(16):1675-83.
[88] Oku M, Hirokawa K, Ikeda S. PHOTOELECTRON SPECTRAL INTENSITIES OF SOME FIRST TRANSITION SERIES ELEMENTS IN METAL CYANIDES CONTAINING INEQUIVALENT ATOMS. Journal of Electron Spectroscopy and Related Phenomena. 1975;6(6):451-8.
[89] Collins PG, Bradley K, Ishigami M, Zettl A. Extreme oxygen sensitivity of electronic properties of carbon nanotubes. Science. 2000;287(5459):1801-4.
[90] Miao HY, Lue JT, Chen SY, Chen SK, Ouyang MS. Growth of carbon nanotubes on transition metal alloys by microwave-enhanced hot-filament deposition. Thin Solid Films. 2005;484(1-2):58-63.
[91] Parthangal PM, Cavicchi RE, Zachariah MR. A generic process of growing aligned carbon nanotube arrays on metals and metal alloys. Nanotechnology. 2007;18(18):5.
[92] Lepro X, Lima MD, Baughman RH. Spinnable carbon nanotube forests grown on thin, flexible metallic substrates. Carbon. 2010;48(12):3621-7.
[93] Kim B, Chung H, Chu KS, Yoon HG, Lee CJ, Kim W. Synthesis of vertically-aligned carbon nanotubes on stainless steel by water-assisted chemical vapor deposition and characterization of their electrochemical properties. Synthetic Metals. 2010;160(7-8):584-7.
[94] Pal SK, Kar S, Lastella S, Kumar A, Vajtai R, Talapatra S, et al. Importance of Cr2O3 layer for growth of carbon nanotubes on superalloys. Carbon. 2010;48(3):844-53.
[95] Cole MT, Hou K, Warner JH, Barnard JS, Ying K, Zhang Y, et al. In-situ deposition of sparse vertically aligned carbon nanofibres on catalytically activated stainless steel mesh for field emission applications. Diamond and Related Materials. 2012;23:66-71.
[96] Shin EC, Jeong GH. Highly efficient carbon nanotube growth on plasma pretreated stainless steel substrates. Thin Solid Films. 2012;521:102-6.
[97] Baker RW. Membrane Technology and Applications. 2nd ed: John Wiley & Sons; 2008.

[98] Hinds WC. Aerosol technology: Properties, behavior, and measurement of airborne particles: Wiley-Interscience; 1982.
[99] Atkinson S. Filtration technology verified to remove arsenic from drinking water. Membrane Technology. 2006;2006(3):8-9.
[100] Li ZJ, Zhou SQ, Qiu JH. Combined treatment of landfill leachate by biological and membrane filtration technology. Environmental Engineering Science. 2007;24(9):1245-56.
[101] Holt JA, inventor Compressor Systems, Inc., assignee. Coalescing device and method for removing particles from a rotary gas compressor. USA. 2000.
[102] Takao Kusuda TM, Masaaki Yonemura, Satoshi Kuwano, inventor Matsushita Electric Industrial Co., Ltd., assignee. Exhaust gas filter. USA. 1987.
[103] Yiannis A. Levendis RFA, inventor Northeastern University, Ceramem Corporation, assignee. Diesel engine exhaust gas recirculation
system for NOx control incorporating a compressed air regenerative
particulate control system. USA. 1995.
[104] Lee C, Baik S. Vertically-aligned carbon nano-tube membrane filters with superhydrophobicity and superoleophilicity. Carbon. 2010;48(8):2192-7.
[105] Masarapu C, Subramanian V, Zhu HW, Wei BQ. Long-Cycle Electrochemical Behavior of Multiwall Carbon Nanotubes Synthesized on Stainless Steel in Li Ion Batteries. Advanced Functional Materials. 2009;19(7):1008-14.
[106] Anwar H, George AE, Hill IG. Vertically-aligned carbon nanotube counter electrodes for dye-sensitized solar cells. Solar Energy. 2013;88:129-36.
[107] Duy DQ, Kim HS, Yoon DM, Lee KJ, Ha JW, Hwang YG, et al. Growth of carbon nanotubes on stainless steel substrates by DC-PECVD. Applied Surface Science. 2009;256(4):1065-8.
[108] Masarapu C, Wei BQ. Direct growth of aligned multiwalled carbon nanotubes on treated stainless steel substrates. Langmuir. 2007;23(17):9046-9.
[109] Yuan LM, Saito K, Hu WC, Chen Z. Ethylene flame synthesis of well-aligned multi-walled carbon nanotubes. Chemical Physics Letters. 2001;346(1-2):23-8.
[110] Park D, Kim YH, Lee JK. Synthesis of carbon nanotubes on metallic substrates by a sequential combination of PECVD and thermal CVD. Carbon. 2003;41(5):1025-9.
[111] Vander Wal RL, Hall LJ. Carbon nanotube synthesis upon stainless steel meshes. Carbon. 2003;41(4):659-72.
[112] Baddour CE, Fadlallah F, Nasuhoglu D, Mitra R, Vandsburger L, Meunier JL. A simple thermal CVD method for carbon nanotube synthesis on stainless steel 304 without the addition of an external catalyst. Carbon. 2009;47(1):313-8.
[113] Karwa M, Iqbal Z, Mitra S. Scaled-up self-assembly of carbon nanotubes inside long stainless steel tubing. Carbon. 2006;44(7):1235-42.
[114] Camilli L, Scarselli M, Del Gobbo S, Castrucci P, Nanni F, Gautron E, et al. The synthesis and characterization of carbon nanotubes grown by chemical vapor deposition using a stainless steel catalyst. Carbon. 2011;49(10):3307-15.
[115] Brown, C. R. Air Filtration: Pergamon Press; 1993.
[116] Li JJ, Srivastava S, Ok JG, Zhang YY, Bedewy M, Kotov NA, et al. Multidirectional Hierarchical Nanocomposites Made by Carbon Nanotube Growth within Layer-by-Layer-Assembled Films. Chemistry of Materials. 2011;23(4):1023-31.
[117] Lv WP, Lee KJ, Li JJ, Park TH, Hwang S, Hart AJ, et al. Anisotropic Janus Catalysts for Spatially Controlled Chemical Reactions. Small. 2012;8(20):3116-22.
[118] Pattinson SW, Viswanath B, Zakharov DN, Li JJ, Stach EA, Hart AJ. Mechanism and Enhanced Yield of Carbon Nanotube Growth on Stainless Steel by Oxygen-Induced Surface Reconstruction. Chemistry of Materials. 2015;27(3):932-7.